

Cyclic and linear photoionizations of acridine derivatives and xanthone investigated by nanosecond laser flash photolysis

Dissertation

zur Erlangung des akademischen Grades
Doctor rerum naturalium (Dr. rer. nat.)

vorgelegt der

Mathematisch-Naturwissenschaftlich-Technischen Fakultät
(mathematisch-naturwissenschaftlicher Bereich)
der Martin-Luther-Universität Halle-Wittenberg

von Herrn M.Sc. Belal Hussein Mohamed Hussein
geb. am 02.01.1970 in Egypt

Gutachter:

1. Prof. Dr. Martin Goez, Halle
2. Prof. Dr. Hans-Gerd Löhmannsröben, Universität Potsdam

Halle (Saale), 2005

Datum der Verteidigung: 06.12.2005

urn:nbn:de:gbv:3-000010143

[<http://nbn-resolving.de/urn/resolver.pl?urn=nbn%3Ade%3Agbv%3A3-000010143>]

Contents

1. Introduction	1
Part I Experimental methodology and theoretical analysis.....	5
2. Experimental section	6
2.1. Steady-state measurements	6
2.2. Laser flash photolysis.....	6
2.3. Materials.....	8
2.4. Determination of triplet-triplet extinction coefficients	9
2.4.1. Relative actinometry	9
2.4.2. Energy transfer	9
2.5. Determination of extinction coefficients and quantum yields of radical ions.....	11
2.6. Analysis of triplet state decay kinetics.....	11
2.6.1. First-order decay	11
2.6.2. Self-quenching	12
2.6.3. Triplet-triplet annihilation.....	12
2.7. Determination of electron absorption.....	13
3. Linear and cyclic photoionizations – Analysis of light intensity dependences	14
3.1. Kinetic formulation of light absorption.....	14
3.2. Linear photoionization processes	15
3.2.1. Consecutive two-photon ionization.....	16
3.2.2. Parallel photoionization of excited singlet and triplet states.....	19
3.2.3. Stepwise photoionization via a three-photon process	20
3.3. Cyclic mechanisms of electron donor photoionizations	22
3.3.1. Singlet or triplet state undergoes photoionization.....	22
3.3.2. Both singlet and triplet states undergo photoionization	25
3.4. Cyclic mechanisms of electron acceptor photoionizations	26

Part II Donor and acceptor photoionizations – Results and discussions	29
Part II.A Electron donor photoionizations.....	30
4. Photoionization of acridone derivatives via their singlet state	30
4.1. Spectroscopic characterization	30
4.2. Triplet and radical cation absorption spectra	32
4.3. Triplet energy transfer	33
4.4. Electron transfer	34
4.5. Cyclic photoionization of N-methylacridone in SDS	35
4.5.1. Possible reaction mechanisms	35
4.5.2. Analysis and simulation of cyclic photoionization mechanism	37
4.6. Cyclic photoionization of acridone in SDS	39
4.7. Two-laser pulse experiments.....	40
4.8. Linear photoionization of acridone derivatives in alcohol-water solution.....	41
4.9. SDS as a sacrificial electron donor	43
5. Photoionization of xanthone via its triplet state.....	45
5.1. Steady-state absorption spectra	45
5.2. Transient absorption spectra.....	45
5.3. Triplet decay analysis.....	46
5.4. Determination of extinction coefficient of xanthone triplet state	48
5.5. Linear photoionization in methanol-water (1:2 v/v) by near UV.....	48
5.6. Cyclic photoionization in aqueous SDS solution at 308 nm.....	51
5.7. Photoionization in aqueous SDS at 355 nm.....	52
5.8. Two-laser two-color laser flash photolysis	53
5.9. Effect of xanthone concentration	54
5.10. Effect of SDS concentration on the photoionization.....	55
6. Photoionization of acridine through singlet and triplet channels	59
6.1. Absorption spectra.....	59
6.2. Fluorescence spectra	60

6.3.	Transient absorption spectra.....	61
6.4.	Triplet energy transfer.....	62
6.5.	Photoionization of acridine in alkaline water.....	63
6.5.1.	Simulation study according to results of Kellmann and Tfibel.....	63
6.5.2.	Interpretation of deviations for the triplet state.....	65
6.6.	Photoionization of acridine in alkaline methanol-water mixture.....	66
6.7.	Cyclic photoionization in SDS.....	68
6.8.	Photoionization quantum yields.....	70
7.	Photoionization of monoprotated Proflavine.....	71
7.1.	Absorption and fluorescence spectra.....	71
7.2.	Transient absorption spectra.....	72
7.3.	Photoionization mechanism at 355 nm.....	74
Part II.B	Electron acceptor photoionization.....	79
8.	Photoionization of xanthone/amine systems.....	79
8.1.	Direct generation of xanthone radical anion.....	79
8.2.	Rate constants for xanthone triplet quenching by amine.....	80
8.3.	Back electron transfer.....	82
8.4.	Secondary reaction of the xanthone ground state.....	82
8.5.	Cyclic photoionization of xanthone radical anion in methanol-water solution ...	83
8.6.	Cyclic photoionization of xanthone anion radical in aqueous SDS solution.....	87
8.7.	Combined triplet state and radical anion of xanthone photoionization pathways	88
8.8.	Two-color two-laser flash photolysis of xanthone /amine system.....	91
8.9.	Linear photoinization of X ^{*-} at green light (532 nm).....	95
9.	Summary / Zusammenfassung.....	99
9.1.	Summary.....	99
9.2.	Zusammenfassung.....	104
10.	References.....	109

1. Introduction

Photoionization plays an important role in biological processes [1-7] e.g., light interaction in chloroplasts during photosynthesis [8] and photoionization of dihydronicotinamide adenine dinucleotide (NADH) [9]. Laser excitation of deoxyribonucleic acid, DNA, may produce breaks, either in a single strand or in complementary double strands [10, 11].

Therefore, photoionization of a variety of organic molecules in polar solvents upon visible and UV-laser excitation has been of considerable interest for kinetic and mechanistic studies [12-26]. Photoejection of an electron occurs via different mechanisms, depending on the available photon energy, the excited state properties of the substrate, and the nature of the solvent [27-31]. If the photon energy of the excitation wavelength is greater than the photoionization threshold, a mono-photon electron ejection from the relaxed or unrelaxed lowest excited singlet state is energetically feasible [32-34]. In other words, increasing the excitation photon energy causes a change from a two-photon into a one-photon ionization process with an increase in the photoionization quantum yield [34].

The two-photon ionization is a relatively common process with visible or near-UV light excitation, where the substrate absorbs the first photon to give the excited state which in turn is ionized by the second photon [35-37]. Laser flash photolysis (LFP) with optical detection is widely used to distinguish between mono- and biphotonic ionization. The non-linear behavior of the electron yield upon variation of the laser intensity indicates a biphotonic ionization [38, 39]. More precisely, the electron yield increases linearly with the square of the laser intensity [40, 41].

Real-time observation of a chemical reaction, which constitutes a primary key for understanding reaction mechanisms, still remains a challenge. Laser techniques are not only important for their study, but have also developed into pivotal tools in science and technology, with significant applications in industry, communication, and medicine. One important example is multi-photon spectroscopy [42], where a high-intensity laser with short pulses causes the absorption of two or several photons.

Multilaser flash photolysis can be used to:

- generate new reactive intermediates,
- give more information about photoreaction mechanisms,

- identify the chemical species during the reaction pathway, and
- open up new reaction pathways.

In addition, the selectivity of lasers allows the multilaser method to be applied to biological activities such as photodynamic therapy [43].

Two-laser chemistry has been extensively investigated by various groups [44-51]. Goetz and his group have reported that photoinduced electron transfer between ketones (such as 4-carboxybenzophenone [52] or 1,5-anthraquinonedisulfonate [53]) and donor molecules produces radical anions and radical cations by the first laser (308 nm). The radical anion absorbs a second photon from the second laser excitation (387.5 nm) giving the original ketone as well as the hydrated electron. The use of two-color laser flash photolysis allows the investigation of the reaction pathways of transient intermediates. The first pulse is adjusted to generate the intermediate, which can then be selectively excited by the second pulse at different wavelengths. The observed bleaching of emission or absorption signals resulting from the second laser stems from the excited state that takes part in the photoionization. The lifetime of either both excited states or one of them must be long enough to absorb the second photon. The resulting reactions can be studied in a qualitative and/or quantitative manner.

Laser excitation can be combined with different detection methods [54, 55] to obtain more information about the photoreaction system. The radical ions resulting from electron transfer and photoionization processes can be studied by transient photoconductivity [56], electron paramagnetic resonance (EPR) [57,58], and chemically induced nuclear polarization (CIDNP) [59,60].

In this work, we studied the photoionization mechanisms of some heterocyclic compounds in the presence of a sacrificial electron donor. In addition to the verification of known linear photoionization mechanisms, the main goal of this thesis is to investigate the cyclic photoionization mechanisms which were first observed through our experiments. Our measurements were based on applying the nanosecond laser flash photolysis technique (LFP) with optical detection. We also compared the behaviour of the detectable species resulting from cyclic photoionizations with that in linear photoionizations.

This thesis is organized into two parts. The first part contains a description of the experimental methodology and the theoretical analysis: Chapter 2 describes the nanosecond laser flash photolysis apparatus with optical detection used in our experiments and discusses

the physical properties of the examined substrates (e.g., quantum yield and lifetime of the triplet state). In Chapter 3, we analyse the light intensity dependence of the concentrations of the excited states, radical ions, and electrons. In this analysis, we distinguish between linear and cyclic photoionization mechanisms. The solution of differential equations for the kinetic models usually gives a closed form expression that can be fitted to the experimental data. In some of our measurements, the solution of these kinetic equations was cumbersome and we used a mathematical software package (Mathematica 4.0) to fit the numerical solutions to the experimental data.

The second part comprising Chapters 4 to 8 includes the main results of this thesis on complex cyclic and linear photoionization mechanisms of acridine derivatives and xanthone. Whereas acridine derivatives serve solely as electron donors in our investigations, we used xanthone both as donor and acceptor depending on the experimental conditions. We will show that the high laser intensities open new reaction pathways of photoionization. For instance, the electron yield in the photoionization for an electron donor (e.g., acridone derivatives) in aqueous sodium dodecylsulfate (SDS) micellar solutions exceeds the initial concentration of the substrate due to a cyclic mechanism (Chapter 4). Furthermore, the radical cation produced during the photoionization process exhibits saturation behaviour at high laser intensities while the electron yield increases linearly. These observations are inconsistent with the linear two-photon ionization process reported previously [36-40, 51], where the concentrations of both electron and radical cation must be identical under the same experimental conditions.

Chapter 5 describes the catalytic cyclic photoionization mechanism of xanthone in aqueous SDS micellar solution, while its photoionization in alcohol-water solution proceeds via a linear two-photon ionization process. In order to give a complete description of the effect of SDS concentration on the photoionization mechanism, we compared the electron yield of the photoreaction system in various SDS concentrations as well as in alcohol-water solution i.e., studied the electron yield as a function of the laser intensity in micelle concentration above and below the critical micelle concentration (cmc).

In addition to the cyclic photoionization of the triplet state (in the case of xanthone) or the singlet state only (in case of acridone derivatives), we will also show that the cyclic photoionization of acridine and proflavine proceeds via both singlet and triplet states (Chapters 6 and 7).

In Chapters 5 and 8, we compare the results of two-laser excitation of the examined systems with those obtained from single laser excitation under similar experimental conditions. Chapter 8 is devoted to the cyclic photoionization of an electron acceptor in the presence of an electron donor. We studied the effect of the amines triethylamine (TEA) and 1,4-diazabicyclo[2.2.2]octane (DABCO) on the photoionization of xanthone. The presence of the amine in this system leads to an electron transfer. The photoionization of xanthone/amine systems at high laser intensity is interesting, as the electron yield is much higher than in the absence of amine under the same experimental conditions. Finally, in Chapter 9 summary of the results of this thesis is given.

Part I

Experimental methodology and theoretical analysis

2. Experimental section

2.1. Steady-state measurements

UV-visible absorption spectra were measured using a Shimadzu UV-2102 spectrophotometer. The absorption was measured directly before irradiation and there was no sign of any chemical interaction between the components in their ground states. The absorption spectra of the examined compounds can be compared to known spectra as reported in the literature. In all cases, the Beer-Lambert plots were found to be linear in the measured range of the ground state concentrations. The concentration of the samples for transient absorption measurements was adjusted to give an absorbance less than 0.2 at the excitation wavelengths in the 1-cm optical path length of the cell.

Steady state fluorescence measurements were carried out using a Perkin-Elmer LS50B spectrometer. The fluorescence quantum yields and the fluorescence lifetimes of the examined substances are known.

2.2. Laser flash photolysis

The transient absorption and fluorescence spectra were measured using a laser flash photolysis apparatus with an excimer laser (Lambda Physik LPX-210i, 308 nm, laser pulse duration 60-80 ns, maximum energy approximately 60 mJ per pulse) and/or a Nd:YAG laser (Continuum Surelite II-10; 355 or 532 nm with a pulse width of 6 ns ; the maximum energy was approximately 52 mJ/pulse for 355 nm and 80 mJ/pulse for 532 nm) as the excitation sources. The intensity of excimer laser was varied by using metal-grid filters while the intensity of the Nd:YAG laser was changed by varying the voltage on the flash lamp pumping the laser head. Apart from intensity dependent measurements, the filters were used to suppress second-order reactions, or to minimize the photoionization of the reaction system, when desired. The dimensions of the excited volume were 2 x 4 x 2 mm, and the optical path length of the detection system was 4 mm.

For the two-laser pulse experiments, a home-made delay generator was used. The delay between the pulses could be chosen in the range of a few nanoseconds to several microseconds. The laser pulses passed through the optical cell in a collinear geometry.

The laser flash photolysis setup is shown schematically in Figure 2.1. The dimensions of the laser pulse at the front of the cell were 3 x 4 mm, from which the central part was selected

by an aperture. The laser pulse impinges on the cell at 90° with respect to the monitoring beam and was optimised for homogeneous illumination of the detection volume.

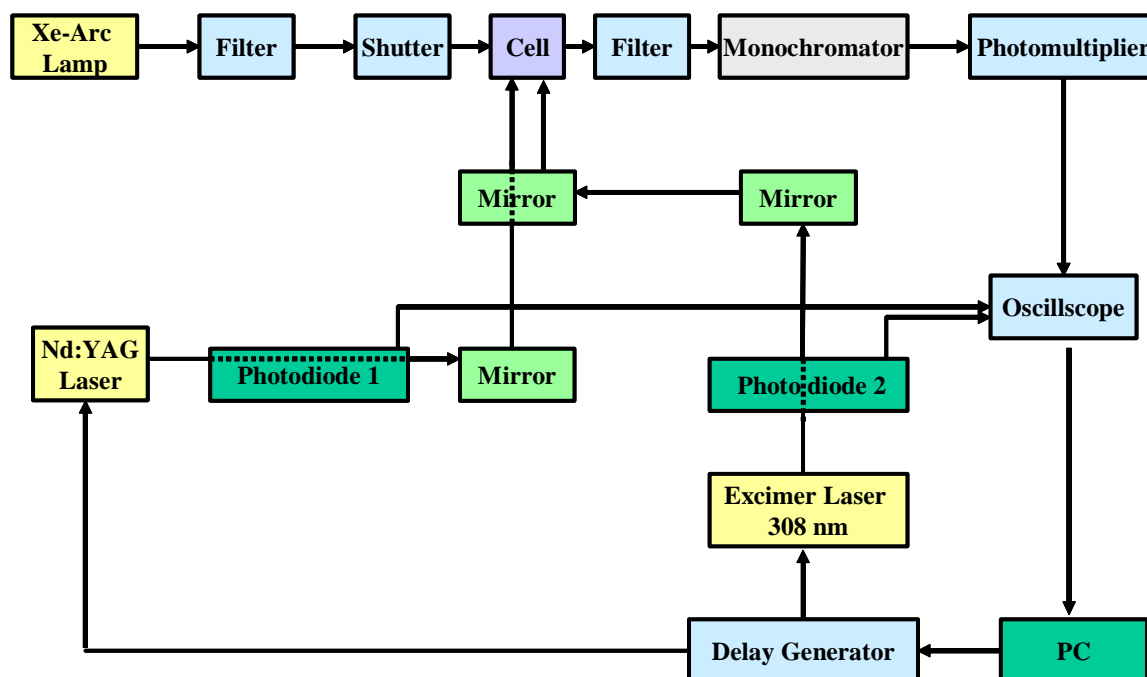


Figure 2.1. Diagram of the experimental setup for nanosecond laser flash photolysis

The detection system measures the change in the photocurrent due to emission or differential absorption of the transient versus time at a selected wavelength. By plotting the intensity of signals versus the monitored wavelength a transient spectrum can be obtained which characterizes this species. A negative absorption by the transient corresponds to a bleaching, where the absorption of the products and/or transients produced in this reaction is smaller than that of the starting materials. The transient spectra obtained under our experimental conditions can be compared to known spectra. Detection of absorbance is done with a high pressure xenon lamp, suitable optical system, filters to suppress the stray light, monochromator, and a photomultiplier with an increased sensitivity in the red (Hamamatsu R 928). The xenon arc lamp for monitoring is used with a shutter to protect the sample from undue photolysis. The shutter was controlled by the PC.

The side-on photomultiplier tube (PMT) is placed at the exit slit of the monochromator, and generates an electrical signal corresponding to the light intensity striking the cathode of the PMT; the photocurrent is amplified in the PMT, controlled by the voltage applied to the dynodes. A digital oscilloscope (Tektronix) is used to convert the PMT output to a digital signal, and to transfer the data to a computer for analysis and storage. The time response of the detection system is 5 ns.

These experiments were generally carried out using a flow system in order to avoid depletion of reactants or accumulation of products. The flow rates were chosen such that each laser shot excited fresh solution, and were maintained during the experiments. Depending on the magnitude of the absorption changes, the transient signals were accumulated at least 64 times in order to obtain a sufficient signal to noise ratio.

The solutions were prepared using ultrapure Millipor MilliQ water (resistance 18.2 M Ω cm⁻¹). Despite its unique properties and obvious biological relevance, one of the major factors that limit the photochemical studies of organic compounds in aqueous solutions is their poor solubility in this medium. Anionic micelles of sodium dodecylsulfate, SDS, can overcome this problem. In all experiments, the micelle concentrations were at least 10 times higher than the substrate concentrations. This ensures that no micelle contains more than one molecule [61, 62]. The micelle concentration [M_s] is given by Equation (2.1)

$$[M_s] = \frac{[S_t] - \text{cmc}}{N_g} \quad \text{Eq. (2.1)}$$

where [S_t], cmc, and N_g are the concentration of SDS, the critical micellar concentration (8 x 10⁻² M [62]), and the aggregation number of SDS (60-62 [62]), respectively.

All experiments were carried out at room temperature in neutral solution or basic solution, where the pH values were adjusted by the addition of NaOH. Simulation fits of the kinetic models were performed by software packages (Origin 6.1 and Mathematica 4.0).

2.3. Materials

Most of the chemicals were obtained commercially in the highest available purity and used without further purification. N-Methylacridone, xanthone, triethylamine, 1,4-diazabicyclo[2.2.2]octane, and benzophenone-4-carboxylate were purchased from Aldrich. Acridone was purchased from Lancaster. Acridine was obtained from Acros. Methylviologen (1,1'-dimethyl-4,4'-bipyridinium chloride) was a Sigma-Aldrich product. Sodium dodecylsulfate was obtained from Sigma. Sodium hydroxide, methanol, and proflavine hemisulfate dihydrate were obtained from Fluka. Xanthone and acridine were crystallized several times from aqueous methanol.

2.4. Determination of triplet-triplet extinction coefficients

2.4.1. Relative actinometry

The extinction coefficient of triplets was determined using the comparative technique [63-66]. This method of determination is valid only if a small fraction of the molecules is excited, so that the absorbance changes remain linear with the laser energy. A substance whose quantum yield (ϕ_T) and extinction coefficient (ε_T) of the triplet state are known is used as the standard, i.e., as an actinometer. In these experiments [67], the concentrations of standard and substance studied are chosen to yield the same optical density at the excitation wavelength. Then, for any given laser energy the number of photons absorbed by each of the two solutions will be identical. Hence, the quantum yield of triplet formation of the substance studied is proportional to the triplet concentration, and Eq. (2.2) can be used to estimate the triplet extinction coefficient of the substance under study, M, or its quantum yield, depending upon which of them is known.

$$\frac{\phi_T^M}{\phi_T^{st}} = \frac{[{}^3M^*]}{[{}^3st^*]} \quad \text{Eq. (2.2)}$$

where ϕ_T^M , $[{}^3M^*]$, ϕ_T^{st} , and $[{}^3st^*]$ are the quantum yield and triplet concentration of the substance under study, quantum yield and triplet concentration of standard substance, respectively. Replacing concentrations with absorbances according to Lambert-Beer's Law in Eq. (2.2) will give

$$\phi_T^M = \phi_T^{st} \frac{E_T^M \cdot \varepsilon_T^{st}}{E_T^{st} \cdot \varepsilon_T^M} \quad \text{Eq. (2.3)}$$

where ε_T^{st} , ε_T^M , E_T^{st} , and E_T^M are the triplet extinction coefficients and the maximum absorbances of the triplet state

2.4.2. Energy transfer

The excited triplet state of the examined substance can be generated by energy transfer from the excited triplet state of a sensitizer [63, 68, 69]. To be an appropriate donor for an energy transfer experiment, its triplet state should be at least 8-5 Kcal/mol higher than that of the acceptor [70]. In this case, the reverse transfer can be neglected. The triplet life of the donor should be long, and the intersystem quantum yield should be relatively high. Its

extinction coefficient, ε_D , should be large at the observation wavelength in order to obtain accurate measurement values.



In this experiment, the solution contains both D and A. Only D should be excited to its singlet state, which converts rapidly to the triplet state which then undergoes triplet-triplet energy transfer. The acceptor molecules should absorb as little as possible of the excitation light, in order to improve the accuracy of the calculations. The decay of the sensitizer triplet will be accompanied by the growth of the transient absorption due to the acceptor triplet. Assuming the two decay pathways of (2.1), and (2.2), for the sensitizer triplet ${}^3D^*$ the efficiency of energy transfer η_{EnT} (i.e., the probability that the triplet donor reacts with acceptor through energy transfer) is

$$\eta_{EnT} = \frac{k_q[A]}{k_q[A] + (\tau_0^D)^{-1}} \quad \text{Eq. (2.4)}$$

where $[A]$ is the acceptor concentration and τ_0^D is the triplet lifetime of the donor in the absence of the acceptor. η_{EnT} approaches unity if $k_q[A] \gg (\tau_0^D)^{-1}$ which shows that $[A]$ should be as high as possible. The concentration of the acceptor triplet formed via energy transfer, is given by Eq. (2.5).

$$[{}^3A^*] = [{}^3D^*] \frac{k_{obs}}{k_{obs} + (\tau_0^D)^{-1}} \quad \text{Eq. (2.5)}$$

where k_{obs} is the decay rate of the donor triplet in the presence of the acceptor [71]. By expressing concentrations in terms of absorptions, one can calculate the triplet extinction coefficient of the examined substance as with Eq. (2.6),

$$\varepsilon_{{}^3A^*} = \frac{E_{{}^3A^*} \varepsilon_{{}^3D^*} k_{obs} + (\tau_0^D)^{-1}}{E_{{}^3D^*} k_{obs}} \quad \text{Eq. (2.6)}$$

where $E_{{}^3D^*}$, $E_{{}^3A^*}$, $\varepsilon_{{}^3D^*}$ and $\varepsilon_{{}^3A^*}$ are the absorptions of donor and acceptor triplet and the extinction coefficients, respectively.

2.5. Determination of extinction coefficients and quantum yields of radical ions

Time-resolved laser flash photolysis permits the direct observation of radical ion intermediates. It is easy to determine the extinction coefficients of radical ions by an electron transfer reaction [72-74], if the extinction coefficient of the other radical ion formed in that process is known. In these experiments, the concentrations of radical cations and radical anions are equal. Therefore, the extinction coefficient of one radical ion can be calculated by application of the Lambert-Beer's Law as in Eq. (2.7),

$$\varepsilon_{M^{\bullet+}} = \frac{E_{M^{\bullet+}} \varepsilon_{A^{\bullet-}}}{E_{A^{\bullet-}}} \quad \text{Eq. (2.7)}$$

where $\varepsilon_{M^{\bullet+}}$, $\varepsilon_{A^{\bullet-}}$, $E_{M^{\bullet+}}$ and $E_{A^{\bullet-}}$ are the radical cation and radical anion extinction coefficients and the maximum absorbances for the radical cation and radical anion, respectively. The absorption of the radical ions should be monitored at the wavelength of their maximum absorptions to give more accurate results.

The quantum yield of the electron transfer can be expressed as in the Eq. (2.8) [75,76]

$$\varphi_{ET} = \varphi_T \cdot \eta_{ET} \quad \text{Eq. (2.8)}$$

where φ_{ET} and φ_T are the quantum yield of electron transfer process and intersystem crossing, respectively. η_{ET} is the efficiency of electron transfer.

2.6. Analysis of triplet state decay kinetics

2.6.1. First-order decay

In dilute solution and in the absence of a quencher, the triplet state ${}^3A^*$ will decay by interaction with solvent molecules. This gives a unimolecular decay rate constant, k_{1st} , according to the following reaction



Since the difference in absorbance of triplet and ground state, $\Delta E({}^3A^*)$, is directly proportional to $[{}^3A^*]$, it follows

$$\Delta E({}^3A^*) = \Delta E_0({}^3A^*) \exp[-k_{1st} t] \quad \text{Eq. (2.9)}$$

where $\Delta E_0({}^3A^*)$ is the initial absorbance difference, i.e., at $t = 0$.

By fitting the experimental absorption decay curve to Eq. (2.9), the rate constant for decay of the excited triplet state, k_{1st} , is obtained.

2.6.2. Self-quenching

For excitation at low laser intensity in the absence of quencher, the excited triplet state will decay according to first-order, but the decay rate increases with an increase of the substrate concentration under the same experimental conditions, i.e., the triplet state can be quenched by the substrate in a pseudo first-order process (Re. (2.4)) [77]. The experimental absorption of the triplet can be fitted as a mono-exponential decay (Eq. (2.10)) with an observed decay rate constant (k_{obs}),



$$\Delta E({}^3A^*) = \Delta E_0({}^3A^*) \exp[-k_{obs} t] \quad \text{Eq. (2.10)}$$

$$\text{where } k_{obs} = k_{1st} + k_{sq} [A] \quad \text{Eq. (2.11)}$$

The rate constant of self-quenching, k_{sq} , can be determined from the slope of a plot of k_{obs} as a function of the substrate concentration. The intercept of this plot yields the intrinsic first-order decay constant k_{1st} .

2.6.3. Triplet-triplet annihilation

At high laser energies, a significant concentration triplet is generated. Their transient absorbance no longer exhibits a mono-exponential decay, and the decay rates are increased by an increase in laser intensity, the reason is that in addition to the described first-order and pseudo first-order deactivation processes, triplet-triplet annihilation occurs [78-82] according to Re. (2.5).



For mixed first- and second-order decay kinetics, Eq. (2.13) is applicable. The decay rate of ${}^3A^*$ is the sum of the individual rates,

$$-\frac{d\Delta E({}^3A^*)}{dt} = (k_{1st} + k_{sq}[A_0])\Delta E({}^3A^*) + \frac{k_{T-T}}{\Delta \varepsilon_\lambda \cdot d} (\Delta E({}^3A^*))^2 \quad \text{Eq. (2.12)}$$

$$\Rightarrow \Delta E({}^3A^*) = \frac{k \Delta E_0({}^3A^*)}{\left\{ k + \frac{k_{T-T}}{\Delta \varepsilon_\lambda \cdot d} \Delta E_0({}^3A^*) \right\} \exp(kt) - \frac{k_{T-T}}{\Delta \varepsilon_\lambda \cdot d} \Delta E_0({}^3A^*)} \quad \text{Eq. (2.13)}$$

where $k = (k_{1st} + k_{sq}[A_0])$ and k_{T-T} is the rate constant of the triplet-triplet annihilation.

If only triplet-triplet annihilation reaction occurs, the decay should follow simple second-order kinetics,

$$[{}^3\text{A}^*] = \frac{[{}^3\text{A}^*]_0}{1 + k_{T-T}[{}^3\text{A}^*]_0 t} \quad \text{Eq. (2.14)}$$

where $[{}^3\text{A}^*]_0$ is the triplet concentration immediately after the end of the laser pulse.

2.7. Determination of electron absorption

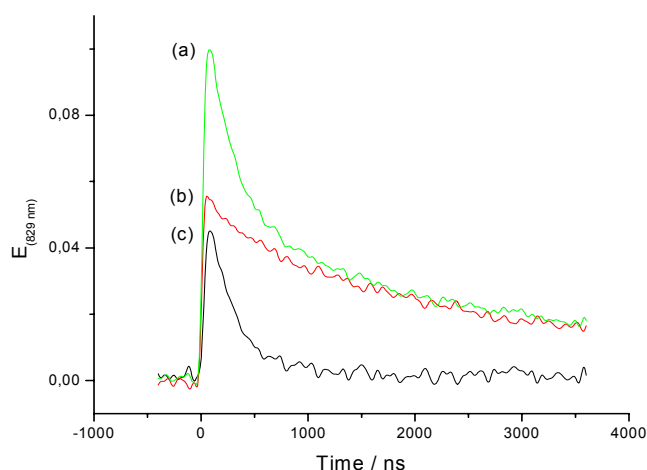
The difference between the absorption signals obtained in argon- and in N_2O -saturated solutions under otherwise identical experimental conditions is taken as the true electron absorption signal as shown in Figure 2.1 (as an example).

Calculation of the concentration of the hydrated electron was carried out using a literature value of $18500 \text{ M}^{-1}\text{cm}^{-1}$ for the molar extinction coefficient at 720 nm in aqueous solution [83]. All measurements based on the study of the electron formation were carried out by measuring its transient absorbance at 830 or 829 nm, because the emission intensities of Xenon lamp at these wavelengths are much higher than that at the absorption maximum of electron (720 nm), i.e., at these wavelengths, the signal/noise ratio is more better than that at 720 nm. The relative extinction coefficients at 720 and 829 (830) nm were determined experimentally. In N_2O -saturated solution, the electron absorption signals are quenched in a few nanoseconds due to Re. (2.6)[83, 84].



When necessary, the hydroxyl radicals produced in Re. (2.6) were removed by adding *tert*-butanol (0.5 M), which reacts with OH^{\bullet} producing a non-reactive radical [85].

Figure 2.1. Kinetic traces recorded at 829 nm of $1.6 \times 10^{-4} \text{ M}$ xanthone in methanol-water (1:2 v/v) following a 308 nm laser pulse (827.7 mJ/cm^2). (a) in argon-saturated solution, (b) in N_2O -saturated solution, and (c) the difference of them.

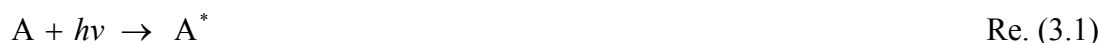


3. Linear and cyclic photoionizations – Analysis of light intensity dependences

Photoionization at high laser intensities can occur by other mechanisms than at low intensities, e.g., with acridone derivatives [86] or the tris-2,2'-bipyridyl ruthenium (II) ion [87, 88], xanthone [89] or benzophenone-4-carboxylate [90] in the presence of the electron donor. This chapter describes different linear and cyclic photoionization mechanisms. We distinguish between these mechanisms kinetically by studying the dependences of the concentrations on the light intensity.

3.1. Kinetic formulation of light absorption

The ground state molecule (A) absorbs a photon to give its excited state (A^{*}) as expressed in Re. (3.1).



The rate, r_i , of conversion of the ground-state molecules into their excited state by light of wavelength λ , depends on the rate $\frac{dI_{abs}}{dt}$ of light absorption by the ground state and on the quantum yield φ_i of the reaction [91]

$$r_i = \frac{-d[A]}{dt} = \varphi_i \frac{dI_{abs}}{dt} \frac{1}{V} \quad \text{Eq. (3.1)}$$

where V is the excited volume. The total intensity I of the exciting light is given by

$$I = \int_0^{\tau} I(t) dt \quad \text{Eq. (3.2)}$$

where τ is the duration of the laser pulse and $I(t)$ is the envelope of the laser pulse.

All solutions in our experiments are optically thin, so all the absorption steps can be treated as first order processes. The Lambert-Beer law can be linearized to give

$$I_{abs} = 2.303 I \varepsilon_{\lambda} [A] d \quad \text{Eq. (3.3)}$$

where ε_{λ} , and d are the extinction coefficient of the substrate at the excitation wavelength and the optical path length of cell. Inserting Eq. (3.3) into (3.1) yields

$$r_i = \frac{2.303 \varphi_i \varepsilon_\lambda}{A} \frac{\lambda}{h c_l N_A} I [\text{A}] \quad \text{Eq. (3.4)}$$

where λ and A are the wavelength of the laser pulse and the irradiated area. N_A , c_l , h are the Avogadro number, speed of the light and Planck's constant.

Therefore, the rate r_i of any photoinduced reaction step is proportional to the concentration of the species that is excited and the light intensity. The associated rate "constant" k_i is time dependent because it depends on $I(t)$,

$$k_i(t) = \kappa_i I(t) \quad \text{Eq. (3.5)}$$

where κ_i is a constant of proportionality. By comparison with Eq. (3.4), the relationship between a kinetic constant κ_i and the quantum yield φ_i of the corresponding process is given by Eq. (3.5) [90].

$$\kappa_i = \frac{2.303 \varphi_i \varepsilon_\lambda}{A} \frac{\lambda}{h c_l N_A} \quad \text{Eq. (3.6)}$$

The constant of proportionality κ_i has the dimension of a reciprocal light intensity, area per energy (cm^2/mJ). It is directly proportional to the pertaining extinction coefficient and quantum yield.

In our calculations, we will assume a rectangular laser pulse i.e.,

$$I(t) = I_{exc} / \tau \quad \text{Eq. (3.7)}$$

where I_{exc} is the total laser intensity. With that solutions of the kinetic equations can be obtained in a closed form and depend only on I_{exc} . Thus the rate constant of a light-driven step can be expressed as a true constant with Eq. (3.8).

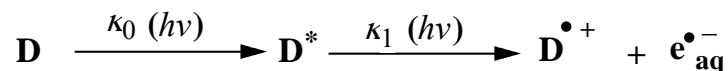
$$k_i = \kappa_i \frac{I_{exc}}{\tau} \quad \text{Eq. (3.8)}$$

3.2. Linear photoionization processes

In this section, we will classify the examined substrates as either an electron donor (D) or an electron acceptor (A), depending on the experimental conditions. D absorbs a photon to generate its excited state (D*) that can be ionized by a further photon. The excited state of an electron acceptor (A*) in the presence of an electron donor (e.g., an amine) is quenched by electron transfer to produce the radical anion (A^{•-}), which can be ionized by a second photon.

3.2.1. Consecutive two-photon ionization

In this process [92-94], the molecule is excited to give D^* by the absorption of one photon with rate constant $\kappa_0 I(t)$. Absorption of the second photon by D^* results in formation of an electron and the radical cation ($D^{\bullet+}$) with rate constant $\kappa_1 I(t)$. The mechanism of that ionization is depicted in Scheme 3.1, which consists of the sequence of two first-order reactions by which the excited state builds up and decays.



Scheme 3.1

The solution of the differential rate equations of this scheme is given by Eqs. (3.9) and (3.10).

$$\frac{[D^*]}{c_0} = \frac{\kappa_0}{\kappa_1 - \kappa_0} \{ \exp(-\kappa_0 I_{\text{exc}}) - \exp(-\kappa_1 I_{\text{exc}}) \} \quad \text{Eq. (3.9)}$$

$$\frac{[e_{\text{aq}}^{\bullet-}]}{c_0} = \frac{[D^{\bullet+}]}{c_0} = 1 - \frac{\kappa_1}{\kappa_1 - \kappa_0} \exp(-\kappa_0 I_{\text{exc}}) - \frac{\kappa_0}{\kappa_1 - \kappa_0} \exp(-\kappa_1 I_{\text{exc}}) \quad \text{Eq. (3.10)}$$

The kinetic constant κ_0 of formation of the excited state can be directly calculated using Eq. (3.6), because the absorption quantum yield is usually equal to unity and the extinction coefficient of the substrate ($\varepsilon_{\text{ground}}$) at the excitation wavelength can be determined experimentally. The kinetic constant κ_1 for photoionization of the excited state could be calculated in the same way, if the extinction coefficient of the excited state, $\varepsilon_{\text{excited}}$, at the excitation wavelength and the quantum yield of photoionization were known. Experimentally, κ_1 is obtained by fitting Eqs. (3.9) and (3.10) to the experimental data. Equation (3.10) shows that the concentrations of both electron and radical cation are identical. Therefore, the measurement of either concentration suffices. The electron curves are identical when κ_0 and κ_1 are interchanged, as shown in Figure 3.1. Also, the form of the curves for D^* remains the same, so they only way to determine which constant is the larger of the two is by measuring the absolute concentrations of D^* .

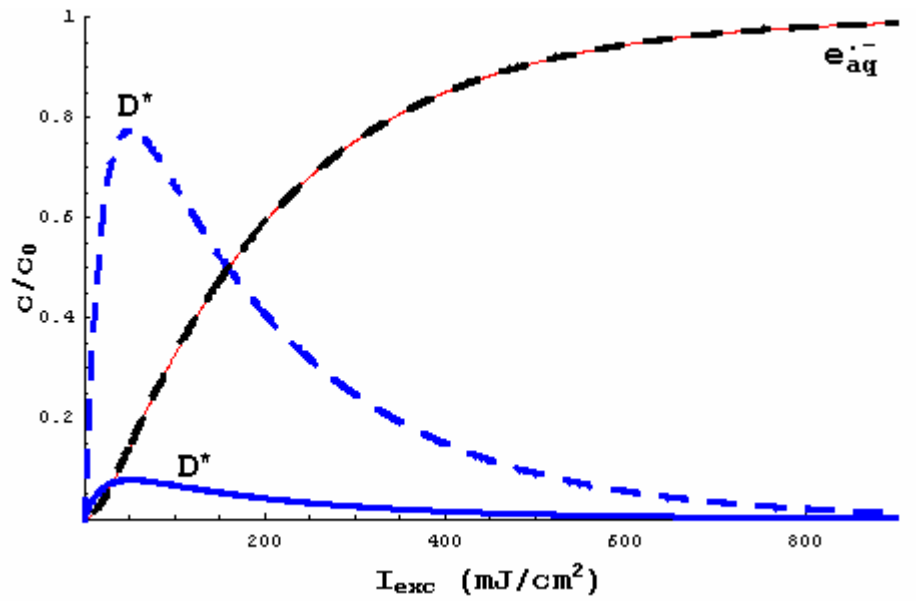


Figure 3.1. Concentrations c of the excited state (D^*), and the electron (e^*_{aq}) relative to the substrate concentration c_0 as functions of the laser intensity I_{exc} for consecutive two-photon ionization. The curves were simulated with Eqs. (3.9) and (3.10). The parameters of simulation were $\kappa_0=0.05 \text{ cm}^2/\text{mJ}$, $\kappa_1=0.005 \text{ cm}^2/\text{mJ}$, solid lines; $\kappa_0=0.005 \text{ cm}^2/\text{mJ}$, $\kappa_1=0.05 \text{ cm}^2/\text{mJ}$, dashed lines. The electron curves are identical in these two cases.

At low laser intensity, the electron curve shows what is called an induction period in a kinetic plot (Figure 3.1), because electron formation requires the formation of an intermediate first. Therefore, in order to distinguish between mono- and biphotonic processes, the laser intensity dependence of the electron yields should be measured at low laser intensities. However, more reliable information is obtained from the concentration of the intermediate at high intensities.

For the special case $\kappa_0 = \kappa_1$, the intensity dependences of the concentrations are given by Eqs. (3.11) and (3.12) for Scheme 3.1.

$$\frac{[D^*]}{c_0} = \kappa_0 I_{exc} \exp(-\kappa_0 I_{exc}) \quad \text{Eq. (3.11)}$$

$$\frac{[e^*_{aq}]}{c_0} = \frac{[D^*]}{c_0} = 1 - \exp(-\kappa_0 I_{exc})(1 + \kappa_0 I_{exc}) \quad \text{Eq. (3.12)}$$

The actual light intensity experienced is affected by D or D^* , other absorbing species (i.e., by an inner filter effect) or re-absorption of emitted radiation, especially when a substance exhibits a high fluorescence quantum yield. When κ_0 is treated as an adjustable parameter in a fit to the experimental data, the best-fit value of κ_0 may be different from the

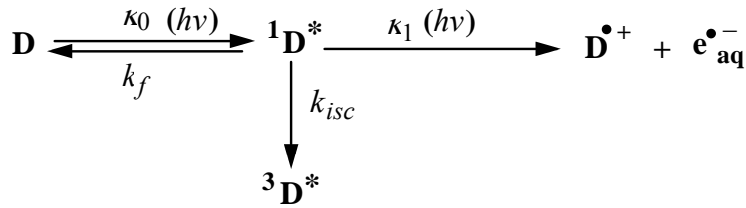
calculated value because of these effects. However, Eq. (3.6) can be used as chemical actinometer for all light-driven steps [90]. Assuming that the quantum yield of excitation of the ground state is unity, the quantum yield of ionization (φ_{ion}) in Scheme 3.1 can be calculated from Eq. (3.13).

$$\varphi_{\text{ion}} = \frac{\kappa_1 \varepsilon_{\text{ground}}}{\kappa_0 \varepsilon_{\text{excited}}} \quad \text{Eq. (3.13)}$$

Also, Eq. (3.6) can be used to obtain the ratio of the quantum yield of photoionization for the same system at different excitation wavelengths as represented in Eq. (3.14)

$$\frac{\varphi_{\text{ion},\lambda_1}}{\varphi_{\text{ion},\lambda_2}} = \frac{(\kappa_1 / \kappa_0)_{\lambda_1} \varepsilon_{\lambda_1(\text{ground})} \varepsilon_{\lambda_2(\text{excited})}}{(\kappa_1 / \kappa_0)_{\lambda_2} \varepsilon_{\lambda_2(\text{ground})} \varepsilon_{\lambda_1(\text{excited})}} \quad \text{Eq. (3.14)}$$

The described two-photon ionization process may be accompanied by deactivation processes of the excited singlet state such as fluorescence emission and triplet state formation ($^3\text{D}^*$) with rate constants k_f and k_{isc} , respectively. The appropriate modification of Scheme 3.1 is shown in Scheme 3.2.



Scheme 3. 2

The laser intensity dependence based on Scheme 3.2 for the singlet and electron concentrations are given by Eqs. (3.15) and (3.16), respectively.

$$\frac{[^1\text{D}^*]}{c_0} = \frac{\kappa_0}{(\kappa_a - \kappa_b)} (\exp(-\kappa_b I_{\text{exc}}) - \exp(-\kappa_a I_{\text{exc}})) \quad \text{Eq.(3. 15)}$$

$$\frac{[e^{\bullet-}_{\text{aq}}]}{c_0} = \frac{\kappa_0 \kappa_1}{\kappa_a \kappa_b} \left(1 - \frac{\kappa_a \exp(-\kappa_b I_{\text{exc}})}{(\kappa_a - \kappa_b)} + \frac{\kappa_b \exp(-\kappa_a I_{\text{exc}})}{(\kappa_a - \kappa_b)} \right) \quad \text{Eq. (3.16)}$$

$$\text{where } \kappa_{a,b} = \frac{1}{2} \left(\kappa_0 + \kappa_1 + \frac{k_f \tau}{I_{\text{exc}}} + \frac{k_{\text{isc}} \tau}{I_{\text{exc}}} \pm \sqrt{(\kappa_0 + \kappa_1 + k_f \frac{\tau}{I_{\text{exc}}} + k_{\text{isc}} \frac{\tau}{I_{\text{exc}}})^2 - 4(\kappa_0 \kappa_1 + \kappa_0 k_{\text{isc}} \frac{\tau}{I_{\text{exc}}})} \right)$$

$$\text{Eq. (3.17)}$$

The functional forms of Eqs. (3.15)-(3.16) and (3.9)-(3.10) are identical ($\kappa_0 \leftrightarrow \kappa_b$, $\kappa_1 \leftrightarrow \kappa_a$), only the leading constant factors are slightly different. The concentration of the excited triplet state is

$$\frac{[{}^3\text{D}^*]}{c_0} = \frac{\kappa_0 k_{isc} \tau / I_{exc}}{\kappa_a \kappa_b} \left(1 - \frac{\kappa_a \exp(-\kappa_b I_{exc})}{(\kappa_a - \kappa_b)} + \frac{\kappa_b \exp(-\kappa_a I_{exc})}{(\kappa_a - \kappa_b)} \right) = \frac{[e^{\bullet-}_{aq}]}{c_0} \frac{k_{isc} \tau / I_{exc}}{\kappa_1} \quad \text{Eq. (3.18)}$$

The term $k_{isc} [{}^1\text{D}^*]$ can be omitted from the differential rate equations that represent Scheme 3.2, when the fluorescence quantum yield is unity. The solutions of the kinetic equations in that case give the same functional form for the singlet and the electron as in Eqs. (3.15) and (3.16), but with

$$\kappa_{a,b} = \frac{1}{2} \left(\kappa_0 + \kappa_1 + \frac{k_f \tau}{I_{exc}} \pm \sqrt{(\kappa_0 + \kappa_1 + \frac{k_f \tau}{I_{exc}})^2 - 4\kappa_0 \kappa_1} \right) \quad \text{Eq. (3.19)}$$

At low intensity ($\kappa_a I_{exc}$, $\kappa_b I_{exc} \ll 1$), the intensity dependences can be approximated by Eqs (3.20) and (3.21).

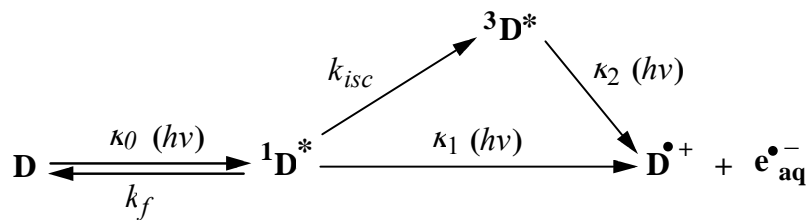
$$\frac{[{}^1\text{D}^*]}{c_0} = \kappa_0 I_{exc} \quad \text{Eq. (3.20)}$$

$$\frac{[e^{\bullet-}_{aq}]}{c_0} = \frac{\kappa_b \kappa_a}{2} I_{exc}^2 \quad \text{Eq. (3.21)}$$

Eq. (3.20) shows that the concentration of the excited singlet state increases linearly with increasing the laser intensity, while Eq. (3.21) shows that the electron concentration increases linearly with the square of the laser intensity.

3.2.2. Parallel photoionization of excited singlet and triplet states

Scheme 3.3 represents that process



Scheme 3.3

The differential rate equations for each species are

$$\frac{d[D]}{dt} = -\kappa_0 I(t)[D] + (k_f)[{}^1D^*] \quad \text{Eq. (3.22)}$$

$$\frac{d[{}^1D^*]}{dt} = \kappa_0 I(t)[D] - (k_f + k_{isc} + \kappa_1 I(t))[{}^1D^*] \quad \text{Eq. (3.23)}$$

$$\frac{d[{}^3D^*]}{dt} = k_{isc}[{}^1D^*] - \kappa_2 I(t)[{}^3D^*] \quad \text{Eq. (3.24)}$$

$$\frac{d[e^{\bullet-}_{aq}]}{dt} = \frac{d[D^{\bullet+}]}{dt} = \kappa_1 I(t)[{}^1D^*] + \kappa_2 I(t)[{}^3D^*] \quad \text{Eq. (3.25)}$$

These equations can be solved by the method of partial fractions. The result for the excited singlet state has already been shown in Eq. (3.15). The solution for the other species are

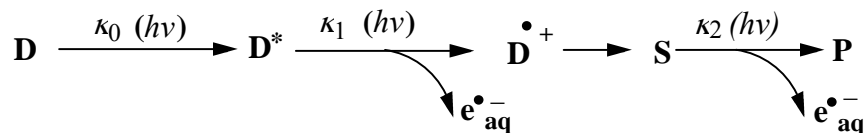
$$\frac{[{}^3D^*]}{c_0} = \frac{\kappa_0 k_{isc} \tau / I_{exc}}{(\kappa_a - \kappa_b)} \left(\frac{(\kappa_a - \kappa_b) \exp(-\kappa_2 I_{exc})}{(\kappa_2 - \kappa_a)(\kappa_2 - \kappa_b)} - \frac{\exp(-\kappa_b I_{exc})}{(\kappa_b - \kappa_2)} + \frac{\exp(-\kappa_a I_{exc})}{(\kappa_a - \kappa_2)} \right) \quad \text{Eq. (3.26)}$$

$$\frac{[e^{\bullet-}_{aq}]}{[c_0]} = \frac{[D^{\bullet+}]}{[c_0]} = 1 - \frac{(\kappa_2 \kappa_a - \kappa_0 \kappa_1) \exp(-\kappa_b I_{ex})}{(\kappa_a - \kappa_b)(\kappa_2 - \kappa_b)} - \frac{\kappa_0 k_{isc} \tau / I_{exc} \exp(-\kappa_2 I_{ex})}{(\kappa_2 - \kappa_a)(\kappa_2 - \kappa_b)} + \frac{(\kappa_2 \kappa_b - \kappa_0 \kappa_1) \exp(-\kappa_a I_{ex})}{(\kappa_a - \kappa_b)(\kappa_2 - \kappa_a)} \quad \text{Eq. (3.27)}$$

where $\kappa_{a, b}$ are given by Equation (3.18). If κ_2 becomes zero, Eq. (3.27) reduces to Eq. (3.16) because $\kappa_0 (\kappa_1 + \kappa_{isc} \tau / I_{exc}) / \kappa_a \kappa_b$ reduces to unity under our conditions.

3.2.3. Stepwise photoionization via a three-photon process

Goez and Zubarev have described the following photoionization [95] with an intervening chemical step that produces a second photoionizable intermediate S.



Scheme 3.4

To simplify the kinetic model, the formation of S is assumed to be fast on the time scale of the laser pulse, so $\kappa_1 I(t)$ can be regarded as the rate constant of the formation of the radical

species (S). Therefore, D^{*+} can be omitted from the kinetic model. The concentration of each species relative to the initial substrate concentration, c_0 is given by

$$\frac{[S]}{[c_0]} = \frac{\kappa_0 \kappa_1 \exp(-\kappa_2 I_{ex})}{(\kappa_0 - \kappa_2)(\kappa_1 - \kappa_2)} + \frac{\kappa_0 \kappa_1 \exp(-\kappa_0 I_{ex})}{(\kappa_0 - \kappa_1)(\kappa_0 - \kappa_2)} - \frac{\kappa_0 \kappa_1 \exp(-\kappa_1 I_{ex})}{(\kappa_0 - \kappa_1)(\kappa_1 - \kappa_2)} \quad \text{Eq.(3.28)}$$

$$\frac{[e_{aq}^{\bullet-}]}{[c_0]} = 2 - \frac{\kappa_0 \kappa_1 \exp(-\kappa_2 I_{ex})}{(\kappa_0 - \kappa_2)(\kappa_1 - \kappa_2)} + \frac{\kappa_1(\kappa_0 - 2\kappa_2) \exp(-\kappa_0 I_{ex})}{(\kappa_0 - \kappa_1)(\kappa_0 - \kappa_2)} - \frac{\kappa_0(\kappa_1 - 2\kappa_2) \exp(-\kappa_1 I_{ex})}{(\kappa_0 - \kappa_1)(\kappa_1 - \kappa_2)} \quad \text{Eq.(3.29)}$$

$$\frac{[P]}{[c_0]} = 1 + \frac{\kappa_0 \kappa_2 \exp(-\kappa_1 I_{ex})}{(\kappa_0 - \kappa_1)(\kappa_1 - \kappa_2)} - \frac{\kappa_0 \kappa_1 \exp(-\kappa_2 I_{ex})}{(\kappa_0 - \kappa_2)(\kappa_1 - \kappa_2)} - \frac{\kappa_2 \kappa_1 \exp(-\kappa_0 I_{ex})}{(\kappa_0 - \kappa_1)(\kappa_0 - \kappa_2)} \quad \text{Eq. (3.30)}$$

For D^* , Eq. (3.9) holds.

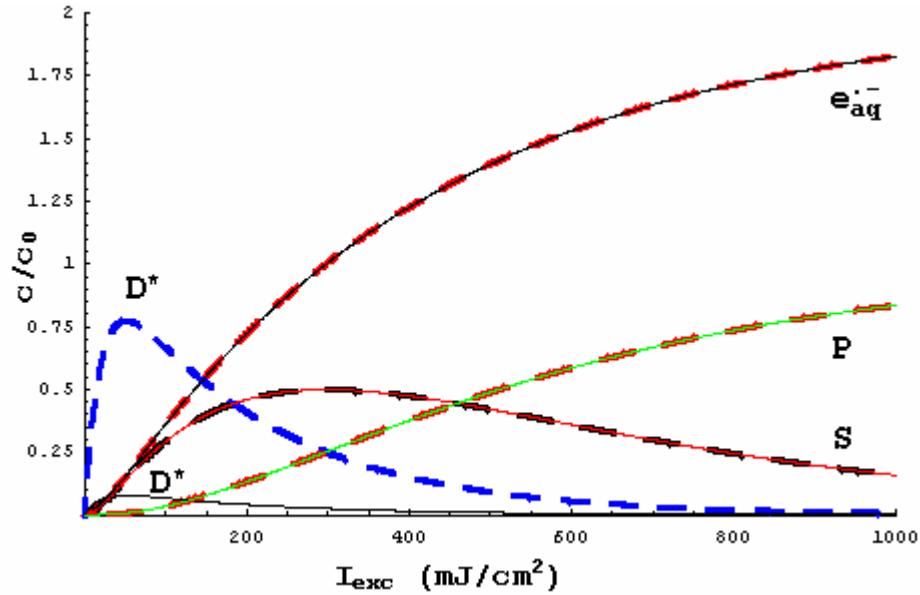


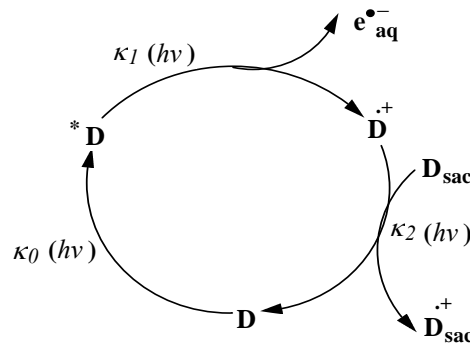
Figure 3.2. Concentrations c of excited state (D^*), intermediate (S), hydrated electron ($e_{aq}^{\bullet-}$) and photoproduct (P) relative to the substrate concentration c_0 as functions of the laser intensity for Scheme 3.4. The curves were calculated with Eqs. (3.9) and (3.28)-(3.30). The parameters of the simulation were: $\kappa_0=0.05 \text{ cm}^2/\text{mJ}$, $\kappa_1 = 0.005 \text{ cm}^2/\text{mJ}$, $\kappa_2 = 0.0025 \text{ cm}^2/\text{mJ}$, (solid lines). $\kappa_0=0.005 \text{ cm}^2/\text{mJ}$, $\kappa_1 = 0.05 \text{ cm}^2/\text{mJ}$, $\kappa_2 = 0.0025 \text{ cm}^2/\text{mJ}$ (dashed lines). The electron curves remain identical when κ_0 and κ_1 were interchanged.

Again, the electron curves cannot help to discriminate between κ_1 and κ_0 parameters as illustrated in Figure 3.2. The electron curves are identical if κ_0 and κ_1 are interchanged, while this interchange has an effect on the curve for the excited state as shown in Figure 3.2.

3.3. Cyclic mechanisms of electron donor photoionizations

3.3.1. Singlet or triplet state undergoes photoionization

We have recently reported [86] that the irradiation of an electron donor D in the presence of a sacrificial electron donor D_{sac} can produce electrons by the catalytic cycle mechanism shown in Scheme 3.5. The radical cation ($D^{\bullet+}$) resulting from the ionization process plays a key role for the reaction mechanism, because it absorbs a third photon and is then reduced by the sacrificial donor (e.g., SDS) to regenerate the ground-state molecule.



Scheme 3.5

The solutions of the corresponding system of differential equations are given by Eqs. (3.31)-(3.33).

$$\frac{[D^*]}{c_0} = \frac{\kappa_0 \kappa_2}{\kappa_a \kappa_b} \left(1 - \frac{\kappa_b (\kappa_a - \kappa_2)}{\kappa_2 (\kappa_a - \kappa_b)} \exp(-\kappa_a I_{\text{exc}}) + \frac{\kappa_a (\kappa_b - \kappa_2)}{\kappa_2 (\kappa_a - \kappa_b)} \exp(-\kappa_b I_{\text{exc}}) \right) \quad \text{Eq. (3.31)}$$

$$\frac{[D^{\bullet+}]}{c_0} = \frac{\kappa_0 \kappa_1}{\kappa_a \kappa_b} \left(1 + \frac{\kappa_b}{(\kappa_a - \kappa_b)} \exp(-\kappa_a I_{\text{exc}}) - \frac{\kappa_a}{(\kappa_a - \kappa_b)} \exp(-\kappa_b I_{\text{exc}}) \right) \quad \text{Eq. (3.32)}$$

$$\frac{[e^{-}_{\text{aq}}]}{c_0} = \frac{\kappa_0 \kappa_1}{\kappa_a \kappa_b} \left(1 + \frac{\kappa_b (\kappa_a - \kappa_2)}{\kappa_a (\kappa_a - \kappa_b)} \exp(-\kappa_a I_{\text{exc}}) - \frac{\kappa_a (\kappa_b - \kappa_2)}{\kappa_b (\kappa_a - \kappa_b)} \exp(-\kappa_b I_{\text{exc}}) - \frac{\kappa_2 (\kappa_a + \kappa_b)}{\kappa_b \kappa_a} + \kappa_2 I_{\text{exc}} \right) \quad \text{Eq. (3.33)}$$

where

$$\kappa_{a,b} = \frac{1}{2} \left(\kappa_0 + \kappa_1 + \kappa_2 \pm \sqrt{(\kappa_0 + \kappa_1 + \kappa_2)^2 - 4(\kappa_0 \kappa_1 + \kappa_0 \kappa_2 + \kappa_1 \kappa_2)} \right) \quad \text{Eq. (3.34)}$$

If κ_2 becomes zero, Scheme 3.5 is transformed into a consecutive two-photon ionization (Scheme 3.1).

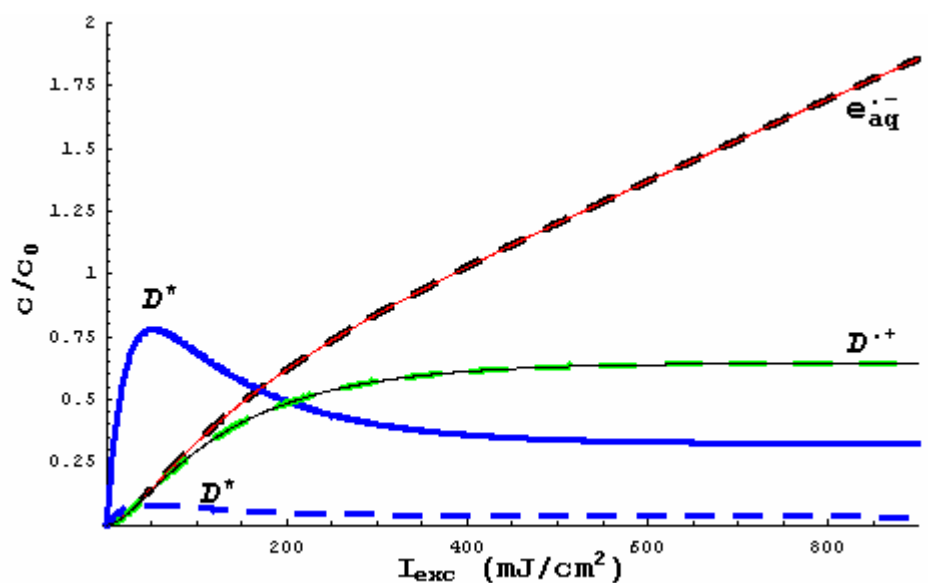


Figure 3.3. Concentrations c of excited state (D^*), electron (e_{aq}^-) and photoproduct ($D^{*\cdot+}$) relative to the substrate concentration c_0 as functions of the laser intensity for the cyclic mechanism of Scheme 3.5. The curves were simulated with Eqs. (3.31)–(3.33). The parameters of the simulations were: $\kappa_0=0.05 \text{ cm}^2/\text{mJ}$, $\kappa_1 = 0.005 \text{ cm}^2/\text{mJ}$, $\kappa_2 = 0.0025 \text{ cm}^2/\text{mJ}$ (solid lines). $\kappa_0=0.005 \text{ cm}^2/\text{mJ}$, $\kappa_1 = 0.05 \text{ cm}^2/\text{mJ}$, $\kappa_2 = 0.0025 \text{ cm}^2/\text{mJ}$ (dashed lines). Both the electron and the radical cation curves remain unchanged when κ_0 and κ_1 are interchanged.

At low laser intensity, the concentrations of the electron and the radical cation are equal, but at high intensities, the electron concentration is always higher. The concentrations both of the excited state and of the radical cation reach a stationary value between zero and c_0 at high intensities while the electron curve increases without bounds and eventually surpasses the initial concentration of the substrate. As opposed to a linear mechanism, the behaviour of the electron curve is thus quite different from that of the radical cation.

As Figure 3.3 shows the concentration of the excited state increases linearly at first before reaching a peak, followed by a gradual decrease towards the steady state. The linear increase indicates that the formation of the excited state is a monophotonic process as expected, and the latter observation provides reliable evidence that regeneration of the excited state occurs through a cyclic reaction.

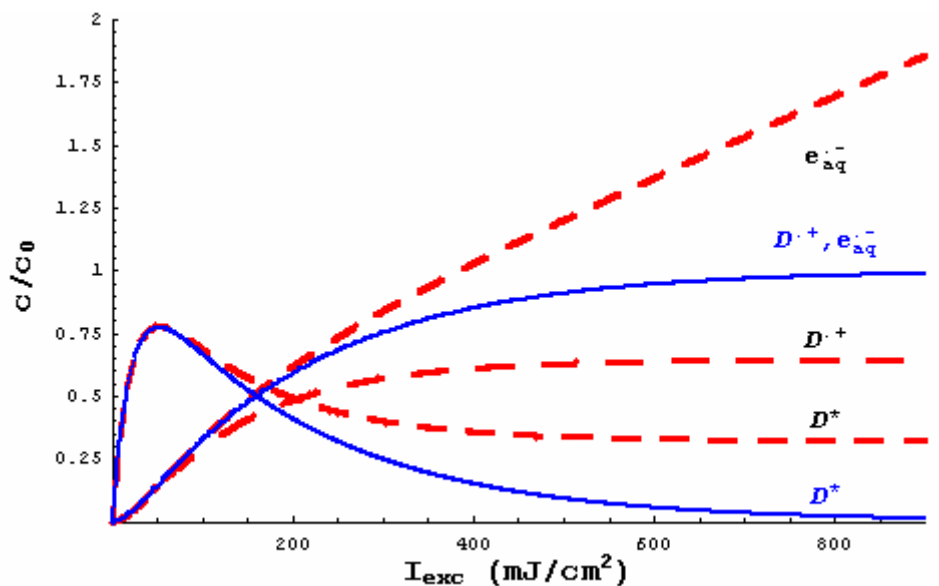
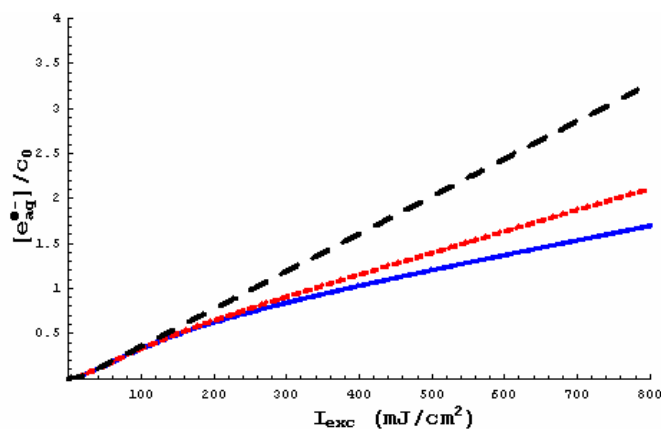


Figure 3.4. Concentration c of the species in Schemes 3.5 and 3.1 relative to the substrate concentration c_0 as functions of the laser intensity. The curves were calculated with Eqs. (3.9)-(3.10) and (3.31)-(3.33). Solid lines: cyclic; $\kappa_0=0.05 \text{ cm}^2/mJ$, $\kappa_1 = 0.005 \text{ cm}^2/mJ$, $\kappa_2=0.0025 \text{ cm}^2/mJ$; dashed lines: consecutive two-photon ionization, $\kappa_0=0.05 \text{ cm}^2/mJ$, $\kappa_1 = 0.005 \text{ cm}^2/mJ$.

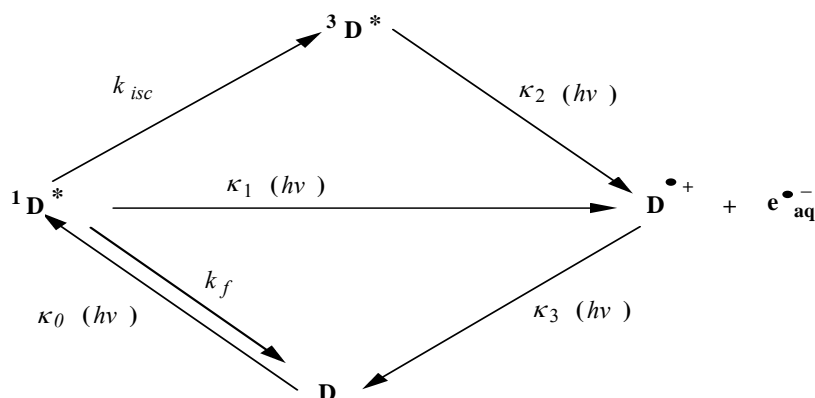
Figure 3.4 displays the behaviour of all species for the cyclic reaction on the one hand, and the consecutive two-photon photoionization process on the other. At low light intensity, a differentiation between the two mechanisms is impossible. However, that differentiation is easy at high light intensity, where the concentration of the excited state approaches a steady state value in the cyclic reaction, but approaches zero in the linear reaction, and where the electron concentration increases linearly in the former but reaches c_0 in the latter reaction. The dependence of the electron curve on κ_2 is shown in more detail in Figure 3.5.

Figure 3.5. The electron concentration relative to the substrate concentration c_0 as functions of the laser intensity. The curves were simulated with Eq (3.33). The kinetic parameters of the simulation were: $\kappa_0=0.05 \text{ cm}^2/mJ$, $\kappa_1 = 0.005 \text{ cm}^2/mJ$ (all curves); $\kappa_2=0.0025 \text{ cm}^2/mJ$ (solid line); $\kappa_2=0.005 \text{ cm}^2/mJ$ (short dashed line); $\kappa_2=0.05 \text{ cm}^2/mJ$ (long dashed line).



3.3.2. Both singlet and triplet states undergo photoionization

The cyclic mechanism of a donor in the presence of a sacrificial donor for ionization of both excited singlet and triplet states is displayed in Scheme 3.6. The rate constants for both ionization steps are $\kappa_1 I(t)$ and $\kappa_2 I(t)$. The radical cation absorbs a photon to regenerate the substrate by a reaction with a sacrificial donor with rate constant $\kappa_3 I(t)$.



Scheme 3.6

The kinetic are described by Eqs (3.35)–(3.39):

$$\frac{d[D]}{dt} = -\kappa_0 I(t)[D] + k_f [{}^1D^*] + \kappa_3 I(t)[D^{\bullet+}] \quad \text{Eq. (3.35)}$$

$$\frac{d[{}^1D^*]}{dt} = \kappa_0 I(t)[D] - (\kappa_1 I(t) + k_f + k_{isc})[{}^1D^*] \quad \text{Eq. (3.36)}$$

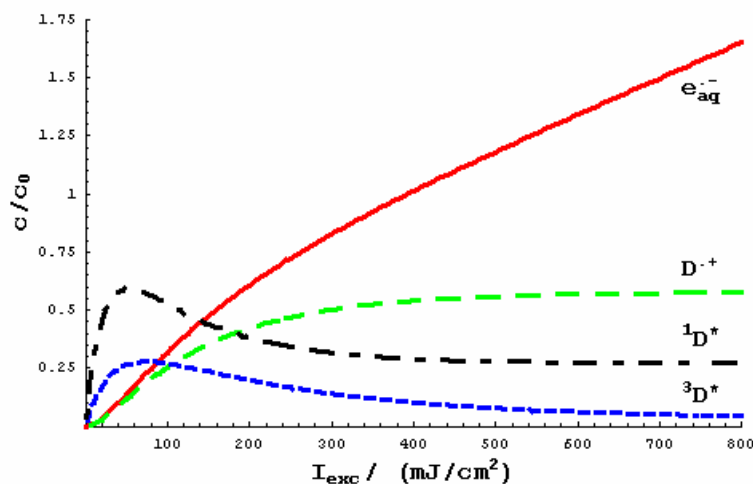
$$\frac{d[{}^3D^*]}{dt} = k_{isc}[{}^1D^*] - \kappa_2 I(t)[{}^3D^*] \quad \text{Eq. (3.37)}$$

$$\frac{d[e^{\bullet-}_{aq}]}{dt} = \kappa_1 I(t)[{}^1D^*] + \kappa_2 I(t)[{}^3D^*] \quad \text{Eq. (3.38)}$$

$$\frac{d[D^{\bullet+}]}{dt} = \kappa_1 I(t)[{}^1D^*] + \kappa_2 I(t)[{}^3D^*] - \kappa_3 I(t)[D^{\bullet+}] \quad \text{Eq. (3.39)}$$

Closed-form solutions of these equations are cumbersome because they contain the roots of a cubic equation, so it is better to solve them numerically. An example is shown in Figure 3.6.

Figure 3.6. Numerical simulation of the laser intensity dependence of the concentrations c relative to the initial concentration of substrate c_0 on the basis of Scheme 3.6 with rate constants $\kappa_0 = 0.05 \text{ cm}^2/\text{mJ}$, $\kappa_1 = 0.005 \text{ cm}^2/\text{mJ}$, $\kappa_2 = 0.005 \text{ cm}^2/\text{mJ}$, $\kappa_3 = 0.0025 \text{ cm}^2/\text{mJ}$, and $k_{isc} = k_f = 5 \times 10^7 \text{ s}^{-1}$, $t = 6 \text{ ns}$.



Qualitatively, $^1\text{D}^*$, $\text{D}^{\bullet+}$ and $e_{\text{aq}}^{\bullet-}$ are seen to behave very similar to $^1\text{D}^*$, $\text{D}^{\bullet+}$ and $e_{\text{aq}}^{\bullet-}$ in Scheme 3.5. In addition, the curves for $^1\text{D}^*$ and $^3\text{D}^*$ in Figure 3.6 have a similar shape.

3.4. Cyclic mechanisms of electron acceptor photoionizations

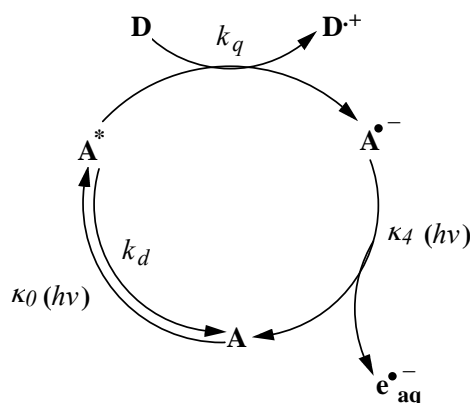
Photoinduced electron transfer from electron donors, such as amines to aromatic ketones in polar solvents produces the radical anion of the ketone and the radical cation of the electron donor [96-100]. Recent studies have revealed that the photoreaction of certain aromatic ketone/amine systems yield electrons, in a concentration that surpasses the initial concentration of the ketone at high laser intensity. Goetz and Zubarev [90] were able to show that the electron concentration as a function of the laser intensity is strongly dependent on the quenching process and the rate constant of excited state formation. If the rate constant of excited state formation is much larger than the rate constant of the quenching process, the electron behaviour exhibits saturation at high laser intensity whereas the electron curve increases linearly when the quenching process is faster than excited state formation.

Scheme 3.7 summarizes the mechanism. The excited state A^* is quenched by electron transfer from the electron donor (D) in its ground state with rate constant k_q to produce its radical anion ($\text{A}^{\bullet-}$) and the radical cation ($\text{D}^{\bullet+}$). The radical anion absorbs a second photon to give an electron and regenerates the substrate with the rate constant $\kappa_4 I(t)$. Radiationless decay of the excited state (k_d) is too slow to compete with the quenching, so it can be neglected. Because of the very low concentration of the substrate A, the small path length of

the reaction cell, and the high concentration of quencher the light dependent steps are first or pseudo-first-order reactions. By using the mass balance, the rate equations are found to be

$$\frac{d[A^*]}{dt} = \kappa_0 I(t)[c_0] - (\kappa_0 I(t) + k_q)[A^*] - \kappa_0 I(t)[A^{\bullet-}] \quad \text{Eq. (3.40)}$$

$$\frac{d[A^{\bullet-}]}{dt} = k_q[A^*] - \kappa_4 I(t)[A^{\bullet-}] \quad \text{Eq. (3.41)}$$



Scheme 3.7

The concentration of the electron can be calculated by the integration of the radical anion concentration over the effective laser pulse width (τ) after multiplication with the rate constant of electron formation ($\kappa_4 I(t)$).

$$[e^{\bullet-}_{aq}] = \int_0^{\tau} \kappa_4 I(t)[A^{\bullet-}] \quad \text{Eq. (3.42)}$$

The efficiency of electron transfer increases with the increase of the quencher concentration, approaching unity. At high quencher concentration, intermediacy of the excited state can be neglected. Thus, the rate of radical anion formation is given by Eq. (3.43).

$$\frac{d[A^{\bullet-}]}{dt} = \kappa_0 I(t)[c_0] - (\kappa_0 + \kappa_4) I(t)[A^{\bullet-}] \quad \text{Eq. (3.43)}$$

Solving Eq. (3.43) gives

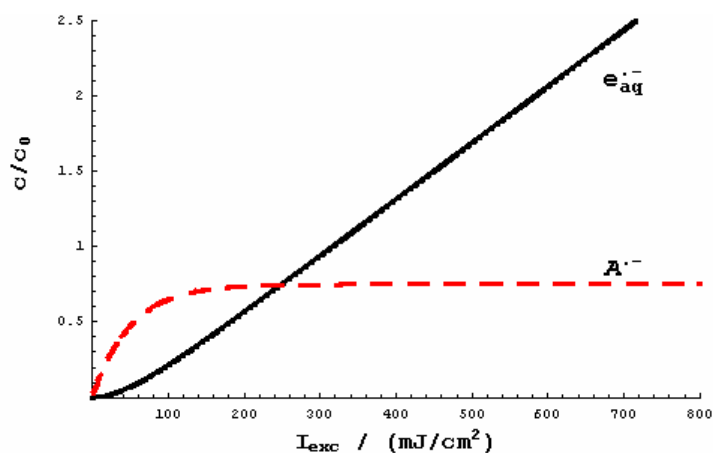
$$\frac{[A^{\bullet-}]}{[c_0]} = \frac{\kappa_0}{\kappa_0 + \kappa_4} (1 - \exp[-(\kappa_0 + \kappa_4) I_{exc}]) \quad \text{Eq. (3.44)}$$

and by integration, one obtains the concentration of the electron

$$\frac{[e^{\bullet-}_{aq}]}{[c_0]} = \frac{\kappa_0 \kappa_4}{(\kappa_0 + \kappa_4)^2} \left(\exp[-(\kappa_0 + \kappa_4) I_{exc}] + (\kappa_0 + \kappa_4) I_{exc} - 1 \right) \quad \text{Eq. (3.45)}$$

Figure 3.7 represents the behaviour of both electron and anion radical curves for fast quenching. In that case, the electron concentration increases linearly with increasing laser intensity, while the radical anion exhibits a saturation behaviour at high laser intensity. This behaviour will be encountered in such a cyclic pathway if both quencher concentration and laser pulse intensity are sufficient.

Figure 3.7. Simulation of the laser intensity dependence of the concentrations c relative to the initial concentration of the substrate c_0 for the radical anion (Eq. (3.44)) and the electron (Eq. (3.45)), with kinetic constants $\kappa_0 = 0.05 \text{ cm}^2/\text{mJ}$ and $\kappa_4 = 0.005 \text{ cm}^2/\text{mJ}$. The solid and the dashed lines represent the hydrated electron and the radical anion.



Application of the steady-state approximation for the radical anion in Eq. (3.43) gives the limiting concentration of radical anion.

$$\frac{[A^{\bullet-}]_{lim}}{[c_0]} = \frac{\kappa_0}{(\kappa_0 + \kappa_4)} \quad \text{Eq. (3.46)}$$

The linear rise of the electron concentration under these conditions is given by

$$\frac{[e^{\bullet-}_{aq}]}{[c_0]} = \frac{\kappa_0}{(\kappa_0 + \kappa_4)} I_{exc} \quad \text{Eq. (3.47)}$$

Part II

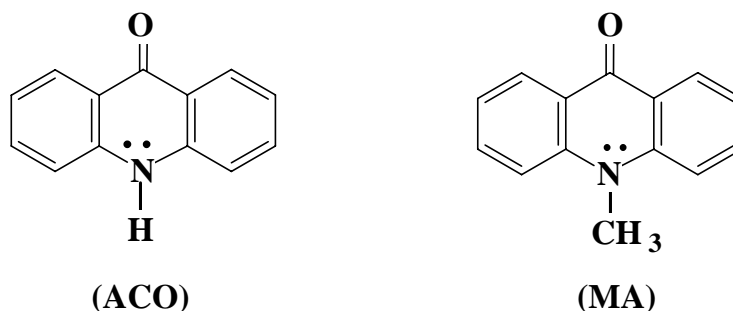
Donor and acceptor photoionizations – Results and discussions

Part II.A

Electron donor photoionizations

4. Photoionization of acridone derivatives via their singlet state

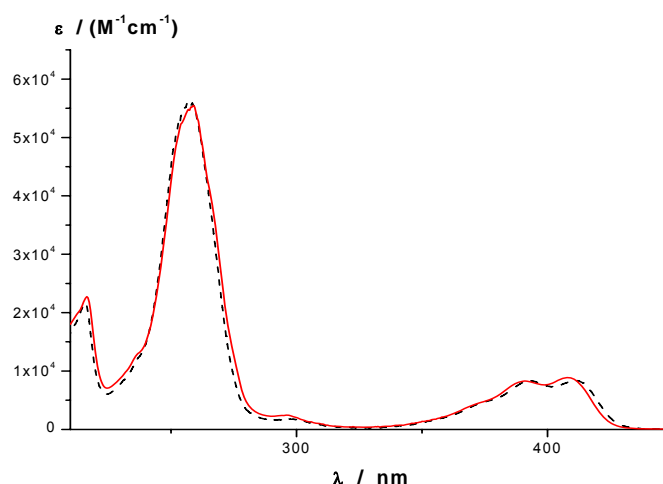
Despite the large number of studies on the electronic relaxation process of acridone derivatives in condensed phase [101-104], laser flash photolysis study of the photoionization of N-methylacridone (MA) and acridone (ACO) has not been reported so far. Much research has been directed to define the mechanism of the photoionization of organic molecules in solution [105-108]. In recent years, it has been shown that the excitation of aromatic compounds in fluid media at high laser intensity may induce a multi-photon ionization, which can make new reaction pathways available [86, 87]. In this chapter, we describe for the first time the cyclic and linear photoionizations of MA and ACO.



4.1. Spectroscopic characterization

The UV-visible absorption spectrum of an aqueous SDS solution of MA, for example, shows absorption peaks at 259 and 411 nm with high molar extinction coefficients ($\epsilon_{259 \text{ nm}} = 5.5 \times 10^4 \text{ M}^{-1}\text{cm}^{-1}$, $\epsilon_{411 \text{ nm}} = 8.89 \times 10^3 \text{ M}^{-1}\text{cm}^{-1}$) as shown in Figure 4.1 [109, 110]. This suggests that the bands have $\pi\text{-}\pi^*$ characters. The concentration of N-methylacridone in aqueous SDS solution was determined from its optical absorption [110]. In all cases, the absorption was measured before irradiation, and there was no sign of any chemical interaction between the components in their ground states.

Figure 4.1. Steady-state absorption spectra of N-methylacridone in 0.05 M aqueous SDS (Solid line) and in ethanol-water mixtures (1:4 v/v) (dashed line), at room temperature



The fluorescence quantum yield, ϕ_f , depends on the nature of the solvent [111-113]. The fluorescence spectrum of MA in aqueous SDS solution exhibits an emission maximum at 430 nm, whereas for ACO, the emission maximum lies at 415 nm [101, 110]. We measured the fluorescence spectra of both MA and ACO at various laser intensities and different laser excitation wavelengths. The fluorescence spectra for each species have the same general form but possess different intensities as shown in Figure 4.2, indicating that the MA and ACO are the only emitting species. Furthermore, the fluorescence is not quenched by SDS under our measurement conditions.

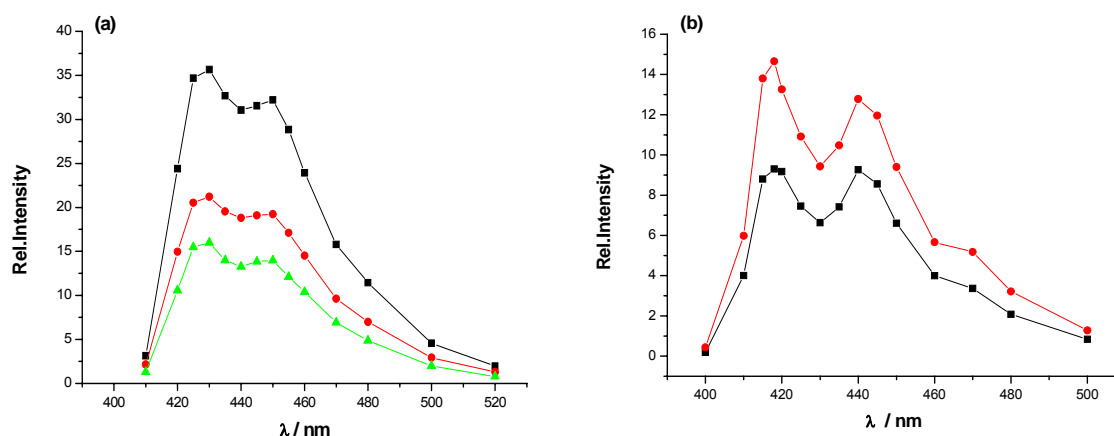
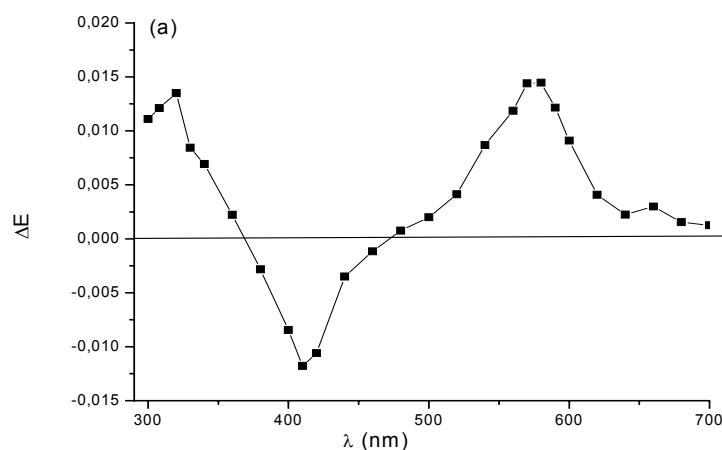


Figure 4.2. Fluorescence spectra of acridone derivatives obtained by 355 nm laser excitation at different laser intensities in N_2O -saturated solution. (a) 5.5×10^{-5} M MA in 0.05 M SDS (squares, 126.6 mJ/cm^2 ; circles, 538 mJ/cm^2 and triangles, 33 mJ/cm^2). (b) 2.4×10^{-5} M ACO in aqueous solution (circles, 33 mJ/cm^2 ; squares, 495 mJ/cm^2).

4.2. Triplet and radical cation absorption spectra

The T-T absorption maximum of N-Methylacridone exhibits a strong blue shift with increasing solvent polarity [113,114]. Following laser flash photolysis of MA in aqueous SDS solution at low laser intensity, we observed that the transient spectrum has maximum absorptions at 580 and 320 nm and a bleaching at around 400 nm due to the depletion of the ground state of MA as shown in Figure 4.3. The transient absorptions at 580 and 320 nm were quenched in oxygen-saturated solution, and were not affected in N₂O-saturated solution. Therefore, the absorption bands at these wavelengths are attributed to the T-T absorption signals.

Figure 4.3. Transient absorption spectrum of 9.89×10^{-5} M MA in N₂O-saturated 0.05 M aqueous SDS solution obtained by 355 nm laser excitation at low intensity (ca., 23.2 mJ /cm²) at room temperature.

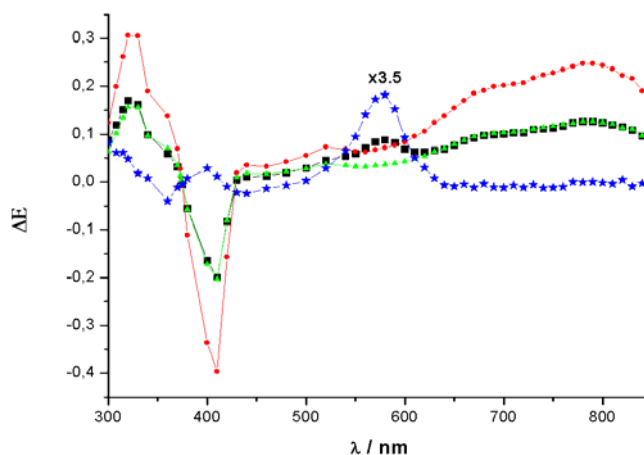


The transient absorption spectrum obtained (Figure 4.4, circles) by laser photolysis at high intensity of an aqueous SDS solution of MA with N₂O saturation following 355 nm light exhibits an additional absorption band at around 780-790 nm. The lifetime of that transient is not affected by the presence of oxygen and is attributable to N-methylacridone radical cation, MA^{•+}. The low absorption at 580 nm illustrates that the main transient is MA^{•+} with a minimal share of ³MA*. MA^{•+} also absorbs at 320 nm.

The spectra of MA^{•+} and ³MA* can be separated by measurements at two different laser intensities (Figure 4.4). At low intensity, both the triplet state and MA^{•+} are present, while at high laser intensity the transient absorption results mainly from MA^{•+} with a very small contribution of the triplet state. The absorption of the triplet state in the range 760-800 nm is negligible. Therefore, the absorptions at these wavelengths characterize MA^{•+}. Hence, within experimental error, one can deduce the pure MA^{•+} absorption spectrum at low laser intensity by multiplying the transient spectrum obtained at high laser intensity by a certain factor. Then, the triplet spectrum can be obtained by subtracting the pure MA^{•+} spectrum from the

transient spectrum at low laser intensity as shown in Figure 4.4. The resulting triplet spectrum is consistent with that found in literature [113] and with direct LFP of MA at very low laser intensity as shown in Figure 4.3.

Figure 4.4. Transient absorption spectra obtained upon 355 nm irradiation of 1.7×10^{-4} M MA in N_2O -saturated 0.05 M aqueous SDS solution. Squares (186.5 mJ/cm^2), circles (604 mJ/cm^2), triangles (calculated spectrum of MA^{*+}), and stars (calculated spectrum of ${}^3\text{MA}^*$, multiplied by 3.5).

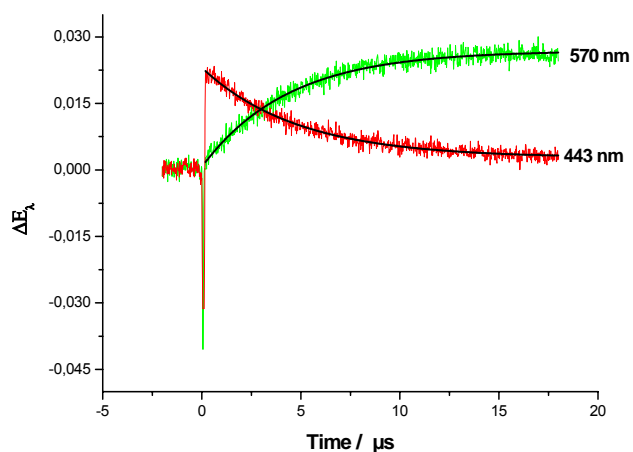


Transient absorption spectra of MA and acridone, ACO, obtained by 355 nm laser excitation at high laser intensity have a broad band with a peak at 720 nm. Addition of oxygen or N_2O quenched the transient absorption at this wavelength, which indicates that the absorption is due to the hydrated electron [84,115]. The transient absorption spectrum of ACO has an absorption band with a maximum at 560 nm, which was quenched by oxygen and was thus identified as the acridone triplet state, ${}^3\text{ACO}^*$ [104].

4.3. Triplet energy transfer

Energy transfer from the excited triplet state of 1,5-naphthalene disulfonate, ${}^3\text{NDS}^*$, to N-methylacridone in aqueous solution is possible since, the energy of ${}^3\text{MA}^*$ (59.6 Kcal/mol [101]) is smaller than that of ${}^3\text{NDS}^*$ (63 Kcal/mol [116]). The triplet energy (E_T) value of MA was obtained from 0-0 bands of phosphorescence spectra [101]. Laser flash photolysis of the aqueous solution containing MA (4.1×10^{-5} M, MA does not absorb at 308 nm under the experimental conditions) and NDS (3.045×10^{-4} M, NDS is known to be a water-soluble triplet sensitizer [116]) gives the transient absorption spectrum which is attributed to the T-T absorption spectrum of MA because of its close resemblance to the spectrum reported previously [113]. Figure 4.5 depicts the absorption decay for ${}^3\text{NDS}^*$ at 443 nm and the growth of the absorption at 570 nm due to the ${}^3\text{MA}^*$ formation as a result of energy transfer process.

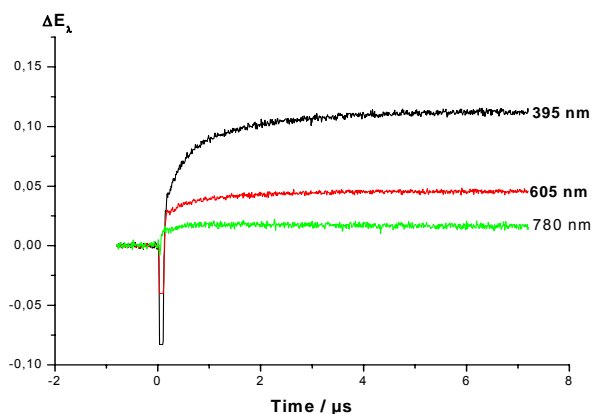
Figure 4.5. Absorption signals as a function of time monitored at 570 nm for the formation of $^3\text{MA}^*$ and 443 nm for the decay of $^3\text{NDS}^*$ for N_2O -saturated aqueous solution containing 4.1×10^{-5} M MA and 3.045×10^{-4} M NDS, generated upon 308 nm irradiation (8.1 mJ/cm^2). The solid lines were the fit curve according to mono-exponential function, where $k_{\text{obs}} = 2.2 \times 10^5 \text{ s}^{-1}$.



4.4. Electron transfer

The photoreaction of MA in methanol-water (1:2 v/v) in the presence of an electron acceptor such as methylviologen dication, MV^{2+} , shows the build up of transient absorption at 390 and 605 nm due to a formation of methylviologen radical cation, $\text{MV}^{\bullet+}$ [117-119], and at 780 nm due to a formation of $\text{MA}^{\bullet+}$, as depicted in Figure 4.6. MV^{2+} ground state does not absorb light at 355 nm under the experimental conditions. Therefore, the electron transfer occurred from $^3\text{MA}^*$ to the ground state of MV^{2+} . An estimate of the rate constant of the triplet decay is difficult because of the overlapping of absorption of both $^3\text{MA}^*$ and $\text{MV}^{\bullet+}$. Assuming that the efficiency of the electron transfer is approximately unity, the extinction coefficient of $\text{MA}^{\bullet+}$ can then be estimated to be $4000 \pm 5\% \text{ M}^{-1}\text{cm}^{-1}$, since the extinction coefficients of $\text{MV}^{\bullet+}$ at 605 and 395 nm are known ($\epsilon_{605} = 11000 \text{ M}^{-1}\text{cm}^{-1}$; $\epsilon_{395} = 3.8 \times 10^4 \text{ M}^{-1}\text{cm}^{-1}$) [120-122].

Figure 4. 6. Laser flash photolysis of 5×10^{-5} M MA in methanol-water (1:2 v/v) at low laser intensity (355 nm, 41.6 mJ/cm^2) in the presence of methylviologen dication (1×10^{-3} M) showed the transient absorption signals at 390 and 605 nm due to $\text{MV}^{\bullet+}$ and 780 nm due to $\text{MA}^{\bullet+}$.



4.5. Cyclic photoionization of N-methylacridone in SDS

By studying possible reaction mechanisms for N-methylacridone in SDS, its cyclic photoionization is deduced. The experimental data are then fitted to the theoretical behaviour of this cyclic mechanism.

4.5.1. Possible reaction mechanisms

The excitation of MA in aqueous SDS solution at high laser intensity produced an electron and the radical cation of N-methylacridone. We have examined the laser intensity dependence of hydrated electron concentration in order to distinguish between one- and multi-photon ionization processes. The electron curve shows a strong non-linear behaviour at low laser intensity, 355 nm (Figure 4.7). Investigation of the electron concentration at high laser intensity showed that it is greater than the initial concentration of MA.

From the previous discussion in Chapter 3, Schemes 3.4-3.7 can account for an electron yield that is greater than the initial concentration of the substrate. Scheme 3.7 is ignored under our experimental conditions.

To determine whether photoionization of MA through the triplet channel or singlet channel is the main pathway of photoionization, we assumed that the absorption quantum yield is unity. Therefore, the sum of the quantum yields of the deactivation processes can be written as

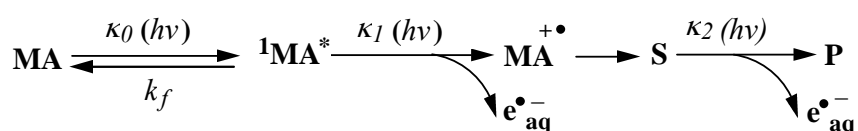
$$\varphi_f + \varphi_{isc} + \varphi_{ic} + \varphi_{pc} = 1 ,$$

where φ_{ic} and φ_{pc} are the internal conversion and the singlet photochemistry quantum yields, respectively. Since, φ_{ic} is often small, the sum of φ_f and φ_{isc} is approximately one when there is no singlet photochemistry. The fluorescence lifetime, τ_f , fluorescence quantum yield and the intersystem crossing quantum yield (φ_{isc}) of the lowest excited singlet state of MA in aqueous SDS solution were determined to be 10 ns, 0.97, and 0.03, [110,113], respectively. One can assume that the maximum quantum yield of $^3\text{MA}^*$ is 0.05. From τ_f , φ_f and φ_{isc} , the rate constant of fluorescence, k_f , and intersystem crossing, k_{isc} , of $^1\text{MA}^*$ in aqueous SDS solution were estimated to be 9.7×10^7 and $5 \times 10^6 \text{ s}^{-1}$, respectively.

Biphotonic triplet ionization under very short laser pulse duration conditions would not be expected, because the intersystem crossing is $5 \times 10^6 \text{ s}^{-1}$ for the reaction in aqueous SDS solution. We note that the inverse of this rate constant (200 ns) is much longer than pulse

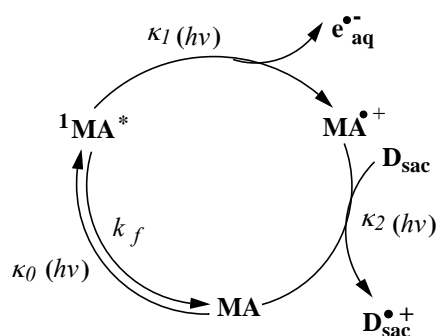
duration (6 ns), whereas $^1\text{MA}^*$ has a lifetime of 10 ns, i.e., only slightly longer than laser pulse duration, which allows for the absorption of a second photon. This allows us to predict that the excited singlet state of MA is the dominant pathway of the photoionization process and the $^3\text{MA}^*$ is not ionized under our experimental condition.

From the above results, the photoionization of MA according to Scheme 3.6 can be neglected. Thus, the photoionization can occur through Scheme 3.4 or 3.5. The fluorescence lifetime of $^1\text{MA}^*$ is comparable to the laser pulse duration. Therefore, both the kinetic schemes must include this step and then Schemes 3.4 and 3.5 will be modified to give Schemes 4.1 and 4.2, respectively.



Scheme 4.1

Owing to the restrictions of the available laser energy, the study of laser dependence of electron absorption alone is not sufficient to distinguish between these mechanisms, because the electron yield obtained by laser flash photolysis exceeds the initial concentration of a substrate by about 70% at the highest available laser intensity. Also, the curves of both radical cation concentration in Scheme 4.2 and the final product concentration in Scheme 4.1 display non-linear behaviour at low intensity and exhibit saturation behaviour at high intensity, i.e., the intensity dependences of their yield have similar behaviours. These observations show the importance of the study of the lowest excited state, by which one can distinguish between the two mechanisms at high laser intensity. The concentration of the lowest excited state in Scheme 4.1 must approach zero at high laser intensity, while in Scheme 4.2 it reaches a steady state, indicating that it is completely consumed in Scheme 4.1 during the photoreaction and regenerated in Scheme 4.2.



Scheme 4.2

4.5.2. Analysis and simulation of cyclic photoionization mechanism

It can be seen that the fluorescence intensity is related to concentration of $^1\text{MA}^*$ and can be used to express the concentration of the $^1\text{MA}^*$. Figure 4.7 illustrates the relationship between the intensity of the fluorescence signals of $^1\text{MA}^*$ and laser intensity.

Initial linear behaviour at low laser intensity is evident up to a maximum value. A subsequent slow decrease in the fluorescence intensity is noticed as the laser intensity increases, reflecting the ionization of the singlet state with a second photon, releasing an electron and the radical cation. Terminal saturation state is reached at high laser intensity supporting the suggestion of $^1\text{MA}^*$ regeneration. We observed a nonlinear dependence of the initial absorbance of $\text{MA}^{\bullet+}$ on laser intensity immediately after the laser pulse.

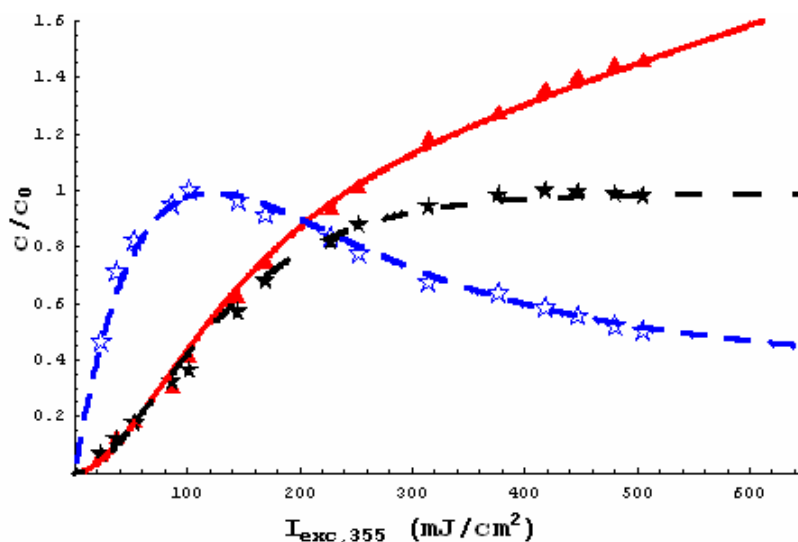


Figure 4.7. Concentrations c (electron; Filled triangles and solid line, $\text{MA}^{\bullet+}$; open stars and long dashed line, $^1\text{MA}^*$; filled squares and short-dashed line) relative to the substrate concentration c_0 as functions of the laser intensity obtained upon 355 nm laser excitation for 5.33×10^{-5} M N-methyl acridone, MA, in 0.1M aqueous SDS solution. The fluorescence intensity was measured at 430 nm and normalized with respect to its maximum intensity. $\text{MA}^{\bullet+}$ absorption was monitored at 780 nm in N_2O -saturated solution and normalized with respect to its maximum absorption. The fit curves were calculated with Eqs. (3.32) for $\text{MA}^{\bullet+}$, (3.33) for $e_{aq}^{\bullet-}$ and (4.2) for the fluorescence intensity of $^1\text{MA}^*$ giving the fitting parameters as $\kappa_1 = 1.74 \times 10^{-2} \text{ cm}^2\text{mJ}^{-1}$, $\kappa_2 = 1.35 \times 10^{-3} \text{ cm}^2\text{mJ}^{-1}$, the scale factor for fluorescence = 6.07, the scale factor for $\text{MA}^{\bullet+} = 1.23$. Constant parameters: $\kappa_0 = 1.17 \times 10^{-2} \text{ cm}^2\text{mJ}^{-1}$, $k_f t = 0.6$, $\chi t = 1.2$.

The curves of $\text{MA}^{\bullet+}$ and $e_{aq}^{\bullet-}$ are similar at low laser intensity, but differ greatly at high laser intensity. $\text{MA}^{\bullet+}$ displays a saturation behaviour while the $e_{aq}^{\bullet-}$ increases linearly with increasing laser intensity. Taken together, our results lead to the conclusion that the postulated

cyclic mechanism (Scheme 4.2) provides a valid description of the photoionization process of N-methyl acridone in aqueous SDS solution.

The solution of the differential rate equations for the postulated scheme 4.2 with respect to the end of laser pulse is represented by Equations (3.31)-(3.33), where

$$\kappa_{a,b} = \frac{1}{2} \left(\kappa_0 + \kappa_1 + \kappa_2 + \frac{k_f \tau}{I_{exc}} \pm \sqrt{(\kappa_0 + \kappa_1 + \kappa_2 + k_f \frac{\tau}{I_{exc}})^2 - 4(\kappa_0 \kappa_1 + \kappa_0 \kappa_2 + \kappa_1 \kappa_2 + \kappa_0 k_f \frac{\tau}{I_{exc}})} \right) \quad \text{Eq. (4.1)}$$

We do not detect the true fluorescence intensity but the convolution of the true signal with the delta-function response of our detection system, $\exp(-x t)$ [123]. Thus, the observed fluorescence signal is given by this convolution, which modifies Eq. (3.31) to Eq. (4.2).

$$I_f \propto \frac{\kappa_0 \kappa_2}{\kappa_a \kappa_b} \left(\begin{aligned} & 1 - \frac{\kappa_b \kappa_a (\chi t / I_{exc} - \kappa_2)}{\kappa_2 (\chi t / I_{exc} - \kappa_a) (\chi t / I_{exc} - \kappa_b)} \exp(-\chi t) + \frac{\kappa_b (\kappa_a - \kappa_2) \chi t / I_{exc}}{\kappa_2 (\kappa_a - \kappa_b) (\chi t / I_{exc} - \kappa_a)} \exp(-\kappa_a I_{exc}) \\ & + \frac{\kappa_a (\kappa_b - \kappa_2)}{\kappa_1 (\kappa_a - \kappa_b) (\chi t / I_{exc} - \kappa_b)} \exp(-\kappa_b I_{exc}) \end{aligned} \right) \quad \text{Eq. (4.2)}$$

Reducing the unknown parameters helps to obtain an excellent fit. ϵ_{GS} and χ can be measured independently. The κ_0 value can be calculated from Eq. (3.6) and k_f was taken from literature [110]. τ and c_0 are known. It is necessary that the resolved equations for fluorescence and radical cation absorption include a scaling factor because the luminescence collection efficiency and the extinction coefficient of $MA^{\bullet+}$ are not known. Scaling factor for radical cation absorption helps to determine its extinction coefficient as explained below. Fitting Eqs. (4.2), (3.32), and (3.33) to the experimental data can evaluate all unknown parameters, particularly the kinetic constants κ_1 and κ_2 . Figure 4.7 shows that the experimental data fit well following Scheme 4.2, providing strong evidence to the postulated cyclic mechanism.

Scaling factor of $MA^{\bullet+}$ ($scale_{MA^{\bullet+}}$) is given by Eq. (4.3)

$$scale_{(MA^{\bullet+}, \lambda)} = \frac{\epsilon_{(MA^{\bullet+}, \lambda)} c_0 d}{E_{(MA^{\bullet+}, \lambda)}^{\max}} \quad \text{Eq. (4.3)}$$

where $\epsilon_{(MA^{\bullet+}, \lambda)}$ and $E_{(MA^{\bullet+}, \lambda)}^{\max}$ are the extinction coefficient and the absorption maximum of $MA^{\bullet+}$ at monitoring wavelength (λ), respectively.

The extinction coefficient of the $MA^{\bullet+}$ at monitoring wavelength can be calculated from Eq. (4.3). It is found to be $3870 \pm 150 \text{ M}^{-1} \text{ cm}^{-1}$ at 780 nm. This value can be used to calibrate

the uncorrected difference absorption spectrum of $\text{MA}^{\bullet+}$, with respect to the ground-state depletion, to give the correct absorption spectrum. The extinction coefficient of $\text{MA}^{\bullet+}$ at excitation wavelength (355 nm) was determined to be $3800 \pm 150 \text{ M}^{-1}\text{cm}^{-1}$. Thus, the quantum yield of the ground-state regeneration is calculated from Eq. (3.13) to be 0.051 ± 0.03 .

The extinction coefficient of the singlet state at the excitation wavelength is not known to date, and the measurement of $\varepsilon(^1\text{MA}^*)$ was not possible due to its short lifetime. Thus the determination of the photoionization quantum yield is not possible.

4.6. Cyclic photoionization of acridone in SDS

The photoionization of the parent compound acridone in aqueous SDS solution at 355 nm is seen to behave very similar to that of N-methylacridone, where the electron yield exceeded the initial concentration of the ACO at high laser intensity. The dependences of acridone fluorescence intensity and the concentration of hydrated electron relative to the initial concentration of acridone on the laser intensity (355 nm) fit well with Eqs. (3.33) and (4.2) (Figure 4.8).

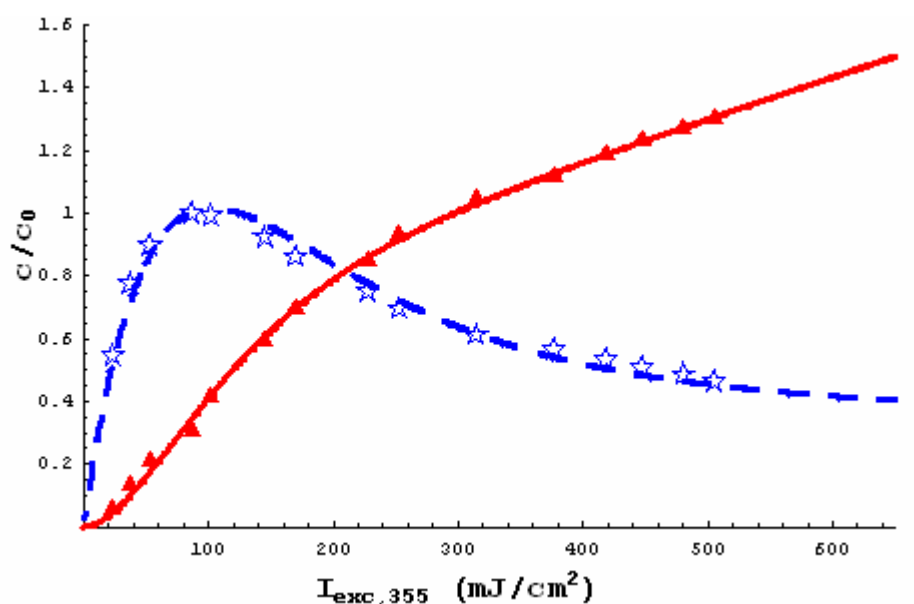


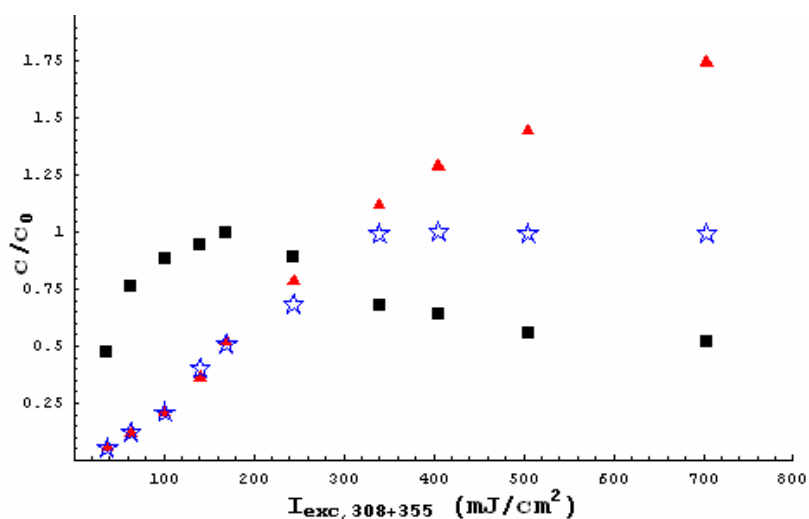
Figure 4.8. Concentrations c of each observed species (electron; Filled triangles and solid line, $^1\text{ACO}^*$: Normalized fluorescence intensity, open stars and short-dashed line) relative to the substrate concentration as functions of the laser intensity obtained upon 355 nm excitation for $5.33 \times 10^{-5} \text{ M}$ acridone, ACO, in 0.1M aqueous SDS solution. The fluorescence intensity was measured at 415 nm and normalized with respect to its maximum intensity. The curves were fitted with Eqs. (3.33) for $e_{\text{aq}}^{\bullet-}$ and (4.2) for $^1\text{ACO}^*$ giving the fitting parameters as $\kappa_1 = 1.44 \times 10^{-2} \text{ cm}^2\text{mJ}^{-1}$, $\kappa_2 = 1.66 \times 10^{-3} \text{ cm}^2\text{mJ}^{-1}$, the scale factor for fluorescence = 3.7 Constant parameters: $\kappa_0 = 1.72 \times 10^{-2} \text{ cm}^2\text{mJ}^{-1}$, $k_f t = 0.6$, $\chi t = 1.2$.

Laser flash photolysis of ACO obtained by 355 nm laser excitation in N₂O-saturated solution does not indicate the presence of any absorbing species other than the triplet state. This means that it is not possible to monitor the acridone radical cation, such that a quantitative detection of the radical cation was not possible.

4.7. Two-laser pulse experiments

To ensure that the photoionization of acridone derivatives occurred via a cyclic mechanism, we have studied their ionization using a two-laser two-color excitation. The 308-nm laser pulse was adjusted to temporally coincide with the 355 nm laser pulses given higher laser intensity than could be obtained with only one laser pulse. The electron concentration produced from the photoionization of MA in aqueous SDS solution at high laser intensity of two superimposed laser pulses exceeds the initial concentration of MA by more than 70% (Figure 4.9).

Figure 4.9. Concentrations c of observed species relative to the substrate concentration c_0 induced by two-laser flash photolysis (superimposed, 308 + 355 nm) for 5.33×10^{-5} M N-methylacridone in 0.2 M aqueous SDS solution as functions of the laser intensity. Open stars (MA^{•+}), squares (normalized fluorescence), and filled triangles (electron).



The lack of differentiation between the behaviour of electron and MA^{•+} at low laser intensity (Figure 4.9) shows that the study of the photoionization at high laser intensity is necessary to distinguish between their behaviour.

The fluorescence intensity of ¹ACO* and the electron yield were measured as a function of the superimposed two-laser irradiation intensity (data not shown). They have the same behaviour as that in Figure 4.9, confirming that the photoionization of ACO and MA in aqueous SDS proceeds via a cyclic mechanism.

4.8. Linear photoionization of acridone derivatives in alcohol-water solution

To confirm that SDS is necessary for photoionization of N-methylacridone via a cyclic mechanism, the photoionization experiments of MA and ACO were investigated in alcohol-water mixture and compared to that in SDS solutions.

Figure 4.10 displays the effect of laser intensity (355 nm) on the electron yield produced from the photoionization of MA in ethanol-water mixture (1:4 v/v). The non-linear behaviour of the electron curve at low laser intensity indicates that the photoionization process requires two 355 nm photons [39,40]. A further increase in the laser intensity results in the electron curve approaching a saturation state. The electron yield of the photoionization of MA in ethanol-water solution is less than the starting concentration of MA even at the highest laser intensity.

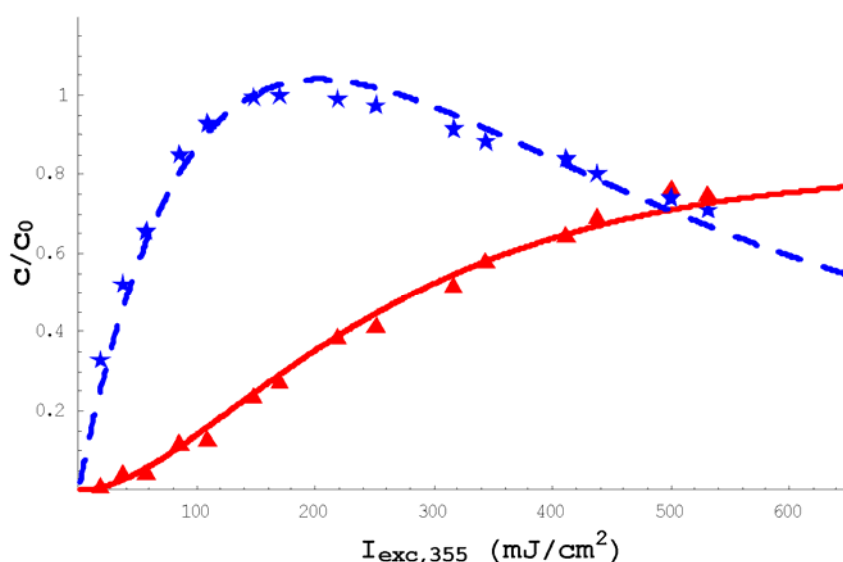


Figure 4.10. Concentrations of each detectable species (electron; filled triangles and solid line, ${}^1\text{MA}^*$: fluorescence intensity was normalized to its maximum intensity and measured at 430 nm, filled stars and dashed line) relative to the concentration of the substrate as functions of the laser intensity obtained upon 355 nm laser excitation of 5.33×10^{-5} M N-methyl acridone, MA, in ethanol-water (1:4 v/v) solution. The curves were fitted with Eqs. (3.16) for $e_{aq}^{\bullet-}$ and (4.4) for ${}^1\text{MA}^*$; the best-fit parameters: $\kappa_1 = 5.9 \times 10^{-3} \text{ cm}^2 \text{ mJ}^{-1}$, the scale factor of fluorescence = 4.6. Constant parameters were $\kappa_0 = 1.17 \times 10^{-2} \text{ cm}^2 \text{ mJ}^{-1}$, $k_f t = 0.6$, $\chi t = 1.2$.

The fluorescence curve of ${}^1\text{MA}^*$ is directly proportional to laser intensity; this linear relationship at low laser intensity is due to formation of ${}^1\text{MA}^*$, and hence this process can be

described as a monophotonic process. The fluorescence curve reaches the maximum intensity, followed by a decrease in intensity due to conversion of $^1\text{MA}^*$ into another species ($\text{MA}^{\bullet+}$), pointing to a biphotonic process for production of $\text{MA}^{\bullet+}$. The observed fluorescence intensity is given by Eq. (4.4).

$$I_f \propto \frac{\kappa_0}{(\kappa_a - \kappa_b)I_{exc}} \left(\frac{(\kappa_a - \kappa_b) \exp(-\chi t)}{(\chi t/I_{exc} - \kappa_a)(\chi t/I_{exc} - \kappa_b)} + \frac{\exp(-\kappa_a I_{exc})}{(\kappa_a - \chi t/I_{exc})} - \frac{\exp(-\kappa_b I_{exc})}{(\kappa_b - \chi t/I_{exc})} \right) \text{ Eq. (4.4)}$$

The excitation of ACO in alcohol-water solvent by light of wavelength 355 nm leads to formation of the hydrated electron. Neither one 355 nm laser pulse nor the superimposed two-laser pulse (308+355 nm) at the available highest intensity produces an electron concentration greater than the initial concentration of ACO, and the electron curve exhibits a simple saturation behaviour at high laser intensities (Figure 4.11). The photoionization of MA and ACO in alcohol-water mixture is consistent with two-photon ionization process as shown in Scheme 3.2.

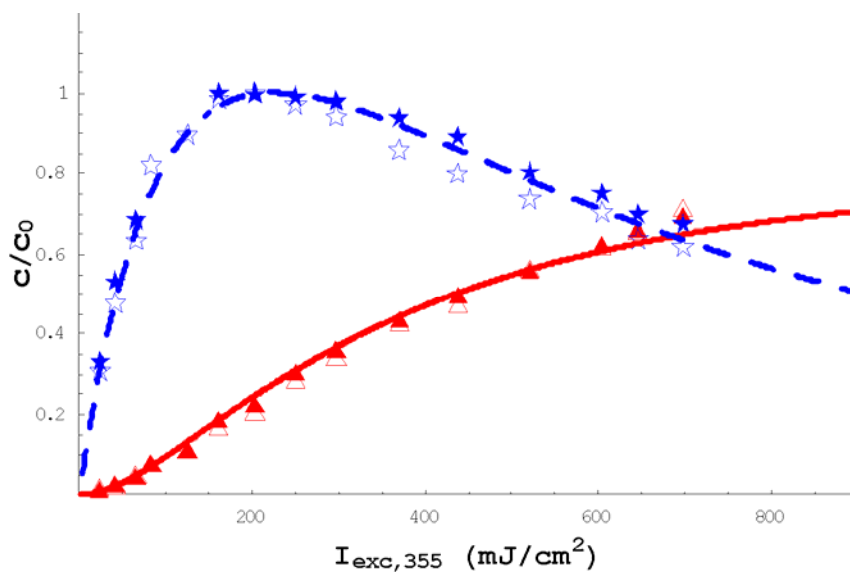


Figure 4.11. Concentrations c relative to the initial concentration of substrate c_0 obtained by 355 nm laser pulse as functions of the laser intensity I_{exc} for acridone in methanol–water (1:2 v/v). Filled symbols (5×10^{-5} M ACO); open symbols (2.25×10^{-5} M); triangles and solid line, electron ($\lambda = 829$ nm); stars and dashed line, normalized fluorescence signal intensity of the $^1\text{ACO}^*$ ($\lambda = 410$ nm, solution saturated with N_2O). The curves were fitted with Eqs. (3.16) for $e_{aq}^{\bullet-}$ and (4.4) for ^1MA giving the fitting parameters as $\kappa_1 = 3 \times 10^{-3} \text{ cm}^2 \text{ mJ}^{-1}$, the scale factor of fluorescence = 3.1. Constant parameters, $\kappa_0 = 1.72 \times 10^{-2} \text{ cm}^2 \text{ mJ}^{-1}$, $k_f t = 0.6$, $\chi t = 1.2$.

4.9. SDS as a sacrificial electron donor

It is clear that the radical cation absorbs a single photon in the presence of SDS to regenerate either the substrate or the excited singlet state. The regeneration of the substrate in its ground state is more energetically favourable than in its excited singlet state. Figure 4.12 illustrates that at low laser intensity the behaviour of the electron curves at different SDS concentrations are similar, while the difference between the electron curves is marked at high laser intensity. The changes of the kinetic parameters due to the effect of SDS on the photoionization were listed in Table 4.1.

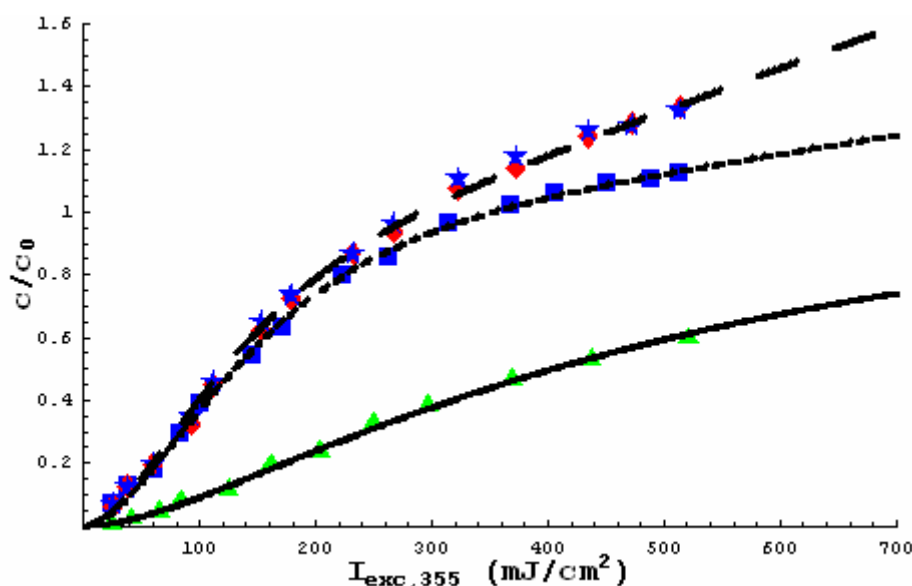


Figure 4. 12. Dependence of the hydrated electron concentration relative to the substrate concentration c_0 for ACO in SDS or in alcohol-water solution on laser intensity (excitation with 6 ns at 355 nm). Concentrations of electron were calculated from their absorption at 830 nm. The curves were fitted with Eq. (3.33) to all data sets. Diamonds, solid line (2.61×10^{-5} M, 0.2 M SDS); stars, long dashed (5.63×10^{-5} M, 0.05 M SDS); squares, short dashed line (2.61×10^{-5} M; 0.01 M SDS) and triangles, long dashed line (2.25×10^{-5} M; methanol-water 1:2 v/v)

The assumption that SDS acts as a sacrificial donor is supported by the effect of SDS concentration on the electron yield and the kinetic parameters, where the electron yield increases along with increase of the SDS concentration from 0.01 M to 0.05 M SDS. Also the data in Table 4.1 show that the κ_2 value in SDS concentration ≥ 0.05 M is greater than that in 0.01 M SDS by almost a factor of 2.5.

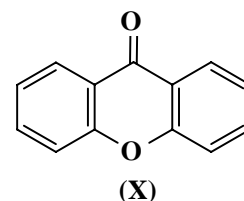
Table 4.1. Effect of SDS concentration on the kinetic parameters. κ_0 was calculated from Eq. (3.6) and set as constant value.

Solvent	Concentration of ACO	(κ_0 cm ² /mJ)	(κ_1 cm ² /mJ)	(κ_2 cm ² /mJ)
MeOH-H ₂ O (1:2, v/v)	2.25 x 10 ⁻⁵ M	0.0172	0.0022	2 x 10 ⁻⁹
0.01 M aqueous SDS	2.61 x 10 ⁻⁵ M	0.0172	0.012	0.00066
0.05 M aqueous SDS	5.63 x 10 ⁻⁵ M	0.0172	0.0138	0.0017
0.2 M aqueous SDS	2.61 x 10 ⁻⁵ M	0.0172	0.0138	0.0017

Replacing the SDS solution with an alcohol-water mixture to explore the solvent effects on the reaction mechanism revealed the fact that the electron concentration does not surpass the initial concentration of MA in both one and two laser pulse experimental designs. This further supports the theory that SDS is an essential component of the cyclic mechanism as a sacrificial electron donor.

5. Photoionization of xanthone via its triplet state

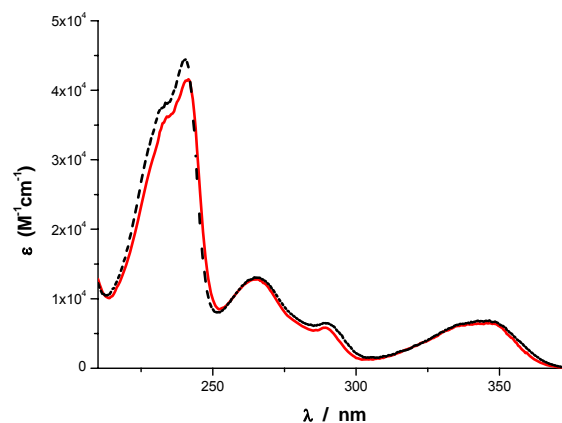
The photoionization of xanthone, X, has received little attention so far. Its photoionization occurs in aqueous SDS solution at 308 nm light via a biphotonic ionization process [124]. Interestingly, we found that the photoionization of xanthone in aqueous SDS solution yields more than one electron at high laser intensity, and the yield of hydrated electron increases with increasing laser intensity. These observations are inconsistent with a consecutive two-photon ionization process. In this chapter, we illustrate the effect of micelle (SDS) environment on the photoionization mechanism of xanthone, and compared the obtained results with that in methanol-water solvent.



5.1. Steady-state absorption spectra

The UV-visible absorption spectrum of X in aqueous SDS solution or in methanol-water (1:2 v/v) show an intense absorption peak at 240 nm with high molar extinction coefficients and a broad absorption band centered at 344 nm [125] (Figure 5.1).

Figure 5.1. Steady-state absorption spectra of xanthone in 0.05 M aqueous SDS solution (solid line) and in methanol-water (1:2 v/v) (dashed line), recorded at room temperature.



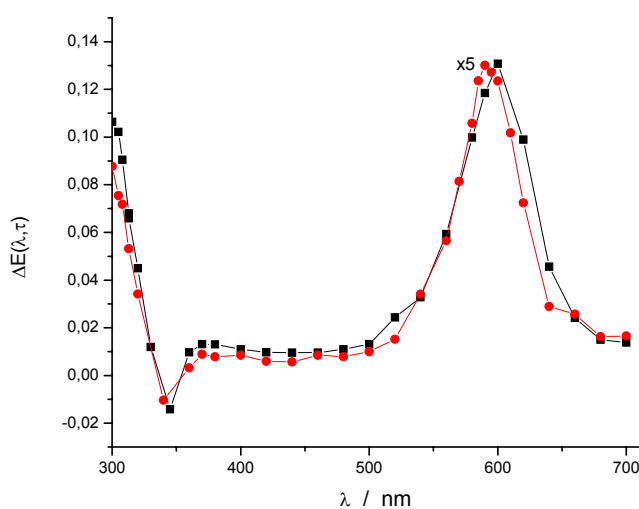
5.2. Transient absorption spectra

The absorption maximum of the triplet state of xanthone, ${}^3X^*$, depends on the nature of the solvent [126]. In non-polar media, xanthone exhibits a highly reactive $n-\pi^*$ triplet state [127], while it has a $\pi-\pi^*$ configuration in polar solvents [128]. Figure 5.2 shows the triplet-triplet absorption spectra of xanthone in 0.05 M aqueous SDS and in methanol-water (1:2 v/v)

solutions recorded at low laser excitation intensity with 308 nm to avoid any contribution from the electron and other intermediates. The triplet spectra exhibit absorption bands at 600 nm in SDS solution and 590 nm in methanol-water solution [126]. Both transients also exhibit an absorption band at 300 nm, in addition to a weak band around 370 nm. The transient absorption bands were quenched quickly in the presence of oxygen, suggesting that the absorption bands are due to the transient absorption of the $^3X^*$.

The transient absorption spectra obtained at high laser intensity are similar to those at low intensity. This means that the transient absorption is due to the same single species at both low and high laser intensities.

Figure 5.2. Triplet-triplet transient difference absorption spectra obtained by 355 nm laser flash photolysis (FWHM~ 6 ns, 35 mJ/cm²) for xanthone in argon-saturated 0.05 M aqueous SDS solution (squares, 4 x 10⁻⁵ M xanthone) and in argon-saturated methanol-water 1:2 v/v (circles, 3.46 x 10⁻⁵ M xanthone). The difference absorption spectrum of xanthone in methanol-water (1:2 v/v) was multiplied by a factor of 5.



5.3. Triplet decay analysis

In absence of self-quenching, the triplet lifetime of xanthone depends strongly on the reactivity of the xanthone triplet towards the solvent [129-131]. We have observed that the first-order rate of the triplet state varied with the variation in the concentration of xanthone, suggesting that $^3X^*$ reacts with xanthone ground state, i.e., self-quenching (Figure 5.3a) [130]. The rate constant of self-quenching of $(6.3 \pm 0.6) \times 10^8 \text{ M}^{-1} \text{ s}^{-1}$ in water-methanol mixture (2:1 v/v) was determined from the slope of a plot of the observed rate constant for the decay of the 590 nm absorption signals as functions of xanthone concentrations (Figure 5.3b).

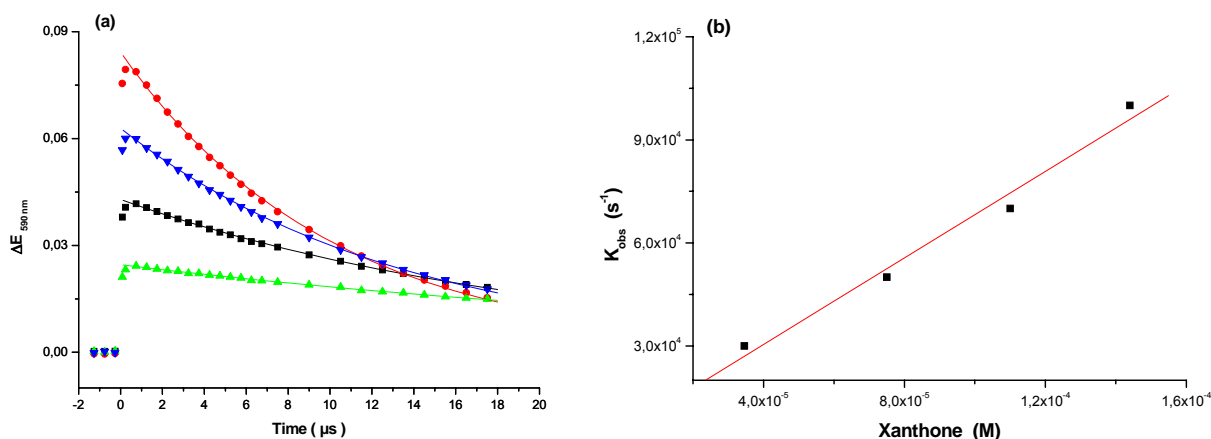
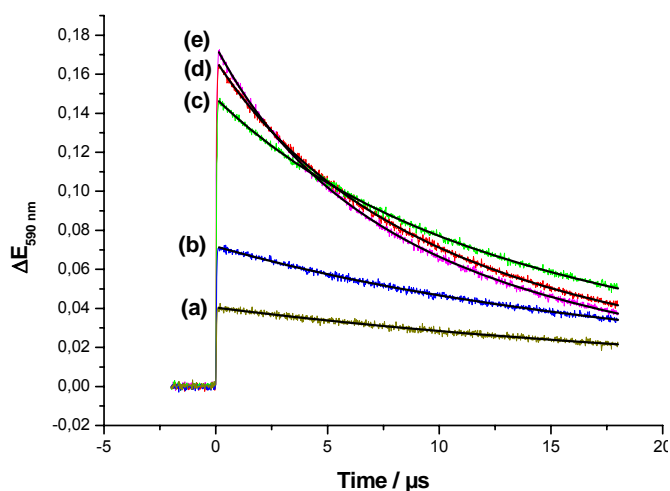


Figure 5.3. (a) Absorption-time profiles at 590 nm of xanthone triplet state with changing the concentration of xanthone as follows: $3.46 \times 10^{-5} \text{ M}$ (triangles), $7.3 \times 10^{-5} \text{ M}$ (squares), $1.0 \times 10^{-4} \text{ M}$ (inverted triangles), $1.44 \times 10^{-4} \text{ M}$ (circles). Decay of the absorption observed after 308-nm laser flash photolysis (7.6 mJ/cm^2) for xanthone in methanol-water (1:2 v/v). The solid curves are the best fit of mono-exponential function. (b) Plot of the observed first-order kinetics, k_{obs} , for xanthone triplet state as functions of xanthone concentrations.

The triplet decay at high laser intensity does not follow the second-order rate reaction and may include both second-order component (triplet-triplet annihilation only) and first-order component (a combination of unimolecular decay and pseudo-first-order processes such as self-quenching by xanthone). Figure 5.4 displays that the absorption of triplet state at high laser intensities fits well according to Equation 2.13.

Figure 5.4. Laser intensity dependence absorption-time profiles of ${}^3\text{X}^*$ at 590 nm obtained by 308 nm laser flash photolysis of xanthone ($4 \times 10^{-5} \text{ M}$) in N_2O -saturated methanol-water (1:2 v/v). The laser excitation intensity increases from trace a (ca. 21.8 mJ/cm^2) to trace e (ca. 394 mJ/cm^2). The solid lines were fitted based on Eq. (2.13).



5.4. Determination of extinction coefficient of xanthone triplet state

It was necessary to know the molar absorption coefficient of the xanthone triplet state. This was estimated using a comparative method. The absorbance of the xanthone triplet state (in methanol-water, 1:2 v/v) and benzophenone-4-carboxylate, BC, (in aqueous solution, pH 12) was compared for the same laser power and at identical absorbance of the ground state at excitation wavelength (308 nm).

We assumed that the intersystem crossing yields for xanthone [132] and benzophenone-4-carboxylate are unity [133]. The molar absorbance coefficient of $5200 \text{ M}^{-1} \text{ cm}^{-1}$ at 545 nm for BC triplet state was taken from reference [133]. The molar absorbance coefficient of the xanthone triplet at 590 nm was found to be $13.5 \times 10^3 \text{ M}^{-1} \text{ cm}^{-1}$. This value is in accordance with that obtained from the best-fit parameters in Figure 5.5.

5.5. Linear photoionization in methanol-water (1:2 v/v) by near UV

A plot of the variation of the absorption intensity signal of the hydrated electron at 829 nm against the laser intensity shows a strong non-linear behaviour at low laser intensity (Figure 5.5). The relationship between the absorbance of the triplet state at 590 nm and the laser intensity shows a linear dependency at low laser intensity. The linear fit passes through the origin when it is extrapolated to zero laser intensity. The absorbance of the triplet state reaches a maximum value and then decreases with an increase in the laser intensity, indicating that the triplet state is the intermediate of that ionization process. Photoionization of xanthone through the triplet channel was also supported by bleaching of the triplet state using the two-laser experiments as discussed in detail below.

Transient absorption spectra produced by 308 nm nanosecond laser flash photolysis of xanthone in both methanol-water mixture and aqueous SDS solutions show no significant absorption bands attributed to the xanthone radical cation. Therefore, effect of laser intensity on its yield is not possible.

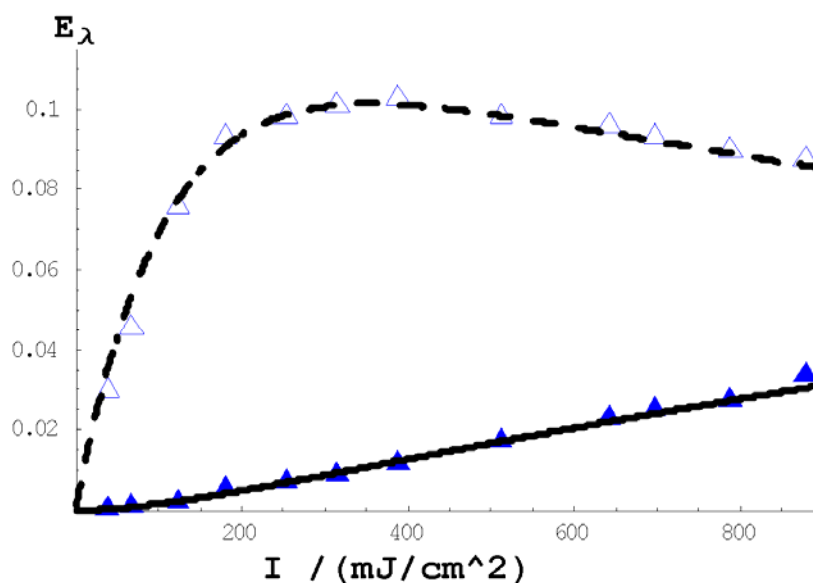


Figure 5.5. Effect of the incident laser intensity (I) on the absorbance (E_λ) of ${}^3X^*$ (open triangles) at 590 nm and on the absorbance of $e_{aq}^{\bullet-}$ (closed triangles) at 829 nm, for the photoionization of xanthone, in methanol-water (1:2 v/v), following 308 nm laser excitation. Pure electron absorptions were calculated from the difference of two measurements with N_2O and without N_2O , the triplet state of xanthone measured in N_2O -saturated solution. The lines (solid line, $e_{aq}^{\bullet-}$; and dashed line, ${}^3X^*$) were calculated with Eqs. (3.9) and (3.10) in the absorption form to the experimental data sets. Fixed parameters, $\kappa_0 = 9.31 \times 10^{-3} \text{ cm}^2/\text{mJ}$, $\varepsilon_{829}(e_{aq}^{\bullet-}) = 13.750 \text{ M}^{-1}\text{cm}^{-1}$, $C_0 = 2.1 \times 10^{-5} \text{ M}$, $d = 0.4 \text{ cm}$; the best-fit parameters were, $\kappa_1 = 4.0 \times 10^{-4} \text{ cm}^2/\text{mJ}$, $\varepsilon_{590}({}^3X^*) = 13.500 \text{ M}^{-1}\text{cm}^{-1}$.

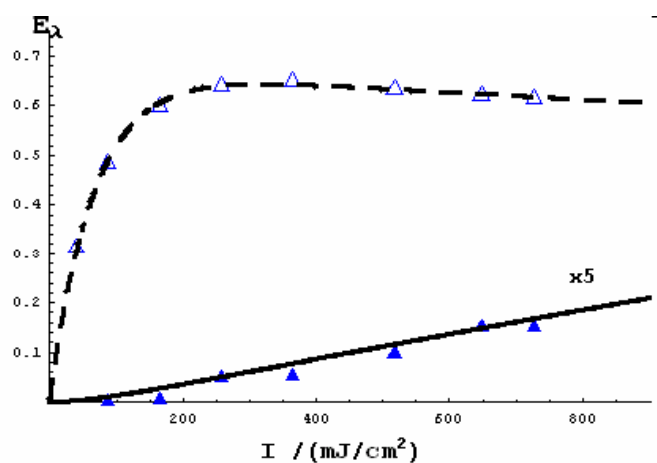
From the laser intensity dependences of the electron and the triplet state absorbances, the mechanism of the photoionization of xanthone is thus a linear two-photon ionization process [40], as in the case of Scheme 3.1. In this scheme, the xanthone ground state absorbs the first photon to give the xanthone excited singlet state which undergoes fast and efficient intersystem crossing leading to the triplet state. This process is much faster than the absorption process, such that the absorption process can be regarded as the rate constant of the triplet state formation, and the excited singlet state can be omitted from the reaction scheme. Damschen et al. [134] reported that the rates of intersystem crossing for xanthone, anthrone and benzophenone are fast and approximately the same. The build up of T-T absorption of xanthone in ethanol following excitation at 355 nm was measured and determined to be $8 \pm 2 \text{ ps}$ [135]. The second photon is absorbed by the xanthone triplet state to give the hydrated electron and the xanthone radical cation, $X^{\bullet+}$.

The number of unknown parameters should be reduced as much as possible to obtain a good fit. κ_0 can be calculated from Eq. 3.6, because the extinction coefficient of xanthone ground state and the quantum yield of the intersystem crossing are known. Also the extinction coefficient of the hydrated electron and the initial concentration of xanthone are known, so that the number of unknown parameters is reduced to two. The simultaneous fit of Eqs. (3.9) and (3.10) in the absorption form to the experimental data can be used to evaluate the κ_2 value and the extinction coefficient of xanthone triplet state as shown in Figure 5.5.

From UV/VIS spectrum of xanthone in aqueous SDS or in the methanol-water solution, the extinction coefficient of xanthone at 355 nm is higher than that at 308 nm by almost factor of 2.5. This means that the concentration of the triplet state formed by 355 nm light is higher than that formed by 308 nm light at the same laser intensity. For this reason we chose to study the photoionization of xanthone by laser excitation at 355 nm.

The laser intensity dependences of the observed species induced by 355 nm have the same behaviour as that induced by 308 nm light. In Figure 5.6 the triplet concentration of xanthone obtained by excitation with 355 nm light is higher than that obtained by excitation with 308 nm light as expected. However, the electron yield of the photoionization of xanthone is lower than that in Figure 5.5. These observations may reflect the different extinction coefficients of the triplet state at these excitation wavelengths. The quantum yield of the photoionization of the X at both excitation wavelengths was found to be $8 \times 10^{-3} \pm 15\%$.

Figure 5.6. Laser intensity dependence of the absorption of the triplet state (open triangles) and the hydrated electron (closed triangles) of 8×10^{-5} M xanthone in methanol-water (1:2 v/v) induced by 355 nm laser excitation. The solid ($e_{aq}^{\bullet-}$) and dashed (${}^3X^*$) lines were the results of fitting based on Eqs. (3.9) and (3.10). The best-fit parameters were $\kappa_0 = 1.52 \times 10^{-2} \text{ cm}^2/\text{mJ}$ and $\kappa_1 = 1.2 \times 10^{-4} \text{ cm}^2/\text{mJ}$.



5.6. Cyclic photoionization in aqueous SDS solution at 308 nm

The laser flash photolysis of xanthone in aqueous SDS solution following 308 nm laser pulses was investigated. The measured concentration of electron relative to the initial concentration of the substrate against laser intensity shows a strong non-linear behaviour at low pulse intensities (Figure 5.7). The electron concentration at high laser intensity is not limited by the depletion of xanthone since it is significantly larger than the initial concentration of xanthone. The usual two-photon ionization scenario (Scheme 3.1) cannot produce an electron concentration higher than the initial concentration of the original substance. Therefore, 308 nm laser flash photolysis experiments at high light intensity suggest an additional reaction pathway responsible for the production of a second electron.

Figure 5.7 demonstrates the relationship between the maximum absorption of the excited triplet state of xanthone at 600 nm and the laser intensity at 308 nm. This relationship displays a linear behaviour at low laser intensity. The triplet absorption reaches its maximum at about 180 mJ/cm^2 . As laser intensity increases, the maximum concentration decreases before reaching a constant level. This means that the triplet state decays by photoreaction. The concentration of the triplet state approaches a saturation behaviour at high laser intensity suggesting regeneration of the triplet excited state during laser pulse.

In light of the above observations, Scheme 3.5 can be considered valid to describe the photoionization process of xanthone in aqueous SDS solution. Scheme 3.5 shows that the photoreaction of the xanthone radical cation regenerates the substrate via the absorption of a third photon. The micelle (SDS) plays an important role in this step and is involved as an electron donor.

Figure 5.7 depicts the fit curves of the detectable species based on Scheme 3.5. The dotted line shows that the results of the fitting of the triplet data according to Eq. (3.31) exhibits some aberration, i.e., at low laser intensity the fitted curve of the triplet state demands a higher concentration than that found in the experimental data. At higher laser intensity, the measured relative concentration is lower than that predicted by the simulation fit.

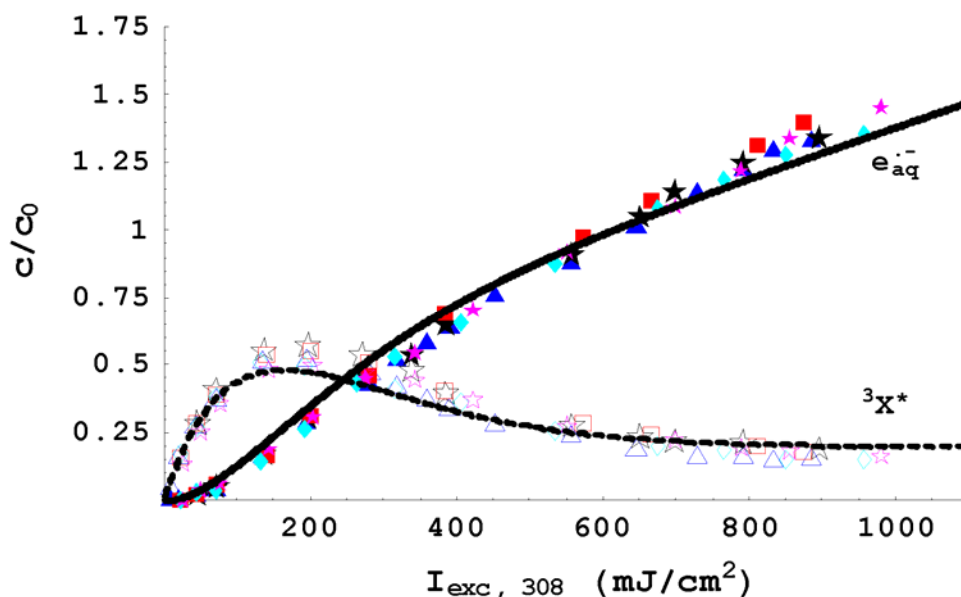


Figure 5.7. Concentrations c of each observed species (electron monitored at 829 nm; Filled symbols and solid line and $^3X^*$ monitored at 600 nm in N_2O -saturated solution; open symbols and dashed line) relative to the concentration of the substrate, c_0 , as a function of the laser intensity obtained upon 308 nm laser excitation of xanthone in 0.05 M aqueous SDS solution. The concentrations of xanthone were 4×10^{-5} (triangles, big stars, squares); 1.93×10^{-5} (diamonds); 2.5×10^{-5} M (small stars). The curves were fitted with Eqs. (3.31) for $^3X^*$ and (3.33) for $e_{aq}^{\cdot-}$, the best-fits parameters were $\kappa_1 = 4.69 \times 10^{-3} \text{ cm}^2 \text{ mJ}^{-1}$, $\kappa_2 = 1.34 \times 10^{-3} \text{ cm}^2 \text{ mJ}^{-1}$. Constant parameter was $\kappa_0 = 8.3 \times 10^{-3} \text{ cm}^2 \text{ mJ}^{-1}$.

5.7. Photoionization in aqueous SDS at 355 nm

The photoionization of X in SDS solution induced by 355 nm was observed. Figure 5.8 shows that the photoionization requires at least two photons, whereas the triplet formation requires only one photon. The electron concentration, relative to the initial concentration of xanthone, remains low and shows no tendency towards saturation at high intensity. The experimental evidence as shown in Figure 5.8 does not give sufficient information to determine whether the overall process occurs via a linear two-photon or cyclic mechanism. There is no evidence supporting the cyclic mechanism, therefore, we may assume that a linear two-photon process occurs in this case.

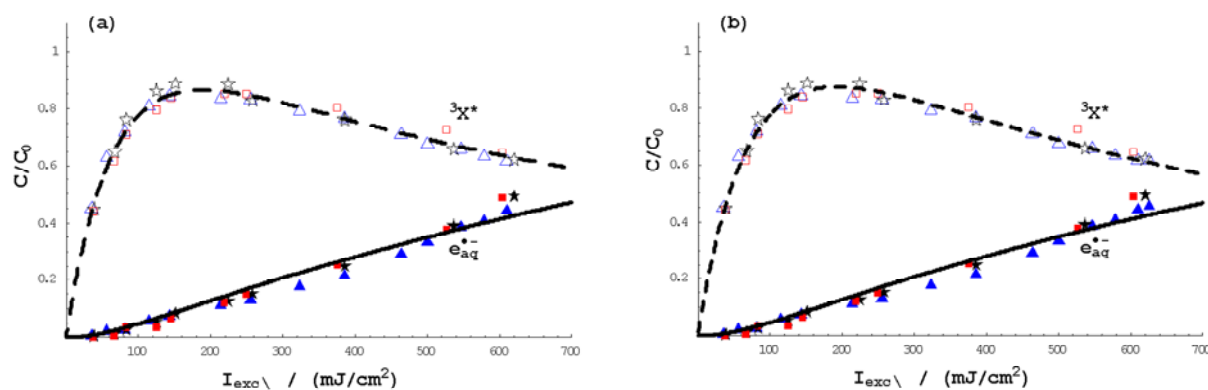


Figure 5.8. Concentration c of ${}^3X^*$ (open symbols) and e_{aq}^- (closed symbols) relative to the initial concentrations c_0 of xanthone 4×10^{-5} M (triangles and stars) and 2.75×10^{-5} M (squares), in 0.05 M aqueous SDS obtained by 355-nm laser pulse (pulse width is about 6 ns) as functions of the laser intensity I_{exc} . a) The curves were fitted with Eqs. (3.31) and (3.33) referring to the cyclic mechanism, yielding the best fit parameters $\kappa_0 = 1.578 \times 10^{-2} \text{ cm}^2 \text{ mJ}^{-1}$, $\kappa_1 = 9.9 \times 10^{-4} \text{ cm}^2 \text{ mJ}^{-1}$, $\kappa_2 = 3.08 \times 10^{-4} \text{ cm}^2 \text{ mJ}^{-1}$. b) The curves were fitted with Eqs. (3.9) and (3.10) referring to the consecutive two-photon ionization process, yielding the best-fit parameters $\kappa_0 = 1.52 \times 10^{-2} \text{ cm}^2 \text{ mJ}^{-1}$, $\kappa_1 = 9.9 \times 10^{-4} \text{ cm}^2 \text{ mJ}^{-1}$.

5.8. Two-laser two-color laser flash photolysis

Two-laser two-color laser flash photolysis was employed to examine the effect of the laser excitation on the excited state behaviour [53–55], particularly that of the triplet state. A pulse at 355 nm was used as a synthesis laser to generate ${}^3X^*$, while the excimer laser at 308 nm was used to ionize the triplet state. This choice resulted from the fact that the extinction coefficient of the xanthone ground state at 355 nm is greater than that at 308 nm, while the extinction coefficient of the triplet state at 308 nm is greater than that at 355 nm. The synthesis laser and ionization laser were incident upon the front of the sample cell and are collinear.

Figure 5.9 shows that the first laser pulse at 355 nm of X produced ${}^3X^*$ from xanthone via ${}^1X^*$, the second laser pulse at 308 nm generates an electron. The delay time of the second 308 nm laser pulse was 1.2 μs after the first laser pulse at 355 nm. The lifetime of triplet xanthone is long enough to absorb a second photon. This long lifetime allows us to shoot the triplet state at different time scales. We compared the electron yield relative to starting concentration of xanthone that was produced from the second pulse at 308 nm with that by a single laser pulse at 308 nm of the same energy. We found that the electron concentration relative to concentration of starting xanthone increases by a factor of approximately two.

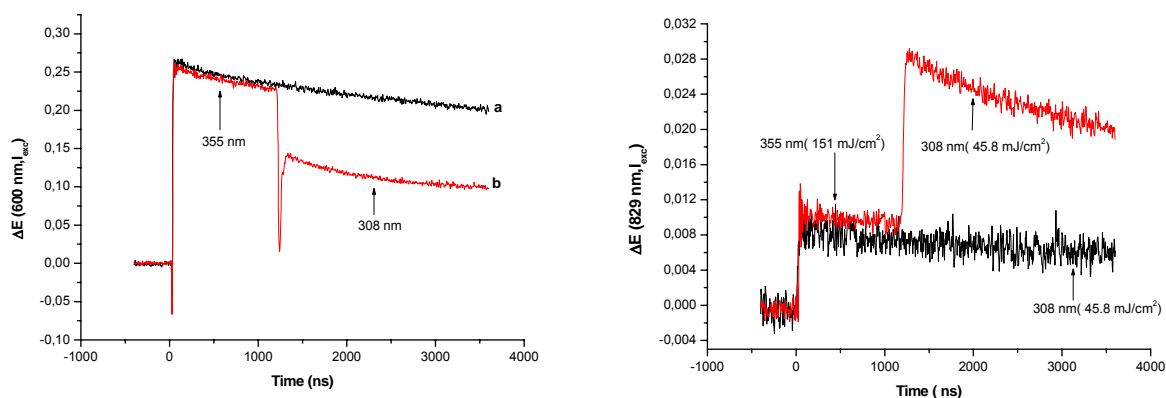


Figure 5.9. Two-laser experiments of 4×10^{-5} M xanthone in 0.05 M aqueous SDS solution, first pulse: at 355 nm (151 mJ/cm^2), second pulse: at 308 nm (45 mJ/cm^2 , 60–80 ns), 1.2 μs delay between the two pulses. Decay profile shows the electron formation that was monitored at 829 nm (right) and triplet bleaching by the second laser pulse, which was detected at the wavelength of its maximum absorption (600 nm) (left).

Direct evidence for the xanthone triplet excited state as the intermediate for photoionization of xanthone was given by comparing the triplet absorption signal after a single 308 nm laser pulse with that following two-laser pulse (308 + 355 nm) excitation. As shown in Figure 5.9a, an appreciable decrease in the triplet absorption signal was observed after the excitation by the second pulse (355 nm). This observation suggests that the triplet state is re-excited and results in the production of the electron (Figure 5.9b).

5.9. Effect of xanthone concentration

The electron concentration obtained from the photoionization of xanthone by 308 nm depends on the xanthone ground state concentration. The electron concentration decreased with increasing the concentration of xanthone as illustrated in Figure 5.10. The electron yield reduced by about 35% when the concentration of xanthone was changed from 4×10^{-5} M to 4×10^{-4} M. This effect is large and results not only from the inner filter effect, which lowers the electron yield, but also from other contributing factors. These effects may be due to xanthone dimerizations in ground or excited state, but no transient absorption attributed to these effects could be found in our experiments. The effect of xanthone concentrations in 0.05 M aqueous SDS solution on the kinetic parameters is listed in Table 5.1.

Figure 5.10. Dependence of the hydrated electron concentration relative to initial concentration of xanthone c_0 in aqueous 0.05 M SDS solution on laser intensity at 308 nm. The concentrations of electron were calculated at 829 nm. The curves were fitted according to Eq 3.33 for data sets. Squares, long and short dashing (2×10^{-4} M X); stars, short dashing (1×10^{-4} M X); open triangles, dotted line (8×10^{-5} M X); and closed triangles, solid line (4×10^{-5} M X).

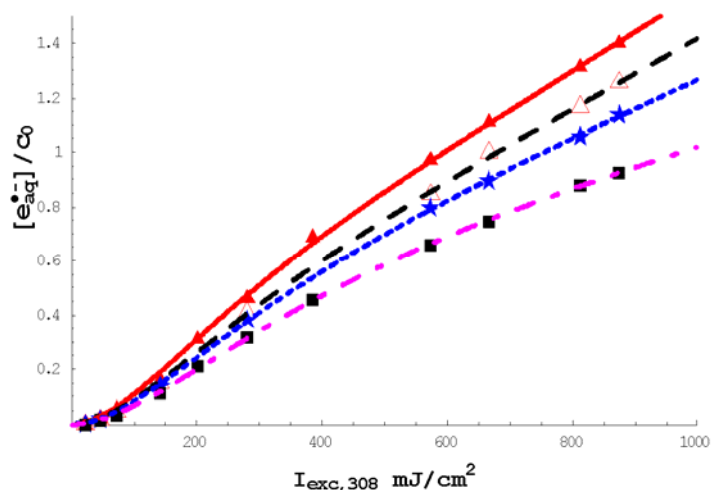


Table 5.1. Effect of xanthone concentrations on the kinetic parameters of Scheme 3.5. k_0 was calculated from Eq.(3.6) and set as fixed constant value.

[xanthone] / M	κ_0 (cm ² /mJ)	κ_1 (cm ² /mJ)	κ_2 (cm ² /mJ)
4×10^{-5}	8.3×10^{-3}	4.0×10^{-3}	3.1×10^{-3}
8×10^{-5}	8.3×10^{-3}	3.2×10^{-3}	2.98×10^{-3}
1×10^{-4}	8.3×10^{-3}	3.0×10^{-3}	2.1×10^{-3}
2×10^{-4}	8.3×10^{-3}	2.3×10^{-3}	1.04×10^{-3}

5.10. Effect of SDS concentration on the photoionization

In subsequent experiments, the effect of the SDS concentration on the electron yields was investigated. Figure 5.11 clearly illustrates that the photoionization reaction of xanthone in aqueous SDS yields an electron concentration higher than the initial concentration of xanthone when the SDS concentration is higher than its critical micellar concentration, cmc (8×10^{-2} M [62]). In contrast, the electron yield does not surpass the concentration of xanthone at SDS concentrations lower than its cmc. Figure 5.11 shows that the laser excitation of xanthone in concentrated SDS solution (i.e., above the cmc) yields more electron concentration than that in SDS concentration lower than cmc.

The electron concentration is directly proportional to the SDS concentration up to a certain SDS concentration (ca. 0.05 M). This finding was further confirmed by studying the electron concentration at different SDS concentrations, where the electron yield was identical in both 0.05 and 0.2 M SDS. The kinetic constant of xanthone regeneration, κ_2 , increases with increasing the concentration of aqueous SDS solution up to a limiting value as displayed in Figure 5.11. For example, a 10-fold increase in the concentration of aqueous SDS (from 0.005 to 0.05 M) results in an increase of the kinetic constant of xanthone regeneration, κ_2 , from 7.5×10^{-4} to $2 \times 10^{-3} \text{ cm}^2/\text{mJ}$. These experiments provide an important evidence that SDS can act as a reducing component in the cyclic reaction. The effect of SDS concentrations on the kinetic constants of both photoionization of triplet state and regeneration of xanthone is listed in Table. 5.2.

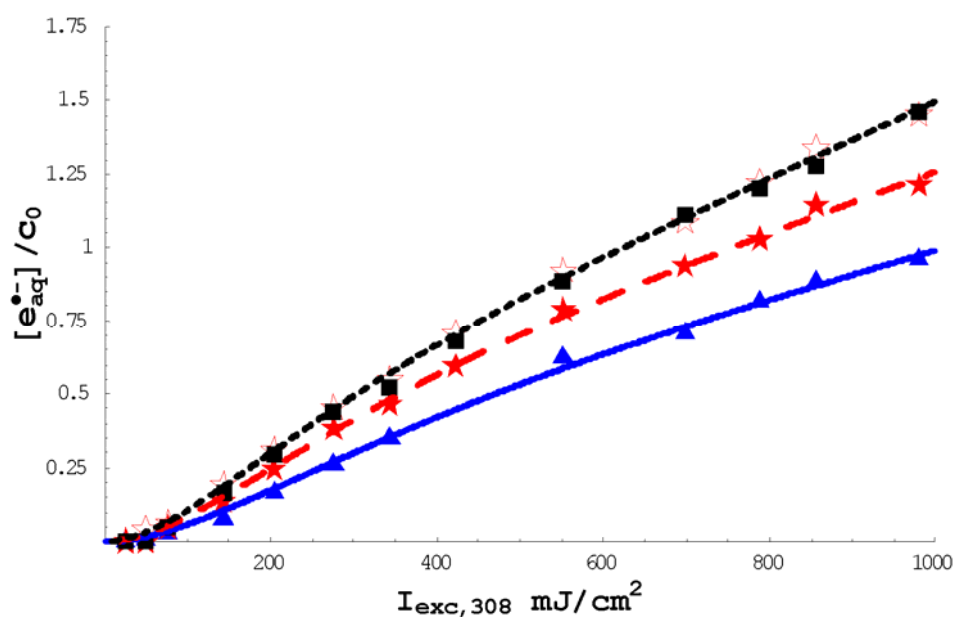


Figure 5.11. Dependence of the hydrated electron concentration relative to initial concentration of substrate for 4×10^{-5} M xanthone in SDS solution on laser intensity at 308 nm. The concentrations of electron were calculated at 829 nm. The curves were fitted with Eq (3.33). Squares, long dashed (0.2 M SDS); open stars, long dashed (0.05 M SDS); stars, dotted line (0.01 M SDS) and triangles, solid line (0.005 M SDS).

Table 5.2. Effect of SDS concentration on the kinetic parameters. κ_0 was calculated from Eq.(3.6) and set as fixed constant value.

Solvent	(κ_0 cm ² /mJ)	(κ_1 cm ² /mJ)	(κ_2 cm ² /mJ)
0.005 M aqueous SDS	0.083	0.002	0.0015
0.01 M aqueous SDS	0.083	0.003	0.0019
0.05 M aqueous SDS	0.083	0.0038	0.0026
0.2 M aqueous SDS	0.083	0.0038	0.0026

The resulting best-fit parameters κ_1 and κ_2 in Tables 5.1 and 5.2 are not identical to those in Figure 5.7. This results from the fact that the data in the former case were fitted for the hydrated electron concentration only. In the latter case, both electron and triplet concentrations were fitted.

All three steps of this reaction mechanism are driven by the same laser pulse, therefore the ionization quantum yield, ϕ_{ion} , of the $^3\text{X}^*$ and the regeneration quantum yield ϕ_{reg} of the xanthone ground state were determined according to the Equation (3.13). Most of the variables were determined independently. The extinction coefficient of $^3\text{X}^*$, ε_i , and that of the xanthone ground state, ε_{GS} , were measurable. The quantum yield of the intersystem crossing was assumed to be unity. κ_0 was calculated from Eq. (3.6). κ_1 and κ_2 were evaluated from the simultaneous fit of Eqs. (3.31) and (3.33) to the experimental data sets of Figure 5.7. The obtained ionization quantum yield at 308 nm was $0.092 \pm 10\%$. The regeneration quantum yield ϕ_{reg} of the xanthone ground state is linearly dependent on the kinetic constant κ_2 . Unfortunately, the extinction coefficient of xanthone radical cation is not measurable under our experimental conditions, so that the regeneration quantum yield of xanthone cannot be determined.

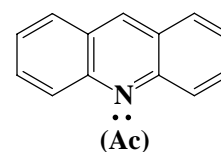
Photoionization quantum yield of xanthone induced by 355 nm laser pulse was found to be $0.06 \pm 10\%$ and was lower by about 35 % compared to that obtained following excitation with 308 nm light. This lower value may be due to the extinction coefficient of the triplet state at 355nm is lower than that at 308 nm. Thus, the photoionization of xanthone via 308 nm is more efficient. The photoionization quantum yield of xanthone in SDS is an order magnitude greater than that in methanol-water solution. It is well known that the photoionization quantum yield in aqueous SDS is higher than that in other solvent media [136], owing to the ability of SDS to decrease the ionization potential of the excited state [137].

Anionic micelles may change the photoionization mechanism from biphotonic to monophotonic as reported by Alkaitis, et al. [138]. Furthermore, in the presence of anionic micelles (SDS), the electron exits rapidly from the micelles into the aqueous phase as a hydrated electron due to the negative charge of the Stern layer of the micelles whereas the radical cation is strongly associated to the anionic micelles due to the electrostatic attraction (neutralization of radical cation). This rapid separation electron/radical cation pair enhances the yield and lifetime of the hydrated electron [139].

The photoionization of xanthone in methanol-water solution (1:2 v/v) differs from that in aqueous SDS in three important aspects. First, the electron yield of the photoionization of xanthone in aqueous SDS at 308 nm light is greater than that in the methanol-water solution. Specifically, the electron concentration displays saturation at high laser intensity in the methanol-water mixture, whereas it increases linearly with increasing laser intensity in aqueous SDS micellar solution. Second, the triplet absorption signal intensity in both cases passes through maximum, followed by a gradual decline to a constant level at high laser intensity in case of SDS or to base line in case of methanol-water solution. Third, the xanthone radical cation in methanol-water solution system does not regenerate xanthone ground state as is one case in aqueous SDS. These observations lead to the conclusion that the photoionization of xanthone is a linear photoionization in methanol-water mixture and a cyclic photoionization in aqueous SDS micelles.

6. Photoionization of acridine through singlet and triplet channels

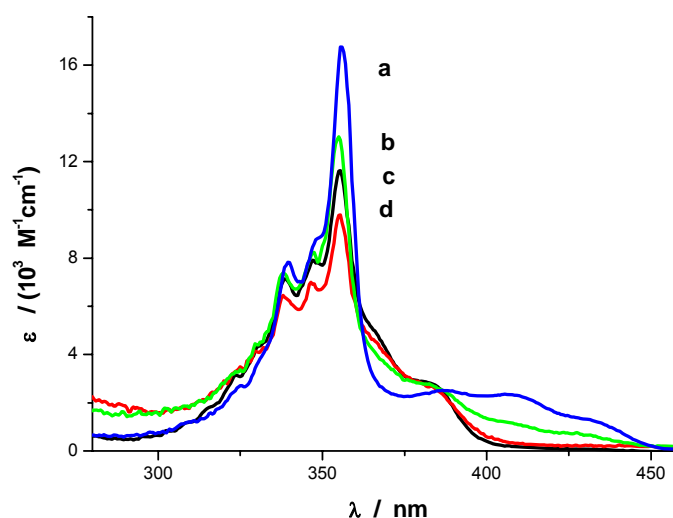
Photoionization of acridine (Ac) in aqueous micelles has not yet been studied, although, Kellmann and Tfibel [140] have investigated its photoionization in alkaline water solution at room temperature. They found that biphotonic ionization proceeds mainly through the singlet and to small extent via the triplet state. We could show for the first time that the photoionization of acridine in SDS micellar solution proceeds via a cyclic mechanism with high photoionization quantum yield.



6.1. Absorption spectra

The UV-visible absorption spectrum of an aqueous SDS solution of acridine (Figure 6.1) shows an absorption peak at 355.5 nm with a molar extinction coefficient of $16700 \text{ M}^{-1}\text{cm}^{-1}$, which suggests that the band has a $\pi\text{-}\pi^*$ character [141,143]. At low pH, the absorption spectrum shows a broad band centered around 410 nm which is not observed in alkaline solution. This band is attributed to the formation of acridinium ion [145]. We have investigated the photoreaction of acridine in alkaline solutions because it is slightly soluble in water ($1.8 \times 10^{-4} \text{ M}$) in absence of SDS [146,147].

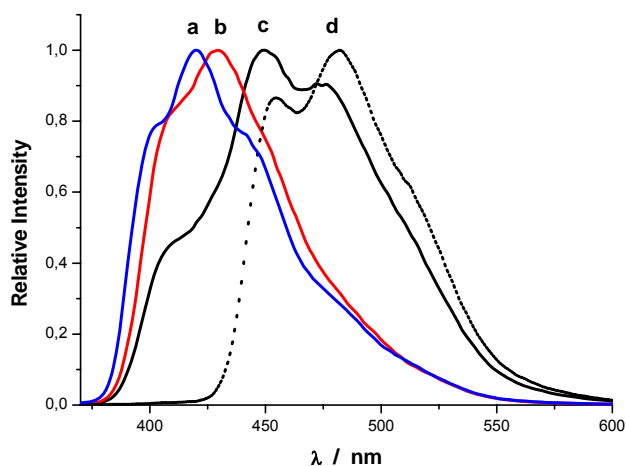
Figure 6.1. Absorption spectra of acridine solutions at room temperature in (a) 0.05 M SDS, (b) water, (c) methanol-water (1:2 v/v) and (d) water at pH 12.



6.2. Fluorescence spectra

The fluorescence spectra of acridine singlet state ($^1\text{Ac}^*$) [146] show maximum emission at approximately 430 (alkaline solution, pH 12), 420 (aqueous SDS, pH 12), and 450 nm (neutral aqueous solution) (Figure 6.2). The fluorescence spectrum of acridine in aqueous SDS solution has two emission maxima, at 480 and 450 nm, due to the presence of the protonated and neutral form of acridine, indicating that there is an acid-base equilibrium. At higher pH value, the emission band at 480 nm was not observed, i.e., the band at 480 nm is due to acridinium ion (AcH^+).

Figure 6.2. Steady-state fluorescence spectra of acridine at room temperature in 0.05 M SDS, pH 12 (a), water, pH 12 (b), water (c), and 0.05 M SDS (d). The samples were excited at 355 nm and normalized with respect to the maximum intensity.



Medeiros et al. [145] reported that the fluorescence decay of acridine in water and aqueous SDS solution at pH 12 was mono-exponential with lifetimes of about 10.04 and 2.3 ns, respectively. The fluorescence quantum yield values of acridine at pH > 11 in SDS and in water were 0.06-0.09 [145, 147] and 0.24 [145], respectively. We determined the fluorescence quantum yield of acridine in methanol-water (1:2 v/v) based on the reported value in methanol [143] and it was found to be 0.1. This value is approximately equal to that in methanol-water mixture (1:2 v/v) at pH 12. From the previous studies of the photophysical properties of acridine, the sum of the rate constants of the radiationless processes of the lowest excited singlet state in different solvents was calculated from the fluorescence lifetime and the rate constant of the fluorescence emission as displayed in Table 6.1. It is seen that the rate constants of the fluorescence emissions of the lowest singlet state of acridine in polar solvents are almost equal.

Table 6.1. Rate constants of deactivation processes of $^1\text{Ac}^*$ in different solvents at pH 12.

Solvent	$\tau_f \times 10^9$ (s)	$k_f \times 10^7$ (s^{-1})	$(k_{isc} + k_{ic}) \times 10^7$ (s^{-1})
H ₂ O [145]	10.4	2.3	7.67
0.05 M SDS [145]	2.3	2.61	19.6
MeOH-H ₂ O 1:2 v/v	4 ^(a)	2.5 ^(b)	22.5 ^(c)

(a) ref. [143]

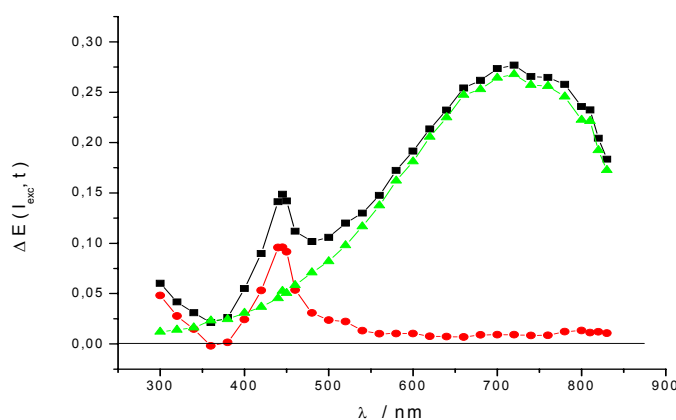
(b) in this work

(c) $k_{ic} + k_{isc} + k_r = 22.5 \times 10^7 \text{ s}^{-1}$; where k_r is the rate constant of the reaction of the singlet state with alcohol

6.3. Transient absorption spectra

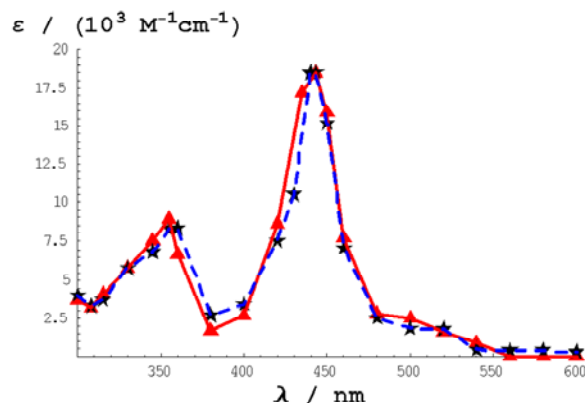
The transient absorption spectra of acridine in aqueous SDS solution under laser excitation wavelength of 355 nm at high laser intensity show absorption bands at 443 nm due to triplet-triplet absorption of acridine [148], and a broad band centered at 720 nm due to the hydrated electron [149] (Figure 6.3). These observations indicate the ionization of acridine.

Figure 6.3. Transient absorption spectra observed in 355 nm laser flash photolysis of acridine solution saturated with argon (squares), N₂O (circles). The incident laser intensity was 590 mJ/cm² pulse. Both curves were recorded at 60 ns; at that time solvated electrons were scavenged completely by N₂O in N₂O-saturated solution. Their difference absorption spectrum is characteristic for hydrated electron (triangles).



Correction of the triplet-triplet absorption spectrum for ground-state depletion yields the absolute absorption spectrum of the triplet state as shown in Figure 6.4. It has two maximum absorption bands at 443 and 355 nm. This correction is based on the extinction coefficient of the triplet state of acridine, $^3\text{Ac}^*$, at 443 nm that is $1.9 \times 10^4 \pm 0.1 \text{ M}^{-1}\text{cm}^{-1}$ [142,143,150].

Figure 6.4. Corrected absorption spectra of triplet–triplet absorption of acridine in 0.05 M aqueous SDS solution at pH 12 (stars, dashed line) or in methanol-water 1:2 v/v (triangles, solid line), following 355 nm laser pulse

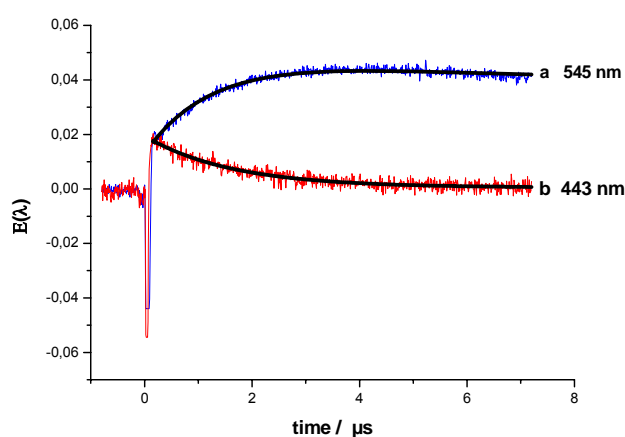


6.4. Triplet energy transfer

The molar extinction coefficients of T-T absorption of acridine in water solution were reported to be 19000 and 14500 $\text{M}^{-1}\text{cm}^{-1}$ at $\lambda_{\text{max}} = 443$ nm, by light–saturation method [151] and the triplet energy transfer method [152], respectively. Since the discrepancy in values cannot be ignored; we re-determined the molar extinction coefficient of the T-T absorption of acridine. The energy transfer from the excited triplet state of benzophenone-4-carboxylate, BC, to acridine in alkaline solution (pH 12) was monitored. The molar extinction coefficient of the triplet state of acridine at 443 nm in alkaline solution was found to be $18500 \pm 5\% \text{M}^{-1}\text{cm}^{-1}$ based on the extinction coefficient of the triplet state of BC at 545 nm ($5200 \text{M}^{-1}\text{cm}^{-1}$) [133].

Figure 6.5 shows the absorption time profile recorded at 443 and 545 nm (obtained by 308 nm laser excitation) for acridine triplet building and benzophenone-4-carboxylate triplet decay as a result of energy transfer process.

Figure 6.5. Transient absorption decay of the solution contained acridine (4.96×10^{-5} M) and benzophenone-4-carboxylate (5.39×10^{-4} M) obtained by 308 nm laser excitation at low intensity, (a) growth transient absorption at 443 nm for formation of acridine triplet and (b) transient absorption decay of the triplet state of benzophenone-4-carboxylate at 545 nm. The solid curves are the fitting of monoexponential function giving $k_{\text{obs}} = 6.2 \times 10^5 \text{s}^{-1}$.



6.5. Photoionization of acridine in alkaline water

We have observed that the electron yield resulting from photoionization of acridine in an aqueous SDS (pH 12) at 355 nm is greater than that in methanol-water, 1:2 v/v at pH 12 by almost a factor of 3 under the same experimental conditions. This observation prompted us to study and compare the photoionization behaviour of acridine in both cases as well as in alkaline water. By simulating photoionization mechanism of acridine in alkaline water as reported by Kellmann and Tfibel [140], we found that an unknown photoproduct of acridine absorbs at the wavelength of maximum absorption of the triplet state.

6.5.1. Simulation study according to results of Kellmann and Tfibel

The laser intensity dependence of the hydrated electron concentration (Figure 6.6) shows an induction period at low laser intensity. Figure 6.6 also includes the relationship between laser intensity and fluorescence intensity of the excited singlet state of acridine, $^1\text{Ac}^*$. The fluorescence intensity passes through a maximum followed by a gradual decline. In addition, formation of $^3\text{Ac}^*$ is a monophotonic process. Kellmann and Tfibel [140] reported that the excited singlet and triplet states are the source of the hydrated electron. Scheme 3.3 in Chapter 3 is thus, proposed for that photoionization. The excited singlet state thermally relaxes and returns back to its ground state with a rate constant k_{ic} (internal conversion). Therefore, Scheme 3.3 must include this step.

The acridine radical cation ($\text{Ac}^{\bullet+}$) has an absorption band at 900 nm [154]. It is important to mention that our nanosecond laser flash photolysis apparatus does not have the capability to detect the transient absorption above 840 nm. Thus, we could not investigate the laser intensity dependence of the yield of the acridine radical cation.

The observed fluorescence intensity is the convolution of the Eq. (3.15) with the response function as given in Eq. (6.1).

$$I_{Fl} \propto \frac{\kappa_0}{I_{exc}(\kappa_a - \kappa_b)} \left(\frac{(\kappa_a - \kappa_b) \exp(-\chi t)}{(-\kappa_b + \chi t/I_{exc})(-\kappa_a + \chi t/I_{exc})} + \frac{\exp(-\kappa_a I_{exc})}{(\kappa_a - \chi t/I_{exc})} - \frac{\exp(-\kappa_b I_{exc})}{(\kappa_b - \chi t/I_{exc})} \right) \quad \text{Eq. (6.1)}$$

where

$$\kappa_{a,b} = \frac{1}{2} \left(\kappa_0 + \kappa_1 + \frac{k_f \tau}{I_{exc}} + \frac{k_{isc} \tau}{I_{exc}} + \frac{k_{ic} \tau}{I_{exc}} \pm \sqrt{(\kappa_0 + \kappa_1 + k_f \frac{\tau}{I_{exc}} + k_{isc} \frac{\tau}{I_{exc}} + \frac{k_{ic} \tau}{I_{exc}})^2 - 4(\kappa_0 \kappa_1 + \kappa_0 k_{isc} \frac{\tau}{I_{exc}})} \right) \quad \text{Eq. (6.2)}$$

The observed triplet concentration, $[^3\text{Ac}^*]_{obs}$, after the end of the pulse will be given by Eq. (6.3)

$$[^3\text{Ac}^*]_{obs} = [^3\text{Ac}^*] + \varphi_{isc} [^1\text{Ac}^*] \quad \text{Eq. (6.3)}$$

where $\varphi_{isc} [^1\text{Ac}^*]$ is the triplet concentration resulting from the acridine singlet state via intersystem crossing after the end of the laser pulse.

It is necessary for the kinetic equation of fluorescence, Eq. (6.1), to include a scaling factor since, the luminescence collection efficiency is not known. Reducing the unknown parameters makes the fit easier, so that κ_0 , χ , τ , k_f , and $k_{ic} + k_{isc}$ were treated as constant values during the fit and were measured independently. Our attempts to fit the experimental data of the observed species based on Eqs. (6.3), (6.1) and (3.27) show that the resulting fit curves of the triplet state and the hydrated electron deviate from the experimental data (Figure 6.6).

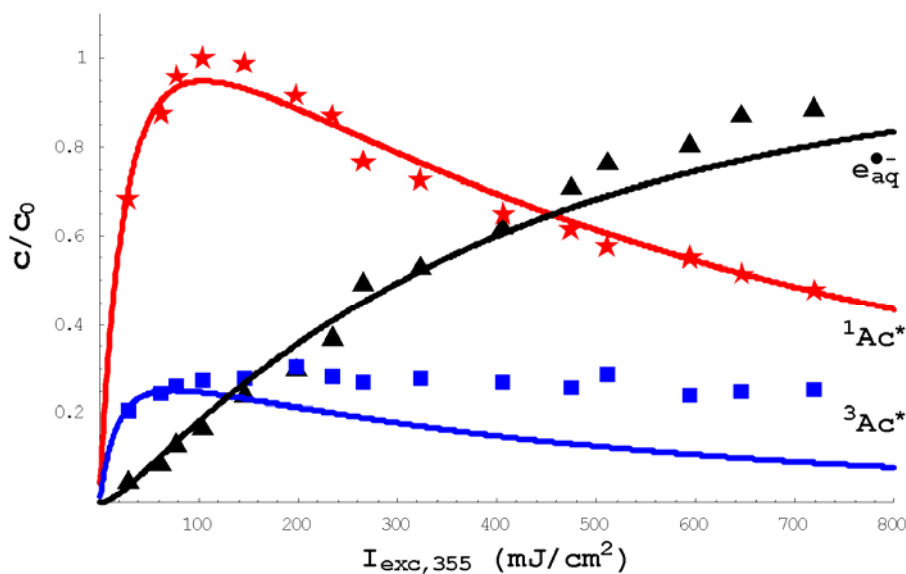


Figure 6. 6. Effect of laser intensity I_{exc} on the fluorescence intensity of $^1\text{Ac}^*$ (stars) and on the concentration of both the hydrated electron (triangles) and the acridine triplet state (squares) relative to the initial concentration of acridine c_0 (2×10^{-5} M) in aqueous solution at pH 12 following 355 nm laser excitation. The curves were fitted with Eqs. (6.1) for $^1\text{Ac}^*$, (6.3) for $^3\text{Ac}^*$ and (3.27) for $e_{aq}^{\bullet-}$. The best-fit parameters were $\kappa_1 = 2.65 \times 10^{-3} \text{ cm}^2\text{mJ}^{-1}$, $\kappa_2 = 1.01 \times 10^{-5} \text{ cm}^2\text{mJ}^{-1}$, $\text{cm}^2\text{mJ}^{-1}$, $k_{ic} \tau = 3.25 \times 10^{-1}$, $k_{isc} \tau = 1.369 \times 10^{-1}$, scale factor for fluorescence 2.3. Constant parameters were $\kappa_0 = 6.7 \times 10^{-2} \text{ cm}^2\text{mJ}^{-1}$, $\chi \tau = 1.2$, $k_f \tau = 1.38 \times 10^{-1}$.

6.5.2. Interpretation of deviations for the triplet state

Kinetic analyses in Figure 6.6 show that the behaviour of the triplet state is analogous to that of the singlet excited state. This implies that the triplet state could pass through a maximum concentration and decrease with increasing laser intensity. However, the absorption at 443 nm increases linearly and reaches a saturation state, indicating that there is another acridine derivative, Ac^d , which has an absorbance at 443 nm. Thus, the transient absorption at 443 nm can be given by Eq. (6.4)

$$\Delta E_{443}^{obs} = E_{(^3\text{Ac}^*,443)} + E_{(\text{Ac}^d,443)} \quad \text{Eq. (6.4)}$$

where $E_{(^3\text{Ac}^*,443)}$ and $E_{(\text{Ac}^d,443)}$ are the absorbances of the excited triplet state of Ac and the acridine derivative at 443 nm, respectively. ΔE_{443}^{obs} is the observed transient absorption at 443 nm. The transient absorption of $^3\text{Ac}^*$ at 443 nm can be represented by Eq. (6.5).

$$E_{(^3\text{Ac}^*,443)} = \varepsilon_{(^3\text{Ac}^*,443)} d C_0 ([^3\text{Ac}^*]_{\text{rel}} + \varphi_{isc} [^1\text{Ac}^*]_{\text{rel}}) \quad \text{Eq. (6.5)}$$

where $\varepsilon_{(^3\text{Ac}^*,443)}$, d , and C_0 are the extinction coefficient of the $^3\text{Ac}^*$ at 443 nm, the path length of the cell used, and the initial concentration of acridine ground state, respectively. $[^3\text{Ac}^*]_{\text{rel}}$ and $[^1\text{Ac}^*]_{\text{rel}}$ are the concentrations of $^3\text{Ac}^*$ and $^1\text{Ac}^*$ relative to the initial concentration of acridine, respectively.

The concentration of the electron must be equal to the concentrations of the acridine radical cation and its subsequent decay products under the same experimental conditions as displayed in Scheme 3.3. Therefore, the concentration of resulting acridine derivative during the photoreaction must be proportional to the electron concentration. The observed transient absorption at 443 nm in N_2O -saturated solution can thus be represented by Eq. (6.6)

$$\Delta E_{443}^{obs} = (\beta [^3\text{Ac}^*]_{\text{rel}} + \varphi_{isc} [^1\text{Ac}^*]_{\text{rel}}) + \gamma [e_{aq}^{\bullet-}]_{\text{rel}} \quad \text{Eq. (6.6)}$$

$$\beta = \varepsilon_{(^3\text{Ac}^*,443)} d C_0 \quad \text{and} \quad \gamma = b \varepsilon_{(\text{Ac}^d,443)} d C_0$$

where b is a scaling factor that gives the ratio of the concentration of acridine derivative to the concentration of the hydrated electron. $\varepsilon_{(\text{Ac}^d,443)}$ is the extinction coefficient of the acridine-derived species at 443 nm.

Fitting Eq. (6.6) to the experimental data at 443 nm, Eq. (3.27) for the hydrated electron, and Eq. (6.1) for the fluorescence intensities were depicted in Figure 6.7. The rate constants of the deactivation process were taken from literature [145]. The best-fit parameters show that

the triplet and singlet states are ionized with the kinetic constants of 2.63×10^{-3} and $5.9 \times 10^{-4} \text{ cm}^2\text{mJ}^{-1}$, respectively. Therefore, the photoionization of acridine in alkaline water proceeds via a linear ionization process through the singlet and triplet excited state channel.

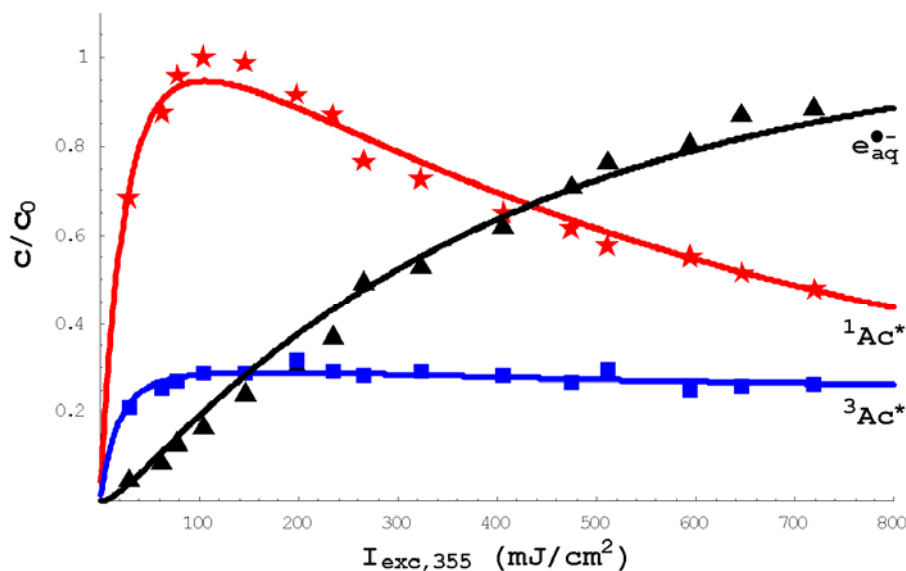


Figure 6.7. Effect of laser intensity $I_{\text{exc},355}$ on the normalized fluorescence intensity of $^1\text{Ac}^*$ (stars), the concentration of the hydrated electron (triangles) relative to the initial concentration of acridine c_0 ($2 \times 10^{-5} \text{ M}$), and the absorption intensity at 443 nm (squares) in aqueous solution at pH 12 following 355 nm laser pulse. The triplet state absorptions were measured at 443 nm in N_2O -saturated solution and multiplied with factor of 5. The curves were fitted with Eqs. (6.1) for the fluorescence of the $^1\text{Ac}^*$, (6.6) for the absorbance at 443 nm, and (3.27) for $e_{\text{aq}}^{\bullet-}$. The best-fit parameters were $\kappa_1 = 2.63 \times 10^{-3} \text{ cm}^2 \text{ mJ}^{-1}$, $\kappa_2 = 5.9 \times 10^{-4} \text{ cm}^2\text{mJ}^{-1}$, $k_{\text{ic}} \tau = 3.25 \times 10^{-1}$, $k_{\text{isc}} \tau = 1.369 \times 10^{-1}$, scale factor for fluorescence 2.3, $\gamma = 0.032$. Constant parameters are $\kappa_0 = 6.7 \times 10^{-2} \text{ cm}^2\text{mJ}^{-1}$, $\chi \tau = 1.2$, $k_f \tau = 1.38 \times 10^{-1}$, $d = 0.4 \text{ cm}$, $\epsilon(^3\text{Ac}^*, 443) = (1.9 \pm 0.1) \times 10^4 \text{ M}^{-1}\text{cm}^{-1}$.

6.6. Photoionization of acridine in alkaline methanol-water mixture

The photoionization of acridine in methanol-water (1:2 v/v) at pH 12 has been investigated for the first time in this work. The behaviour of the observed species (Figure 6.8) was similar to that in alkaline water at pH 12. The fluorescence quantum yield of the acridine singlet state varies from solvent to solvent [155], due to the interaction between the $^1\text{Ac}^*$ and the solvent molecules, which results in the electronic change of the excited states. An additional deactivation pathway of the excited state of acridine in hydrogen-donating solvents such as alcohol was reported previously [156,143]. The excited singlet state of acridine abstracts a hydrogen atom from alcohol to produce N-hydroacridine radical (carbon centered

radical) with the rate constant, k_r , of $5 \times 10^7 \text{ s}^{-1}$ [143]. Thus, this step must be included in the differential equation of the singlet state (Eq. (6.7)).

$$\frac{d[{}^1\text{Ac}^*]}{dt} = \kappa_1 I(t)[\text{Ac}] - (k_f + k_{isc} + k_{ic} + k_r + \kappa_2 I(t))[{}^1\text{Ac}^*] \quad \text{Eq. (6.7)}$$

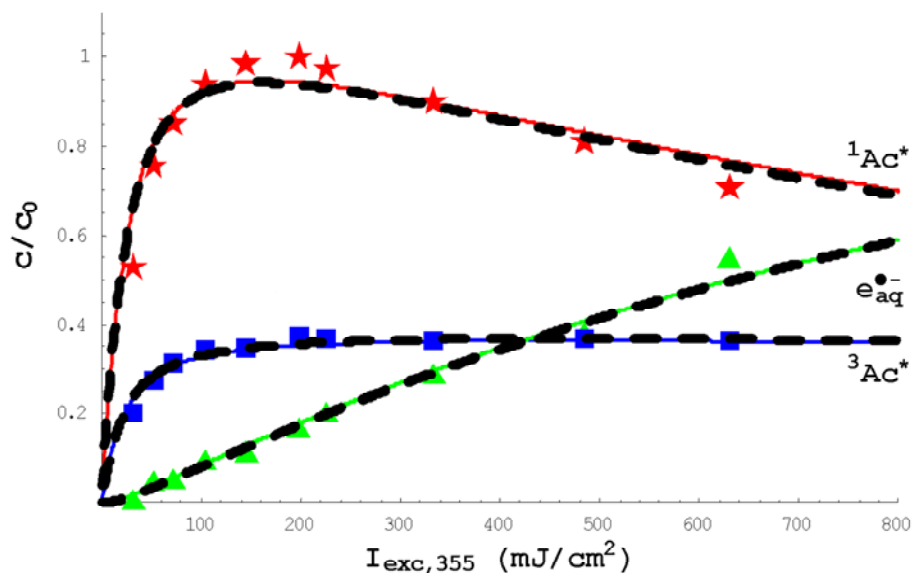


Figure 6.8. Effect of laser intensity $I_{\text{exc},355}$ on the fluorescence intensity of ${}^1\text{Ac}^*$ (stars), the absorption intensity at 443 nm measured in N_2O -saturated solution (squares), and the concentration of the hydrated electron (triangles) relative to the initial concentration of acridine c_0 ($2 \times 10^{-5}\text{M}$) in methanol-water (1:2 v/v) at pH 12 following 355 nm laser pulse. The fluorescence was normalized and measured in argon- or N_2O -saturated solution at 430 nm. The absorptions at 443 nm and the corresponding equation were multiplied with factor of 5. The solid lines were fitted with Eqs. (6.1) for ${}^1\text{Ac}^*$, (6.6) for the absorbance at 443 nm, and (3.27) for $e_{\text{aq}}^{\bullet-}$; the best-fit parameters $\kappa_1 = 1.16 \times 10^{-3} \text{ cm}^2\text{mJ}^{-1}$, $\kappa_2 = 3.0 \times 10^{-4} \text{ cm}^2\text{mJ}^{-1}$, where the dashed lines were fitted with Eqs. (6.1) for ${}^1\text{Ac}^*$, (6.6) for the absorbance at 443 nm, and (3.27) for $e_{\text{aq}}^{\bullet-}$ ($\kappa_{a,b}$ as in Eq.(6.8)) with the best-fit parameters $\kappa_1 = 1.2 \times 10^{-3} \text{ cm}^2\text{mJ}^{-1}$, $\kappa_2 = 3.8 \times 10^{-4} \text{ cm}^2\text{mJ}^{-1}$, $k_f \tau = 3 \times 10^{-3}$. The other best-fit parameters were equal in both cases and had the following values: $k_{isc} \tau = 3.91 \times 10^{-1}$, $k_{ic} \tau = 1.01$, scale factor for fluorescence 2.47, $\gamma = 0.06$. Constant parameters in both cases are $\kappa_0 = 7.5 \times 10^{-2} \text{ cm}^2\text{mJ}^{-1}$, $k_f \tau = 1.5 \times 10^{-1}$, $\chi \tau = 1.2$, $d = 0.4 \text{ cm}$, $\epsilon({}^3\text{Ac}^*, 443) = 1.9 \times 10^4 \pm 0.1 \text{ M}^{-1}\text{cm}^{-1}$.

The solution of the differential equations corresponding to the photoreaction of acridine in methanol-water solution based on Scheme 3.3 is given by Eqs. (3.15) for the singlet state, (3.26) for the triplet state, and (3.27) for the electron, where κ_a and κ_b are given by Eq. (6.8)

$$\kappa_{a,b} = \frac{1}{2} \left(\kappa_0 + \kappa_1 + \frac{k_f \tau}{I_{exc}} + \frac{k_{isc} \tau}{I_{exc}} + \frac{k_{ic} \tau}{I_{exc}} + \frac{k_r \tau}{I_{exc}} \pm \sqrt{\left(\kappa_0 + \kappa_1 + \frac{k_f \tau}{I_{exc}} + \frac{k_{isc} \tau}{I_{exc}} + \frac{k_{ic} \tau}{I_{exc}} + \frac{k_r \tau}{I_{exc}} \right)^2 - 4 \kappa_0 \left(\kappa_1 + \frac{k_{isc} \tau}{I_{exc}} + \frac{k_r \tau}{I_{exc}} \right)} \right) \quad \text{Eq. (6.8)}$$

In our system the mole fraction of methanol in water is 0.18. Therefore, the quantum yield of the N-hydroacridine radical, ϕ_r , may be less than the value reported previously. From the best-fit parameters, k_r and ϕ_r were found to be $5 \times 10^5 \text{ s}^{-1}$ and 2×10^{-3} , respectively. The kinetic constant of the photoionization of the singlet state is greater than that of the triplet state, indicating that the photoionization of acridine occurs mainly via the acridine excited singlet state with a small contribution from the excited triplet state.

6.7. Cyclic photoionization in SDS

Owing to the ejection of more than one electron from the photoionization of acridine in aqueous SDS solution (pH 12) following 355 nm laser excitation, we focused our attention on the investigation of photoionization mechanism.

It should be mentioned that the acridine radical cation in alkaline solution deprotonates to give the corresponding acridine neutral radical (Ac^\bullet), Re. (6.1), which is stable on the time-scale of microseconds (100 μs) and has an absorption band at 600 nm [140].



The deprotonation process occurs over a longer time (200 ns) than the duration of the laser pulse. However, both cation radical and neutral radical could have very similar spectra as suggested for indole and tryptophan cation and their neutral radicals by Bent and Hayon [157]. Thus, the deprotonation step may be difficult to observe. The acridine radical (Ac^\bullet) can absorb a photon to produce an electron and the acridine cation, Ac^+ , as displayed in Re. (6.2)



It is clear that the source of the second electron is not the excitation of the acridine species resulting from the deprotonation process for two reasons. Firstly, this process takes place over a much longer time period than the duration of the laser pulse. Secondly, the behaviour of the singlet and the triplet excited states is not in line with the linear photoionization mechanism, where the concentration of both states does not fall back to zero with an increase in the laser intensity but reaches a constant level indicating the regeneration of both states during photoreaction within the duration of the laser pulse (Figure 6.9).

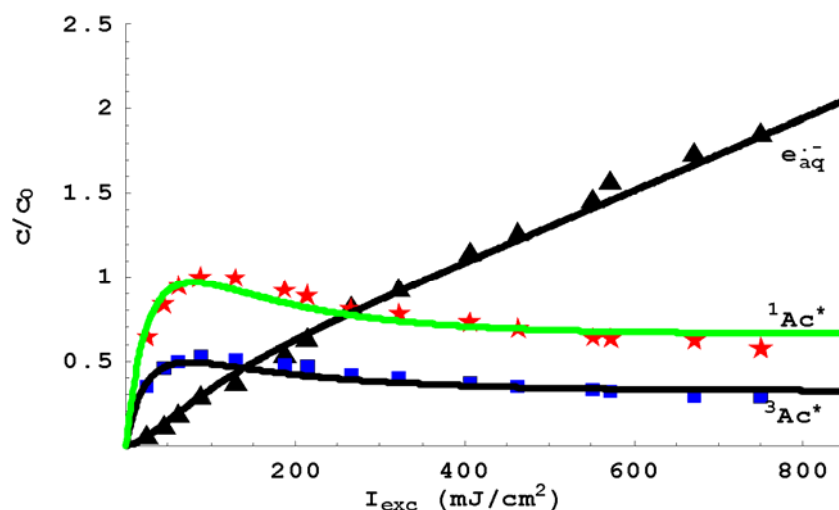


Figure 6.9. Laser intensity dependence I_{exc} of the fluorescence intensity of $^1\text{Ac}^*$ (stars), the absorption intensity at 443 nm (squares), and the concentration of the hydrated electron (triangles) relative to the initial concentration of substrate obtained upon 355 nm laser excitation of acridine c_0 (2×10^{-5} M) in 0.05 M aqueous SDS solution at pH 12. The fluorescence was normalized and measured at 420 nm. The electron concentrations were calculated from absorption signal at 829 nm. The solid lines were calculated based on Scheme 3.6. The best-fit parameters were $\kappa_1 = 7.72 \times 10^{-3} \text{ cm}^2 \text{ mJ}^{-1}$, $\kappa_2 = 1.1 \times 10^{-3} \text{ cm}^2 \text{ mJ}^{-1}$, $\kappa_3 = 3.1 \times 10^{-3} \text{ cm}^2 \text{ mJ}^{-1}$, $k_{\text{isc}} \tau = 1.23$, $k_{\text{ic}} \tau = 1.22$, scale factor of fluorescence is 4.626, $\gamma = 6.74 \times 10^{-3}$. Constant parameters were $\kappa_0 = 6.4 \times 10^{-2}$, $k_f \tau = 1.58 \times 10^{-1}$, $\chi \tau = 1.2$, $d = 0.4$ cm, $\epsilon(^3\text{Ac}^*, 443) = 1.9 \times 10^4 \pm 0.15 \text{ M}^{-1} \text{ cm}^{-1}$. Both the absorption intensity and respective kinetic model were multiplied by a factor of 5.

Furthermore, the electron concentration at the end of the laser pulse increases continuously with increasing laser intensity and exceeds the initial concentration of the substrate. These observations are very strong evidence that the photoionization of acridine in aqueous solution (pH 12) involves both singlet and triplet excited states through a cyclic photoionization mechanism as displayed in Scheme 3.6.

Kinetic analysis of differential equations corresponding to Scheme 3.6 will be carried out by numerical integration. All deactivation processes of $^1\text{Ac}^*$ were taken from literature [145,147]. The transient absorption at 443 nm and the fluorescence intensity were treated as in the case of alkaline water system. The fit curves in Figure 6.9 based on Scheme 3.6 are consistent with experimental data.

We assumed that the photoionization of acridine in alkaline water occurs via a cyclic mechanism as is the case with SDS solution. Fitting the experimental data of the detectable species based on the modification of Scheme 3.6 shows that the results are almost similar to that based on Scheme 3.3. The differentiation between the two mechanisms is very difficult under the available experimental conditions.

6.8. Photoionization quantum yields

Photoionization quantum yields of both singlet and triplet states of acridine were determined from the best-fit parameters and Eq. (3.13) or Eq. (3.6). It was assumed that the extinction coefficients of the singlet-singlet absorption in the three polar solvents used have approximately the same values. The extinction coefficient value of $^1\text{Ac}^*$ at 355 nm ($20000 \text{ M}^{-1}\text{cm}^{-1}$) was taken from reference [140]. The net photoionization quantum yield (φ_{net}) is given by

$$\varphi_{\text{ion}}^{\text{net}} = \varphi_{\text{ion}}^{\text{sin}} + \varphi_{\text{ion}}^{\text{trip}} \quad \text{Eq. (6.9)}$$

where $\varphi_{\text{ion}}^{\text{sin}}$ and $\varphi_{\text{ion}}^{\text{trip}}$ are the photoionization quantum yields of both the singlet and the triplet states, respectively. The photoionization quantum yields of acridine are listed in Table 6.2.

Table 6.2. Photoionization quantum yields of acridine in different solvents at pH 12 following 355 nm laser excitation.

Solvent	$\varphi_{\text{ion}}^{\text{sin}}$	$\varphi_{\text{ion}}^{\text{trip}}$	$\varphi_{\text{ion}}^{\text{net}}$	$\varepsilon(^3\text{Ac}^*, 355) \text{ M}^{-1}\text{cm}^{-1}$
H ₂ O	0.019	0.012	0.031	7000 [140]
MeOH-H ₂ O (1:2 v/v)	0.0085	0.0049	0.0134	8900
0.05 M SDS	0.056	0.019	0.075	8300

The data in Table 6.2 show that the photoionization of the excited singlet state is more efficient than that of the triplet state, where the photoionization quantum yield of the singlet state is three times greater than that of the triplet state. Generally, the photoionization quantum yield of acridine in SDS is greater than that in water or methanol-water solution, owing to the ability of SDS micelles to enhance the photoionization. This has been discussed in Chapter 5.

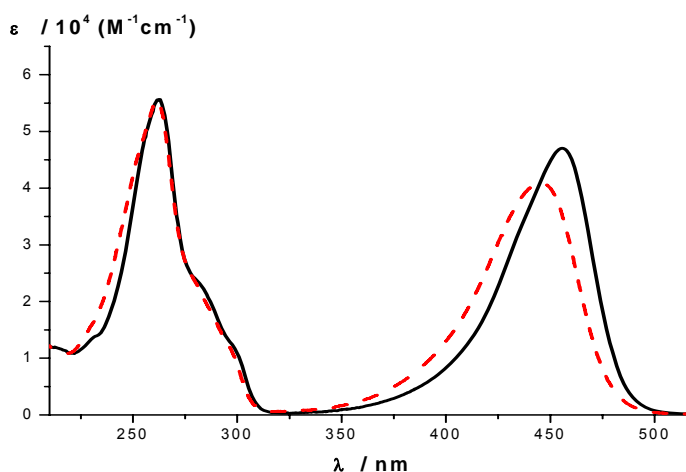
7. Photoionization of monoprotonated Proflavine

Extensive studies have been made on the photochemistry of proflavine, P, because of its interesting spectroscopic and photochemical properties [161]. Mono-protonated proflavine, PH^+ is frequently used as a photosensitizer in various devices for solar energy utilization [162]. Its photoionization occurred via a biphotonic process in aqueous SDS while it was a monophotonic process in aqueous solution as reported previously [163, 164]. Our investigations ruled out the monophotonic ionization of PH^+ in aqueous solution. Furthermore, we found that the electron concentration resulting from the photoionization of PH^+ following a 355 nm laser pulse surpasses the initial concentration of the substrate at the highest available laser intensity. This encouraged us to reinvestigate its photoionization in aqueous and SDS solutions.

7.1. Absorption and fluorescence spectra

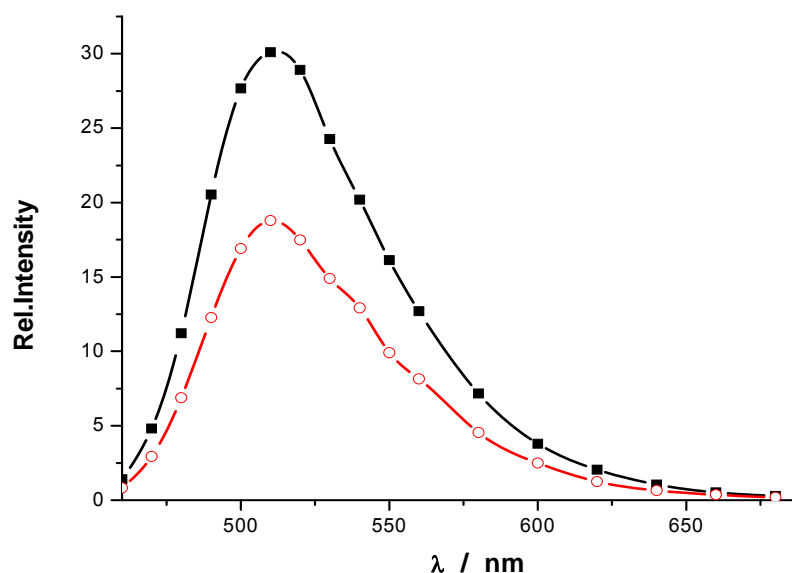
The UV-visible absorption spectrum of aqueous SDS solution of mono-protonated proflavine (PH^+) exhibits a maximum absorption band at 455 nm [164], whereas it exhibits a maximum at 445 nm in aqueous solution [165,166] with high molar extinction coefficients, suggesting π,π^* character bands [167, 168] (Figure 7.1). The parent proflavine (P) has a maximum absorption band at 400 nm in aqueous SDS solution as well as in water [164,166]. The concentration of PH^+ solution was determined from its optical absorption using a molar extinction coefficient of $4.1 \times 10^4 \text{ M}^{-1}\text{cm}^{-1}$ at 445 nm [167] before and after irradiation, where $[\text{PH}^+]$ was changed during measurements due to its adsorption on the wall of the cell.

Figure 7.1. Steady-state UV-visible absorption spectra of PH^+ in 0.05 M aqueous SDS solution (solid line) and in aqueous solution (dashed line) at room temperature.



The fluorescence behaviour of proflavine depends on the pH value of the solution as well as the nature of the solvent. The fluorescence lifetime of proflavine was reported as 5 ns in both aqueous SDS and water solutions in the pH range 5-10 [164]. The fluorescence quantum yield of PH^+ was determined to be 0.37 ± 0.03 based on what is reported previously [164,167]. Figure 7.2 shows the fluorescence spectra of PH^+ in aqueous solution with maximum at 510 nm [167a, 169] following 355 nm laser excitation at two different light intensities. The fluorescence spectrum of $^1\text{PH}^{+*}$ at low laser intensity has the same shape as that at high intensity, differing only in signal intensity, indicating that the PH^+ singlet state is the only emitting species.

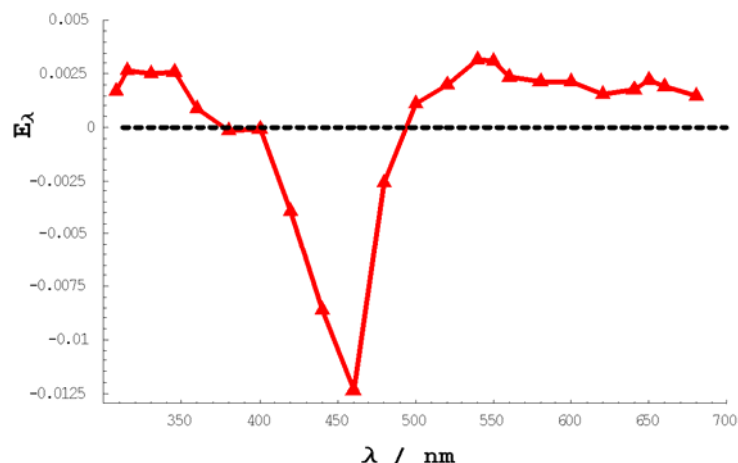
Figure 7.2. Fluorescence spectra of an aqueous solution of 1.85×10^{-5} M PH^+ obtained by 355 nm laser excitation at two different laser intensities. Squares (575 mJ/cm^2) and circles (15 mJ/cm^2).



7.2. Transient absorption spectra

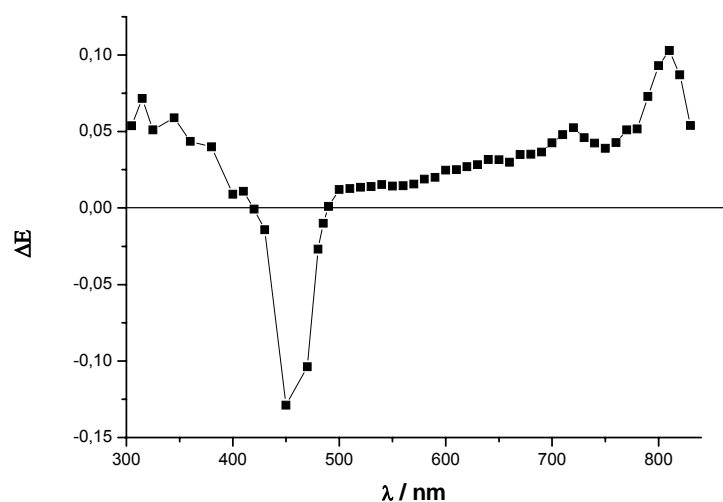
At very low laser intensity, the transient absorption spectrum of PH^+ in aqueous SDS solution obtained immediately after the laser pulse (355 nm) shows absorption bands around 540-550 nm and at 650 nm. These absorptions were quenched by molecular oxygen and were attributed to the triplet state [170,171]. The transient also shows a strong bleaching centered at around 450 nm due to ground state absorption of PH^+ as shown in Figure 7.3.

Figure 7.3. Triplet-triplet transient absorption spectrum of 2.84×10^{-5} M PH^+ of 0.05 M aqueous SDS solution in N_2O -saturated solution obtained via 355 nm laser excitation at low intensity, ca., 24 mJ / cm^2 , at room temperature.



The transient absorption spectrum of PH^+ following 355 nm laser pulse at high intensity exhibits a maximum at 810 nm and a shoulder around 730 nm (Figure 7.4). Molecular oxygen has no significant influence on the absorption decay curves at these wavelengths. This transient absorption has already been identified as the monoprotonated proflavine radical cation, $\text{PH}^{2+\bullet}$, [172,173].

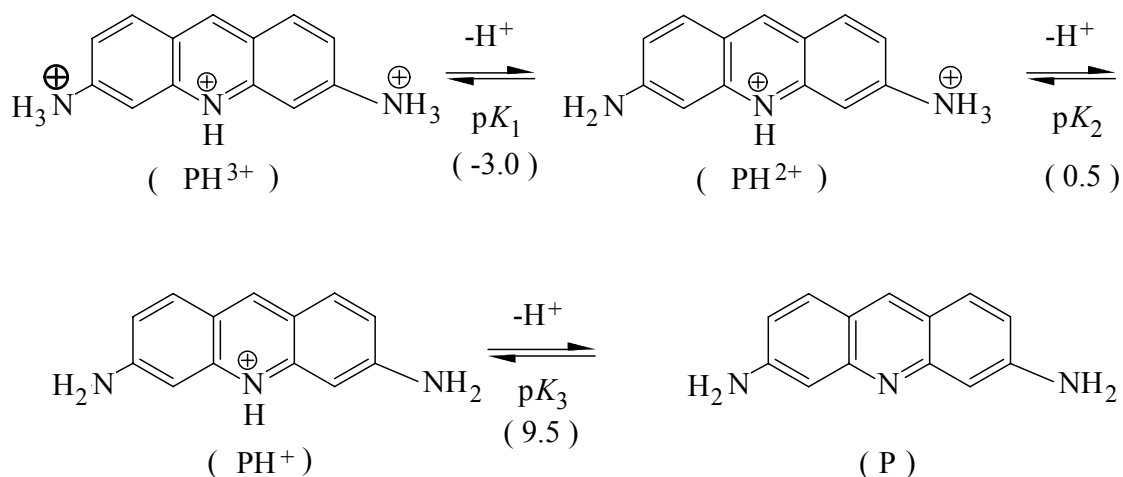
Figure 7.4. Transient absorption spectrum of 2.53×10^{-5} M PH^+ in N_2O -saturated aqueous solution obtained via 355 nm laser excitation at high intensity (ca., 678.5 mJ / cm^2) at room temperature.



Transient absorption spectra resulting from laser flash photolysis in aqueous media were measured in the range 500-830 nm at various laser intensities. The transient absorption spectra obtained under excitation conditions possess the same shape with different intensities, confirming that only a single species is responsible for the transient absorption spectra, which was identified as the $\text{PH}^{2+\bullet}$.

7.3. Photoionization mechanism at 355 nm

The proflavine molecule has three nitrogen atoms; all of which can accept a proton to form a protonated proflavine. Therefore, the structure of proflavine depends strongly on the pH of solution. The pK values for the acid-base equilibrium of proflavine in aqueous solution as shown in Scheme 7.1 were reported previously [174]. Our measurements were carried out in the pH range 3-8. In this pH range, the ground state and the excited state species are mainly the PH^+ , corresponding to protonation of the central tertiary nitrogen [164].



Scheme 7.1

To verify the photoionization mechanism of PH^+ in aqueous SDS solution following 355 nm laser pulse, we studied the effect of laser intensity on electron yield, the $\text{PH}^{2+\bullet}$ yield measured at 810 nm and the fluorescence intensity of the monoprotonated proflavine singlet state, ${}^1\text{PH}^{+\bullet}$ measured at 510 nm.

Laser intensity dependence of the hydrated electron curve shows a non-linear behaviour at low laser intensity. The electron yield increases along with the increase of the laser intensity and its concentration exceeds the initial concentration of the substrate. The effect of laser intensity on the fluorescence intensity of ${}^1\text{PH}^{+\bullet}$ was investigated as depicted in Figure 7.5. At low laser intensity, the fluorescence intensity increases linearly with an increased the laser intensity and passes through a maximum intensity, followed by a gradual decline. This behaviour of fluorescence intensity is a strong evidence that photoionization from singlet state

can be an important pathway. Unfortunately, the triplet state of PH^+ has a very low absorption under our experimental settings. Therefore, it is not possible to investigate the effect of laser intensity on its yield.

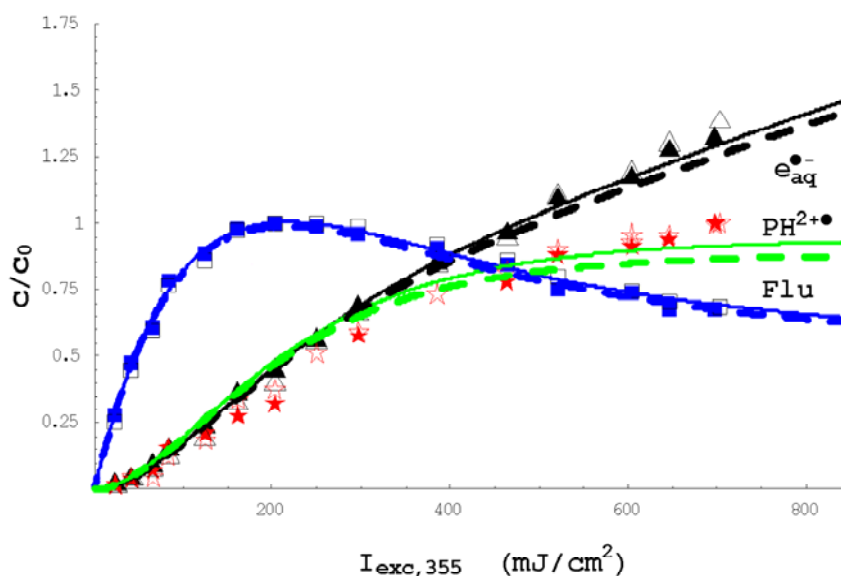


Figure 7.5. Laser intensity dependence I_{exc} of the fluorescence intensity of ${}^1\text{PH}^{2+}$ (squares), the normalized absorption of the PH^{2+} (stars) and the concentration of the hydrated electron (triangles) relative to the initial concentration of substrate obtained upon 355 nm laser excitation of monoprotonated proflavine c_0 (open symbols; $2.84 \times 10^{-5}\text{M}$ and filled symbols; $1.8 \times 10^{-5}\text{M}$) in 0.05 M aqueous SDS solution. The fluorescence was normalized and measured at 510 nm. The absorption of PH^{2+} and the hydrated electron were monitored and calculated at 810 and 829 nm, respectively. The solid and dashed lines were calculated based on Schemes 3.6 and 7.2, respectively. The best-fit parameters were found to be $\kappa_1 = 8.9 \times 10^{-3}\text{cm}^2\text{mJ}^{-1}$, $\kappa_2 = 1.04 \times 10^{-3}\text{cm}^2\text{mJ}^{-1}$, $\kappa_3 = 1.31 \times 10^{-3}\text{cm}^2\text{mJ}^{-1}$ (Scheme 3.6); $\kappa_1 = 9.2 \times 10^{-3}\text{cm}^2\text{mJ}^{-1}$, $\kappa_3 = 1.35 \times 10^{-3}\text{cm}^2\text{mJ}^{-1}$ (Scheme 7.2). The other best-fit parameters were equal in both cases and were found to be scale factor of the fluorescence is 7.6, scale factor for product = 1.32. Constant parameters were $\kappa_0 = 7.9 \times 10^{-3}$, $k_f \tau = 4.4 \times 10^{-1}$, $k_{\text{isc}} \tau = 0.756$, $\chi T = 1.2$.

A nonlinear dependence between the laser intensity and the initial absorbance of PH^{2+} at 810 nm was observed. These observations are a strong indication that the photoionization of PH^+ in aqueous SDS involves more than two photons.

Photoionization of PH^+ in aqueous solution yields more than one electron. The behaviour of all observed species resulting from the photoreaction of PH^+ in aqueous solution (Figure 7.6) following 355 nm light is analogous to that in aqueous SDS solution. On the basis of

laser flash photolysis, Pileni and Gräzel [164] reported that PH^+ in water photoionizes monophotonically to its respective radical cation and the hydrated electron. Our laser flash photolysis measurements showed that the formation of both the hydrated electron and PH^{2+} proceeds through a multi-photonic mechanism.

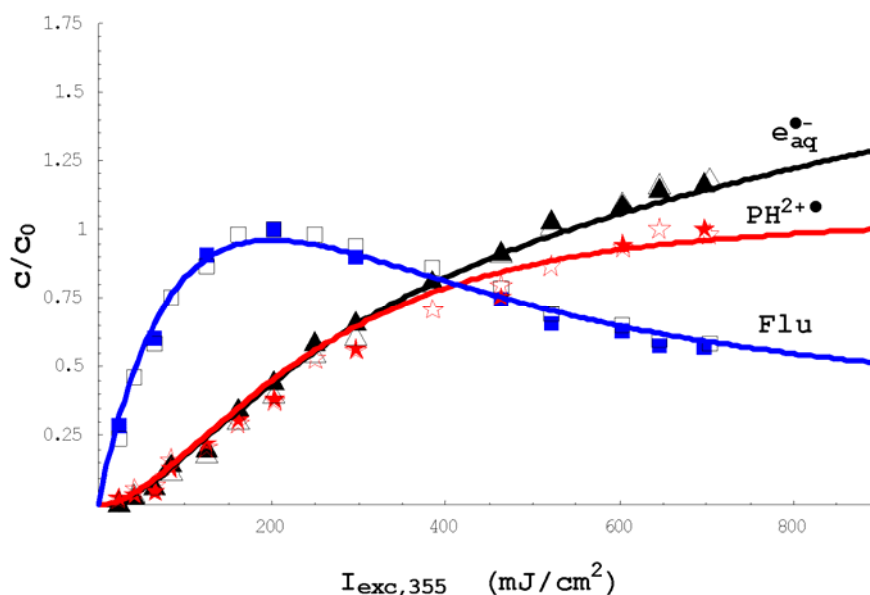
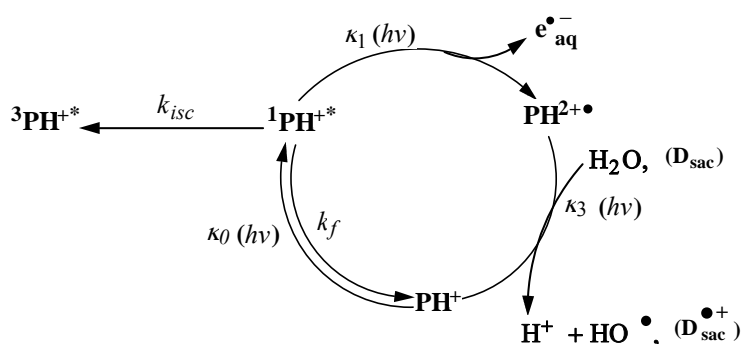


Figure 7.6. Laser intensity dependence $I_{\text{exc},355}$ of the fluorescence intensity (Flu) of $^1\text{PH}^{2+}$ (squares), the normalized absorption of the $\text{PH}^{2+\bullet}$ (stars), and the concentration of the hydrated electron (triangles) relative to the initial concentration of substrate obtained upon 355 nm laser excitation of monoprotonated proflavine c_0 (open symbols; $2.84 \times 10^{-5}\text{M}$ and filled symbols; $1.8 \times 10^{-5}\text{M}$) in aqueous solution. The fluorescence was normalized and measured at 510 nm. The absorption of $\text{PH}^{2+\bullet}$ and the hydrated electron were monitored and calculated at 810 and 829 nm, respectively. The solid lines were calculated based on Scheme 3.6. The best calculated parameters were found to be $\kappa_1 = 5.1 \times 10^{-3}\text{ cm}^2\text{mJ}^{-1}$, $\kappa_2 = 2 \times 10^{-3}\text{ cm}^2\text{mJ}^{-1}$, $\kappa_3 = 6.1 \times 10^{-4}\text{ cm}^2\text{mJ}^{-1}$, fluorescence scale factor = 4.7, product scale factor = 1.23. Constant parameters were $\kappa_0 = 1.38 \times 10^{-2}\text{ cm}^2\text{mJ}^{-1}$, $k_f \tau = 0.44$, $k_{\text{isc}} \tau = 0.756$, $\chi \tau = 1.2$.

The fluorescence signal intensity does not reach zero at $I_{\text{exc}} \rightarrow \infty$ as in the case of linear photoionization mechanism. Furthermore, the electron concentration was measured at the end of the laser pulse and found to be greater than the concentration of substrate, indicating that the photoionization completely ended within the time period of the laser pulse (6 ns). Therefore, the photoionization of PH^+ occurs through a cyclic mechanism. The photoreaction involves only the proflavine-derived species and either water or SDS and water. Hence, the mechanism of such a photoionization involves water or SDS as a reducing agent.

Photoreduction of the oxidized species by its photoreaction with water was also observed in the photoionization process of the tris(bipyridyl)ruthenium ion [87,88].



Scheme 7.2

Owing to the lack of triplet absorption of PH^+ , we consider two reaction mechanisms for photoionization of PH^+ . First, photoionization proceeds via a cyclic mechanism involving the singlet state channel according to Scheme 7.2. Second, photoionization proceeds with both excited singlet and triplet state channels based on Scheme 3.6. The rate constant of the internal conversion of the $^1\text{PH}^{+*}$ (k_{ic}) has not been reported till date and can be neglected. We calculate the curves of the observed species numerically using the known parameters k_f and k_{isc} . χ and τ were measured. κ_0 was calculated from Eq. (3.6). Therefore, the number of unknown parameters reduces to κ_1 , κ_3 , the scale factor for $\text{PH}^{2+\bullet}$, the fluorescence of $^1\text{PH}^{+*}$, and/or κ_2 . Our attempts to fit the experimental data for all detectable species based on Scheme 7.2 give good results for the experimental data of electron and fluorescence of $^1\text{PH}^{+*}$ but not for the $\text{PH}^{2+\bullet}$ (Figure 7.5). In other words, the kinetic model is incomplete.

Fitting the experimental data of the observed species according to Scheme 3.6 displays that the result is somewhat better than that based on Scheme 7.2. When the kinetic constant of the triplet photoionization (κ_2) approaches a zero value, the photoionization would proceed via singlet-excited state channel only, but the outcome of the fit process in Figure 7.5 displays that the κ_2 value is $1.04 \times 10^{-3} \text{ cm}^2\text{mJ}^{-1}$. Therefore, it is evident that the photoionization of PH^+ in water and SDS proceeds via a cyclic reaction with both excited singlet and triplet states as displayed in Scheme 3.6.

The lack of the saturation of the absorption at 810 nm may be due to the contribution for the absorption of $\text{PH}^{2+\bullet}$ by another absorbing proflavine derived species, PH^d , which may be derived from $\text{PH}^{2+\bullet}$. Thus, the absorption of PH^d is related to the electron concentration, and then, the absorption at 810 nm can be expressed as:

$$\Delta E_{810}^{obs} = (\beta([PH^{2+\bullet}]_{rel} + \gamma[e_{aq}^{\bullet-}]_{rel})) \quad \text{Eq. (7.1)}$$

$$\beta = \varepsilon_{(PH^{2+\bullet}, 810)} d C_0 \quad \text{and} \quad \gamma = b \varepsilon_{(PH^d, 810)} d C_0$$

where b is a scaling factor that gives the ratio of the concentration of PH^d to the concentration of the hydrated electron at 810 nm. $\varepsilon_{(PH^d, 810)}$ and $\varepsilon_{(PH^{2+\bullet}, 810)}$ are the extinction coefficients of PH^d and $PH^{2+\bullet}$ at 810 nm, respectively.

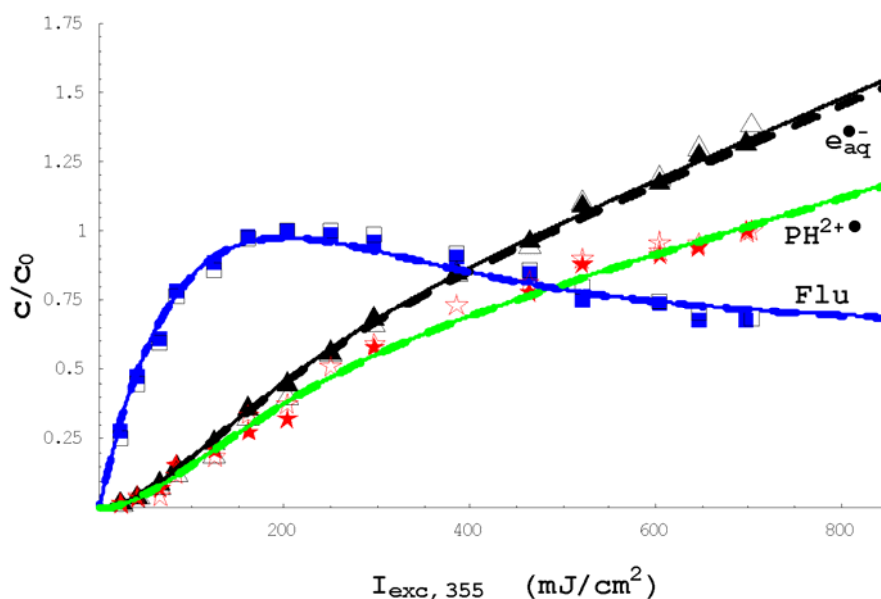


Figure 7.7. Effect of laser intensity on the observed species as in Figure 7.5. The solid and dashed lines were calculated based on Scheme 3.6 and 7.2, respectively. The best parameter was found to be $\kappa_3 = 2.2 \times 10^{-3} \text{ cm}^2 \text{ mJ}^{-1}$. The other best-fit parameters were equal in both cases and were found to be $\kappa_1 = 1.12 \times 10^{-3} \text{ cm}^2 \text{ mJ}^{-1}$, $\kappa_2 = 3.63 \times 10^{-4}$, $k_{isc} \tau = 0.756$, $\chi \tau = 1.2 \text{ cm}^2 \text{ mJ}^{-1}$, the scale factor of the fluorescence was 8.28, the scale factor for product = 0.174, the scale factor for $PH^d = 0.687$. Constant parameters were $\kappa_0 = 7.9 \times 10^{-3}$, $k_f \tau = 4.4 \times 10^{-1}$.

The simultaneous fit based on Scheme 3.6 for electron and fluorescence and according to Eq. (7.1) for the absorbance at 810 nm was depicted in Figure 7.7 and is somewhat better than that of Scheme 3.6. The fit curves show that the κ_1 value is greater than that of κ_2 . This result is a strong evidence that photoionization from singlet state can be a dominant pathway. The latter results are in agreement with the previously reported results by Kalyanasundaram and Dung [163], where they proposed that the triplet state yields an electron concentration of less than 10%. The electron yield of photoreaction of PH^+ in aqueous SDS solution is more than that in water, where SDS enhances the photoionization quantum yield and respective rate constant [139].

Part II.B

Electron acceptor photoionization

8. Photoionization of xanthone/amine systems

Quenching of carbonyl triplet state can occur through different mechanisms depending on the nature of the quencher as well as the carbonyl compound [175-182]. The photoionization of an electron acceptor (e.g., aromatic ketones) in the presence of amine was studied by laser flash photolysis [52, 53, 89]. Photoinduced electron transfer of such system produced a radical anion that can be ionized by absorption of a photon. Our investigations of X/amine show that the electron yield in the presence of amine in high concentration is about 5 times higher than that without amine in methanol-water solution. In this chapter we provide evidence that the photoionization of xanthone radical anion, $X^{\bullet-}$, is a one-photon ionization process at 308 and 355 nm, whereas it is a two-photon ionization process at 532 nm.

8.1. Direct generation of xanthone radical anion

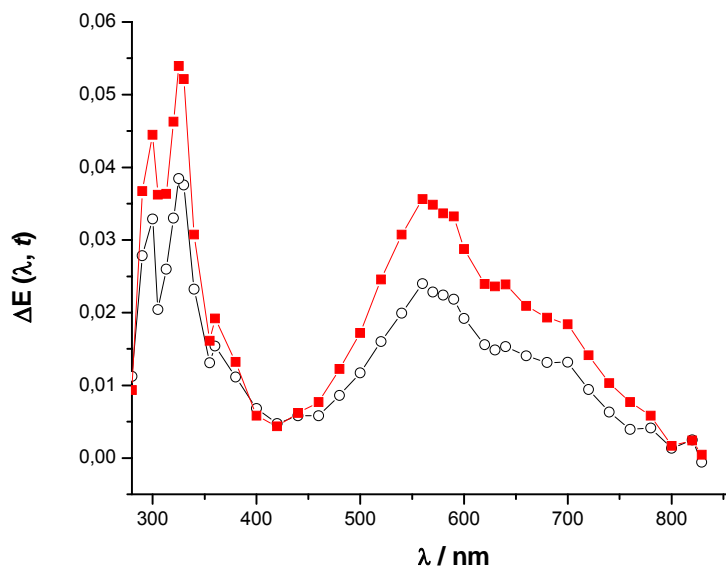
Excitation of xanthone at 308 nm in the presence of a relatively high concentration of TEA (0.3 M) in N_2O -saturated aqueous 0.05 M SDS solution produces a transient absorption spectrum corresponding to the xanthone radical anion, $X^{\bullet-}$, (Figure 8.1). The transient spectra show maximum absorptions at 325 nm and at around 560-750 nm [185]. A similar transient absorption spectrum was observed 20.5 μ s after laser excitation, indicating that there is a secondary reaction, which produces the same xanthone-derived species that results from the electron transfer process.

The ϵ ($X^{\bullet-}$) value in methanol-water mixture was determined, by complete conversion of the starting xanthone, to be $2000 \pm 10\% \text{ l M}^{-1}\text{cm}^{-1}$ at 590 nm. The corrected absorption spectrum of the $X^{\bullet-}$ was obtained by applying a correction for the amount of the parent X depleted.

The transient absorption due to xanthone ketyl radical has an absorption maximum at around 500 nm [126a, 183]. However, we did not observe an absorption in this region, possibly due to the fact that the molar extinction coefficient of the ketyl radical is too small. Abe, et al. [184] found that the benzophenone radical anion is produced instead of benzophenone ketyl radical or the amine complex following 308 nm laser flash photolysis of

the benzophenone/TEA system in polar solvents with a dielectric constant greater than 11. Furthermore, xanthone ketyl radical is not formed at a high pH value [52].

Figure 8.1. Transient absorption spectra of the xanthone radical anion in N₂O-saturated solution at room temperature obtained from 2×10^{-4} M xanthone in aqueous 0.05 M SDS solution in the presence 0.3 M TEA obtained by 308 nm laser excitation (16.33 mJ/cm^2). The time delay is 500 ns (open circles) and $20.5 \mu\text{s}$ (squares) after laser pulse.



8.2. Rate constants for xanthone triplet quenching by amine

The effects of the concentration of the electron donor (e.g., TEA or DABCO) on the triplet lifetime of $^3\text{X}^*$ were examined (see Figure 8.2 and 8.3). It is evident that the rate of decay of $^3\text{X}^*$ is significantly increased with an increase in the concentration of amine. The decay of the triplet in the presence of TEA led to a residual absorption with a long lifetime, which can be attributed to the X radical anion, and hence the absorbance response curves can be approximated as follows:

$$\Delta E(\lambda, t) = A \exp[-k_{obs}.t] + B \quad \text{Eq. (8.1)}$$

where $k_{obs} = k_q [Q]$. A and Q are pre-exponential factor and the quencher concentration, respectively. B is the residual absorption.

The second-order rate constant, k_q , was obtained by plotting k_{obs} versus amine concentrations. The obtained k_q values were found to be $1.5 \times 10^9 \text{ M}^{-1}\text{s}^{-1}$ for TEA and $1.7 \times 10^9 \text{ M}^{-1}\text{s}^{-1}$ for DABCO. The concentration of amine necessary to reduce the triplet lifetime to a few nanoseconds can be easily determined from the previous experimental measurements.

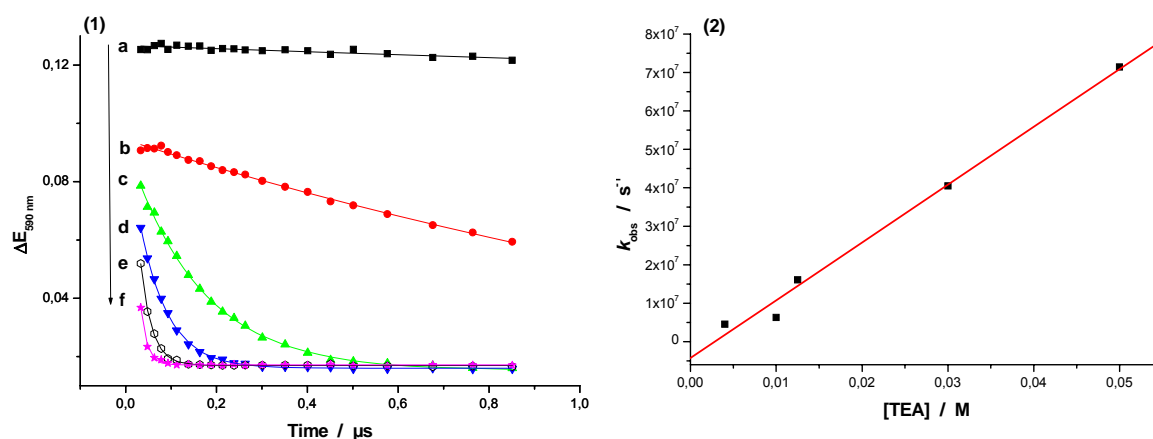


Figure 8.2. (1) Absorption–time profiles at 590 nm of xanthone triplet state in the presence different concentrations of TEA obtained by 355 nm laser excitation (29.17 mJ/cm^2). The concentrations of TEA are as follows: without amine (squares), 0.004 M TEA (closed circle), 0.01 M (triangles), 0.0125 M (inverted triangles), 0.03 M (open circles), 0.05 M (stars). The solid curves are the best fitting of Eq. (8.1). (2) The relationship between observed rate constant (k_{obs}) of quenching the triplet state of xanthone versus the concentrations of TEA.

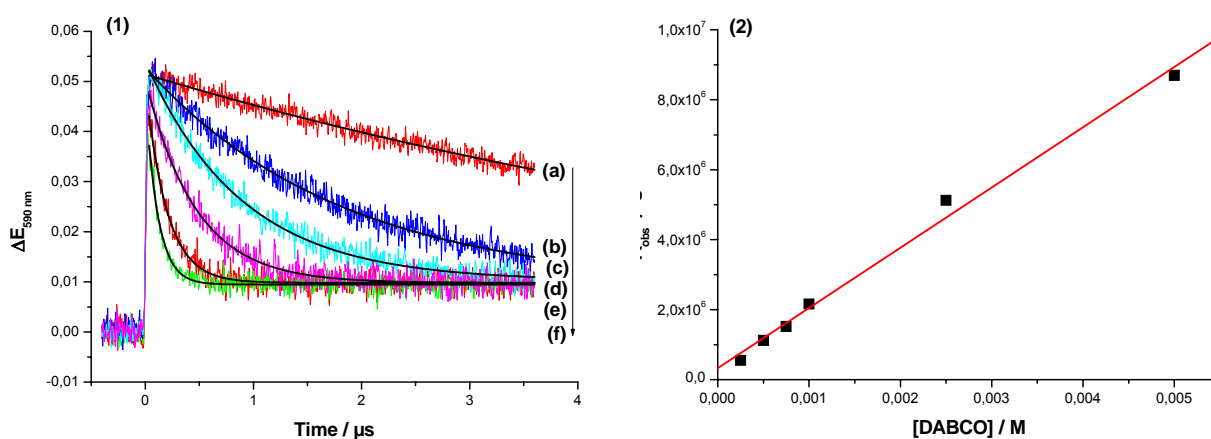
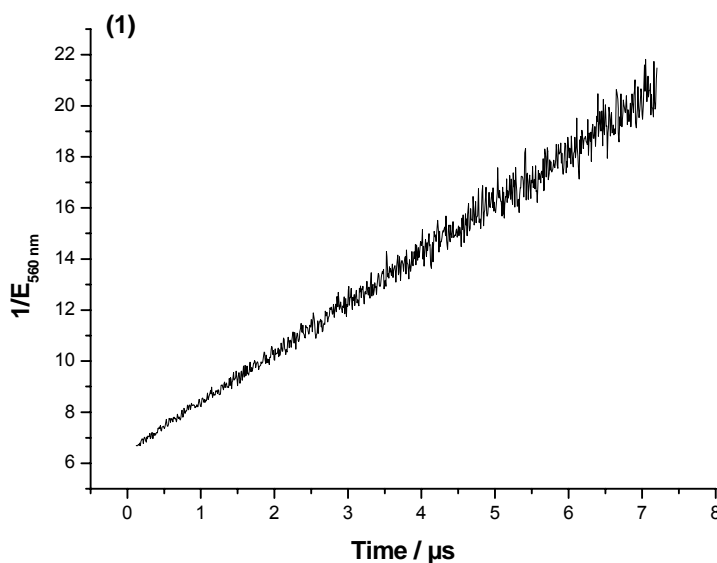


Figure 8.3. (1) Absorption–time profiles at 590 nm of the xanthone triplet state in the presence of different concentrations of DABCO obtained by 308 nm laser excitation (15.6 mJ/cm^2). The concentrations of DABCO were: (a) $2.5 \times 10^{-4} \text{ M}$; (b), $5 \times 10^{-4} \text{ M}$; (c), $7.5 \times 10^{-4} \text{ M}$; (d), $1 \times 10^{-3} \text{ M}$; (e), $2.5 \times 10^{-3} \text{ M}$; (f), $5 \times 10^{-3} \text{ M}$. The solid curves show the best fits to Eq. (8.1). (2) The relationship between pseudo-first-order rate constant (k_{obs}) for the decay transient absorption of the xanthone triplet state vs DABCO concentrations.

8.3. Back electron transfer

Figure 8.4 displays the time dependence of the reciprocal of the absorption of $X^{\bullet-}$ at 560 nm. The decay time profile of the absorption radical anion follows second-order kinetics [Eq. (8.2)] suggesting that a back electron transfer process (k_{bet}) takes place from $X^{\bullet-}$ to $DABCO^{\bullet+}$ [193].

Figure 8.4. Time dependence of the reciprocal of the absorption of $X^{\bullet-}$ at 560 nm. Excitation of 2.1×10^{-4} M X in the presence of 0.2 M DABCO in methanol-water (1:2 v/v), pH 11 at 355 nm light (FWHM~ 6 ns, 172 mJ/cm²)



$$\frac{1}{E(\lambda, t)} = \frac{1}{E(\lambda, 0)} + \frac{k_{bet}}{\varepsilon_{\lambda} d} t \quad \text{Eq. (8.2)}$$

A plot of the reciprocal of the absorbance versus time is linear. Thus, the bimolecular rate constant reaction between $X^{\bullet-}$ and $DABCO^{\bullet+}$ was calculated to be $1.5 \times 10^9 \text{ M}^{-1} \text{ s}^{-1}$.

8.4. Secondary reaction of the xanthone ground state

Figure 8.5 (1) shows the measurements of the product rise due to the $X^{\bullet-}$ at 560 nm in N_2O -saturated solution at four different xanthone concentrations in the range (2×10^{-5} – 2×10^{-4} M). The pseudo-first-order rate constants (k_{obs}) for the slow formation of xanthone radical anion increase with an increase in xanthone concentration. The kinetic absorbance of the growth curves was fitted by a single exponential rise function.

A plot of the rate constant k_{obs} versus the xanthone concentration (Figure 8.5 (2)) yields a straight line whose slope of $(2.1 \pm 0.3) \times 10^9 \text{ l mol}^{-1} \text{ s}^{-1}$ represents the bimolecular rate constant reaction between xanthone ground state and α -aminoalkyl radical [89].

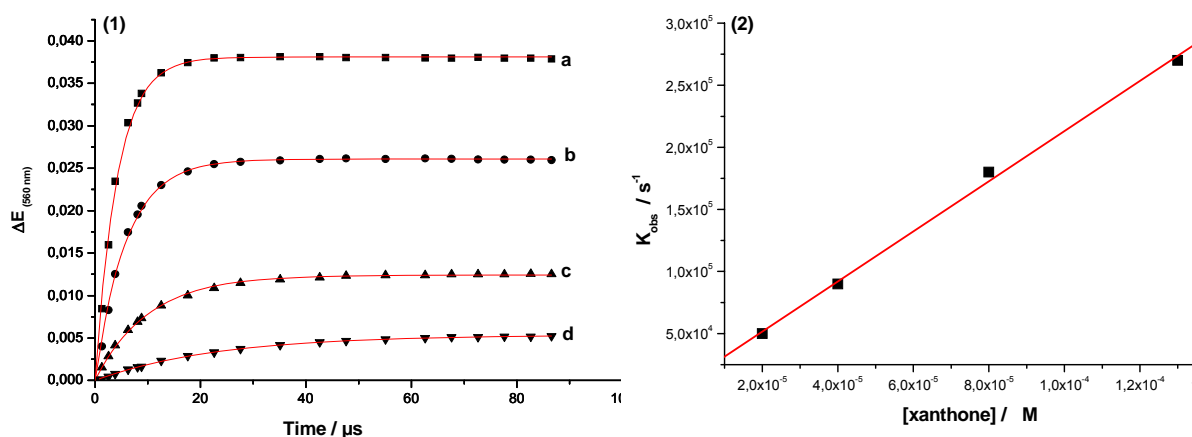


Figure 8.5. (1) The time–profile of the transient absorption due to xanthone radical anion with different initial concentrations of xanthone ground state in the presence of 0.15 M TEA produced by 355 nm excitation (29 mJ/cm^2) in methanol-water 1:2 v/v. Concentrations of xanthone were: $2 \times 10^{-5} \text{ M}$ (inverted triangles); $4 \times 10^{-5} \text{ M}$ (triangles); $8 \times 10^{-5} \text{ M}$ (circles); $1.3 \times 10^{-4} \text{ M}$ (squares). The curves were fitted with a monoexponential rise function. **(2)** The relationship between Pseudo-first-order rate constant (k_{obs}) for the transient absorption of xanthone radical anion vs initial xanthone concentration.

8.5. Cyclic photoionization of xanthone radical anion in methanol-water solution

The presence of absorption characteristic of the aqueous electron in the X/amine system following laser flash photolysis excitation indicates the photoionization of this system. To obtain information about the mechanism of laser photoionization of X/amine in methanol-water solution following a 308 nm laser pulse, the dependence of the absorption of $e_{\text{aq}}^{\bullet -}$ on the laser intensity was investigated as shown in Figure 8.6. The absorption curve exhibits an induction period at low laser intensity, suggesting that a monophotonic process can be ruled out. The induction period is followed by a linear increase of the electron absorption with increasing laser intensity.

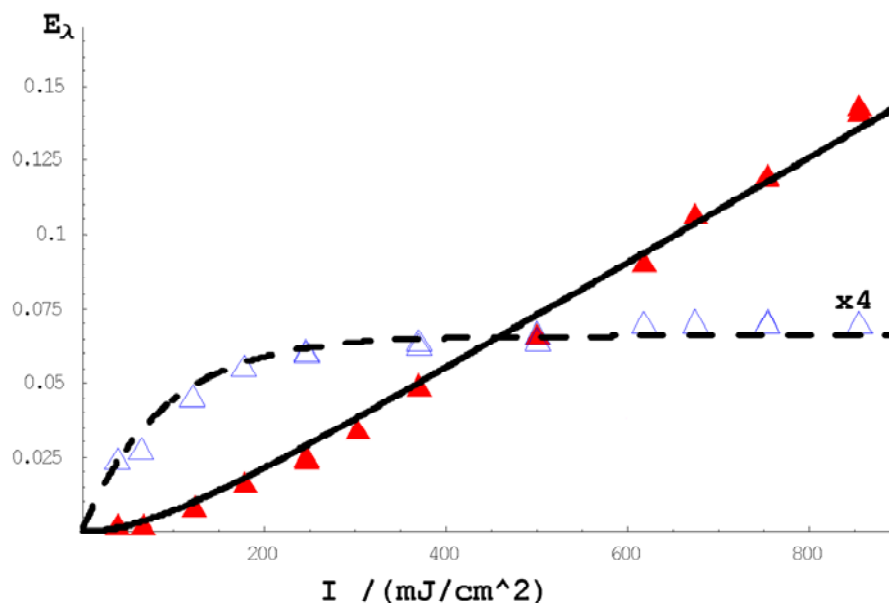


Figure 8.6. Absorbances of the hydrated electron (closed triangles, soiled lines) and the xanthone radical anion (open triangles, dashed line) resulting from the photoreaction of 2.1×10^{-5} M xanthone in methanol-water 1:2 v/v, pH 11, in the presence of 0.3M TEA versus laser intensity (308 nm). The lines represent a global fit of Eqs. (3.44) and (3.45) to the experimental data sets. The absorption data and the fit curve of the xanthone radical anion ($\lambda = 560$ nm, solution saturated with N_2O) multiplied with factor of 4. Constant parameters as in Fig 5.5. Fitting parameters were $\kappa_4 = 1.9 \times 10^{-3} \text{ cm}^2\text{mJ}^{-1}$, $\varepsilon_{560}(X^{\bullet-}) = 2100 \text{ M}^{-1}\text{cm}^{-1}$. When $\varepsilon_{560}(X^{\bullet-})$ was treated as a constant parameter and κ_0 as an adjustable parameter, the best-fit parameters were: $\kappa_0 = 8.6 \times 10^{-3} \text{ cm}^2\text{mJ}^{-1}$, $\kappa_4 = 1.9 \times 10^{-3} \text{ cm}^2\text{mJ}^{-1}$.

The electron concentration at the highest laser intensity is greater than the initial concentration of the substrate by almost 30 %. The absorbance of $X^{\bullet-}$ increases linearly with increasing laser intensity, followed by saturation behaviour at high laser intensity (Figure 8.6), where the photoinduced electron transfer is a monophotonic process. From these results, Scheme 3.7 provides a valid description of the photoreaction of the X/amine system. The intensity dependences of the concentrations of the detectable species can be expressed in the form of the absorption. A good result of the fitting processes of Eqs. (3.44) and (3.45) in the form of the absorption to the data sets is shown in Figure 8.6.

As a result of the electron transfer process in the X/DABCO system, the concentration of both $DABCO^{\bullet+}$ and $X^{\bullet-}$ are equal at the given laser intensity. Scheme 3.7 shows that the xanthone anion radical can be photoionized to produce a hydrated electron. Therefore, the concentration of $DABCO^{\bullet+}$ in this system is given by

$$[\text{DABCO}^{\bullet+}] = [\text{X}^{\bullet-}] + [\text{e}^{\bullet-}_{\text{aq}}] \quad \text{Eq. (8.3)}$$

The transient absorption at 460 nm [194] is not only due to $\text{DABCO}^{\bullet+}$ but also to $\text{X}^{\bullet-}$. The absorption can therefore, be expressed as

$$E_{\lambda} = E_{\lambda, \text{X}^{\bullet-}} + E_{\lambda, \text{DABCO}^{\bullet+}} \quad \text{Eq. (8.4)}$$

$$E_{\lambda} = E_{\lambda, \text{X}^{\bullet-}} + \varepsilon_{\lambda, \text{DABCO}^{\bullet+}} [\text{DABCO}^{\bullet+}] \cdot d \quad \text{Eq. (8.5)}$$

Combination of Eq. (8.3) with Eq. (8.5) yields

$$E_{\lambda} = (\varepsilon_{\lambda, \text{X}^{\bullet-}} + \varepsilon_{\lambda, \text{DABCO}^{\bullet+}}) [\text{X}^{\bullet-}] d + \varepsilon_{\lambda, \text{DABCO}^{\bullet+}} [\text{e}^{\bullet-}_{\text{aq}}] \cdot d \quad \text{Eq. (8.6)}$$

$$E_{\lambda} = (\varepsilon_{\lambda, \text{X}^{\bullet-}} + \varepsilon_{\lambda, \text{DABCO}^{\bullet+}}) [\text{X}^{\bullet-}] d + \frac{\varepsilon_{\lambda, \text{DABCO}^{\bullet+}}}{\varepsilon_{\lambda, \text{e}^{\bullet-}_{\text{aq}}}} E_{\lambda, \text{e}^{\bullet-}_{\text{aq}}} \quad \text{Eq. (8.7)}$$

Figure 8.7 displays that the signal intensity of the absorption at 460 nm due to both radicals is directly proportional to the signal intensity at 829 nm due to the hydrated electron absorption. The slope of this relationship represents the ratio of the extinction coefficient of $\text{DABCO}^{\bullet+}$ at 460 nm to that of $\text{e}^{\bullet-}_{\text{aq}}$ at 829 nm. $\varepsilon(\text{DABCO}^{\bullet+})$ at 460 nm was found to be $2000 \pm 10\% \text{ M}^{-1} \text{ cm}^{-1}$ [195].

Figure 8.7. Plots of the absorbance of radicals (measured at 460 nm in N_2O -saturated solution) versus the absorption of the hydrated electron obtained upon 308 nm excitation of xanthone (closed triangles 2.25×10^{-5} ; open triangles, 4×10^{-5} M) in methanol-water (1:2 v/v), pH 11. Each point of the absorption for radicals and electron was taken at the same laser intensity.

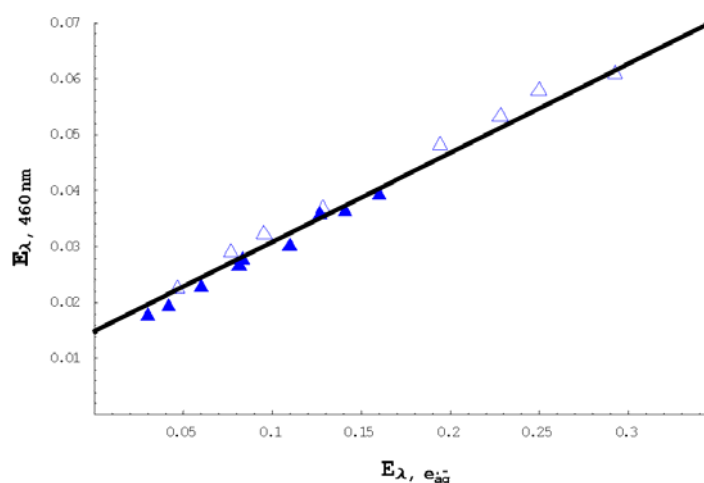


Figure 8.8 describes the effect of laser intensity on the absorption due to all species produced by the photoreaction of the X/DABCO system. In this system, the electron absorption increases with increasing the laser intensity.

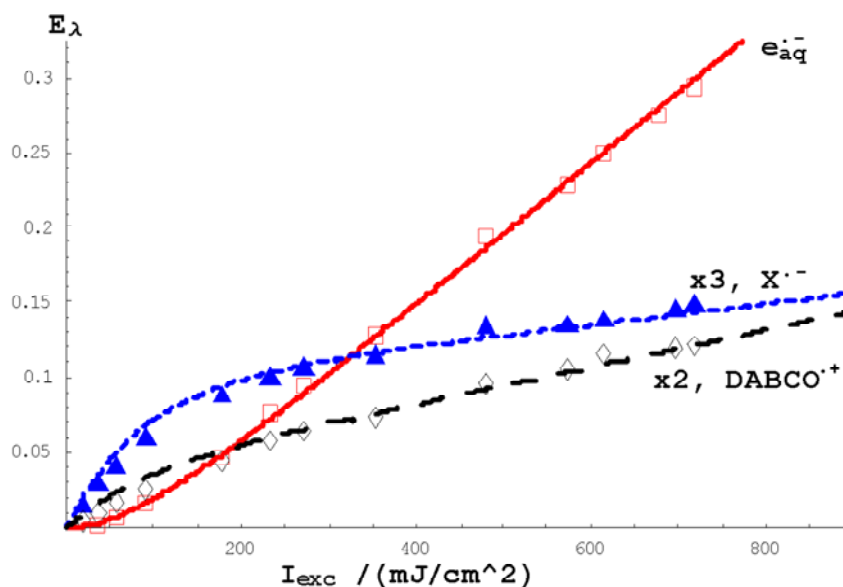


Figure 8.8. Absorbances (E_λ) due to radicals (measured at 460 nm, open triangles, short dashed line; 560 nm, closed triangles, long dashed line in N_2O -saturated solution) and the hydrated electron (measured at 829 nm, open square, solid line) obtained upon 308 nm excitation of $4 \times 10^{-5} M$ xanthone in the presence of 0.15 M DABCO in methanol-water (1:2 v/v), pH 11. The curves were fitted with Eqs. (8.6) for radicals and (3.45) for electron. Constant parameters as in Figure 8.9. The best-fit parameters were $\kappa_4 = 2.7 \times 10^{-3} \text{ cm}^2 \text{ mJ}^{-1}$, $\epsilon(460 \text{ nm, DABCO}^{\bullet+}) = 1800 \text{ M}^{-1} \text{ cm}^{-1}$, $\epsilon(560 \text{ nm, X}^{\bullet-}) = 2000 \text{ M}^{-1} \text{ cm}^{-1}$.

The fit of the experimental data for $X^{\bullet-}$ at 560 nm according to Eq. (3.44) does not give a reasonable result, so that this equation should be modified to Eq. (8.6), where both radicals have appreciable absorption at this wavelength. The extinction coefficient of DABCO radical cation at 460 nm was evaluated from the fitting process and found to be $1800 \text{ M}^{-1} \text{ cm}^{-1}$. This value is lowered than that displayed in Figure 8.7 by 10%.

The kinetic behaviour of the hydrated electron and xanthone radical anion curves obtained by the excitation of X/amine at 355 nm (Figure 8.9) is similar to that obtained at 308 nm. The quantum yield of the photoionization of the $X^{\bullet-}$ could be calculated from Eq. (3.13), and is found to be $0.07 \pm 10\%$ for excitation of X/TEA in methanol-water (1:2 v/v, pH 11), whereas it was found to be $0.086 \pm 10\%$ for excitation of X/DABCO system at both wavelengths (308 and 355 nm)

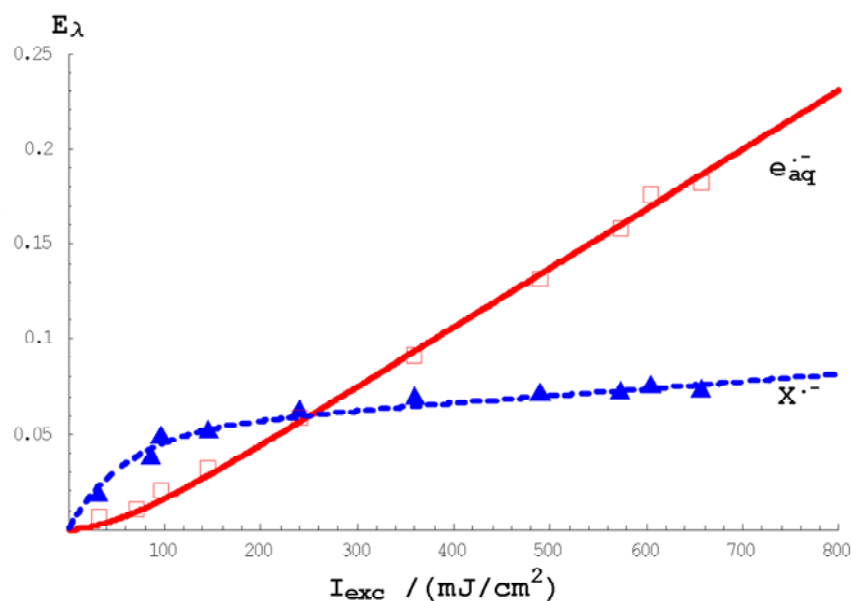


Figure 8.9. Absorbances of radical anion (measured at 560 nm, closed triangles, dashed line in N_2O -saturated solution) and the hydrated electron (measured at 829 nm, open square, solid line) obtained upon 355 nm excitation of $4 \times 10^{-5} M$ xanthone in the presence of 0.15 M DABCO in methanol-water 1:2 v/v, pH 11. The curves were fitted with Eqs. (8.6) for radical ions and (3.45) for $e_{aq}^{\cdot-}$. Fixed parameter $C_0 = 4 \times 10^{-5} M$, $d = 0.4$ cm. The best-fit parameters were $\kappa_0 = 1.52 \times 10^{-2} cm^2 mJ^{-1}$, $\kappa_4 = 1.5 \times 10^{-3} cm^2 mJ^{-1}$.

8.6. Cyclic photoionization of xanthone anion radical in aqueous SDS solution

Addition of electron donor such as TEA in aqueous SDS solution containing xanthone leads to the disappearance of the absorption due to the xanthone triplet. This does not mean that the triplet state is not formed, but rather that the quenching of the triplet state via electron transfer takes place in a time shorter than the laser pulse of the excitation source. This quenching process suggests the presence of X and TEA in the same micelle.

Laser excitation at 308 nm or at 355 nm of a solution containing 0.3 M DABCO in 0.05 M aqueous SDS solution did not produce a transient absorption at any wavelength, corroborating the notion that the transient absorptions result from excitation of xanthone.

The dependence of electron and xanthone radical anion concentration resulting from the excitation of X/amine in aqueous SDS solution on the laser intensity is similar to that in methanol-water solution as shown in Figure 8.10. The electron yield was studied in two different SDS concentrations. The electron yield and the kinetic constant of photoionization increase with an increase in SDS concentration from 0.01 M to 0.05 M (Figure 8.10).

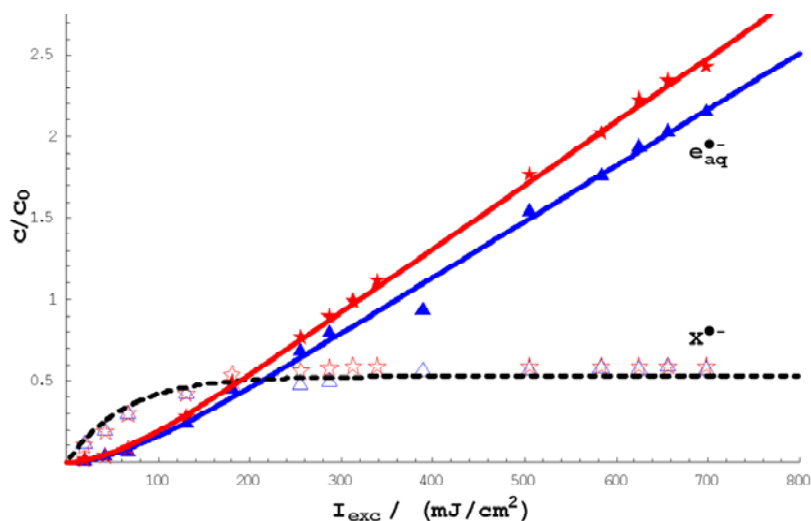
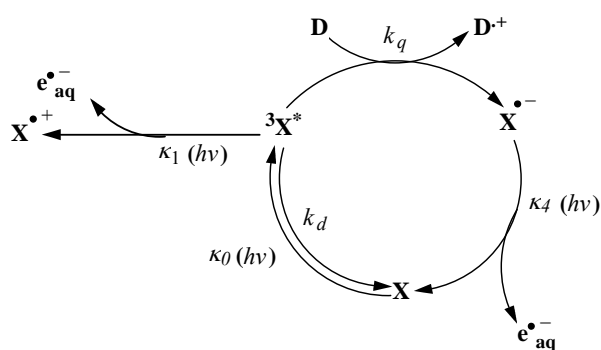


Figure 8.10. Concentrations c of the hydrated electron, $e_{aq}^{\bullet-}$, (closed symbols, soiled lines) and the xanthone radical anion, $X^{\bullet-}$, (open symbols, dotted line) relative to the initial concentration of xanthone c_0 resulting from the photoreaction of 4×10^{-5} M xanthone in aqueous SDS, in the presence of 0.3 M TEA as functions of the laser intensity (308 nm). The lines represent the best fits of the experimental data sets according to Eqs (3.44) for $X^{\bullet-}$ and (3.45) for $e_{aq}^{\bullet-}$; best-fit parameters: $\kappa_4 = 7.4 \times 10^{-3} \text{ cm}^2 \text{ mJ}^{-1}$ (0.05 M SDS), $\kappa_4 = 6 \times 10^{-3} \text{ cm}^2 \text{ mJ}^{-1}$ (0.01 M SDS). Constant parameter: $\kappa_0 = 8.3 \times 10^{-3} \text{ cm}^2 \text{ mJ}^{-1}$.

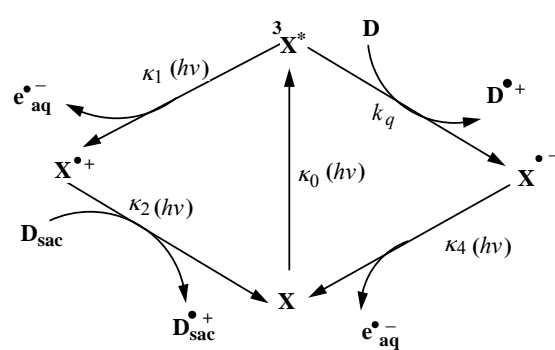
8.7. Combined triplet state and radical anion of xanthone photoionization pathways

Both triplet state and xanthone radical anion have appreciable absorption at the excitation wavelengths. The triplet state could play a role as a source of the hydrated electron at low quencher concentration as well as the radical anion, because the intermediacy of both cannot be neglected. If the radical anion formation is faster than triplet formation, the concentration of triplet at the end of the laser pulse could be neglected. Therefore, the radical anion is the predominant source of hydrated electrons.

Schemes 8.1 and 8.2 show the combination of both pathways in methanol-water (1:2 v/v) and 0.05 M aqueous SDS solution, respectively. The solution of the rate equations gives a complex closed-form expression, so that the numerical analysis of the effect of laser intensity on the electron concentrations at various quencher concentrations can be employed to verify the reaction mechanism and the obtained parameters.



Scheme 8.1



Scheme 8.2

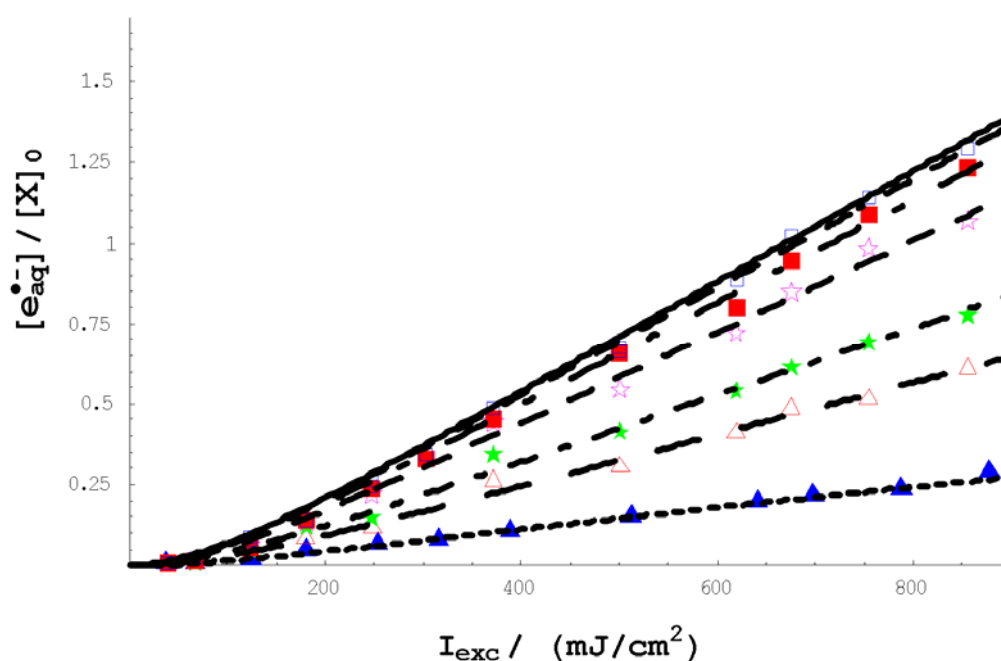


Figure 8.11. Concentration of the hydrated electron $e_{aq}^{\bullet-}$ relative to the starting xanthone concentration $[X]_0$ resulting from the photoionization of 2.25×10^{-5} M xanthone in methanol-water (1:2 v/v), pH 11, in the presence of different concentrations of DABCO as functions of laser intensity (308 nm). The DABCO concentrations: open triangles, 0.006 M; stars, 0.0125 M; open stars, 0.035 M; closed squares, 0.15 M; open squares, 0.3 M; closed triangles, without DABCO. The soiled line represents the limiting curve at 1×10^{10} M DABCO. The kinetic parameters were taken from the former measurements (see text).

Figure 8.11 depicts the effect of the quencher concentration on both electron concentration and kinetic parameters. The curves in Figure 8.11 are numerically calculated based on Scheme 8.1, and all kinetic parameters were known from the previous results, where k_q and κ_0 were taken from the quenching experiments and from Eq. 3.6, respectively. Both κ_1

and κ_4 were estimated from the resulting fit in Figures 5.5 and 8.6. The number of adjusted parameters is therefore zero. The meaningful kinetic parameters can be extracted from these measurements. The fact that the kinetic constant of $X^{\bullet-}$ photoionization (κ_4) in methanol-water solution is almost five times greater than that of ${}^3X^*$ photoionization (κ_1), emphasizes that the photoionization of the radical anion is dominant over that of the triplet, even at moderate donor concentrations. These measurements can determine the quencher concentration required to reach the limit of independence from the quencher concentration.

Photoionization of the xanthone/amine system in SDS solution at various quencher concentrations could be represented as in Figure 8.12. Both the triplet state and radical anion must be considered as sources of the hydrated electron.

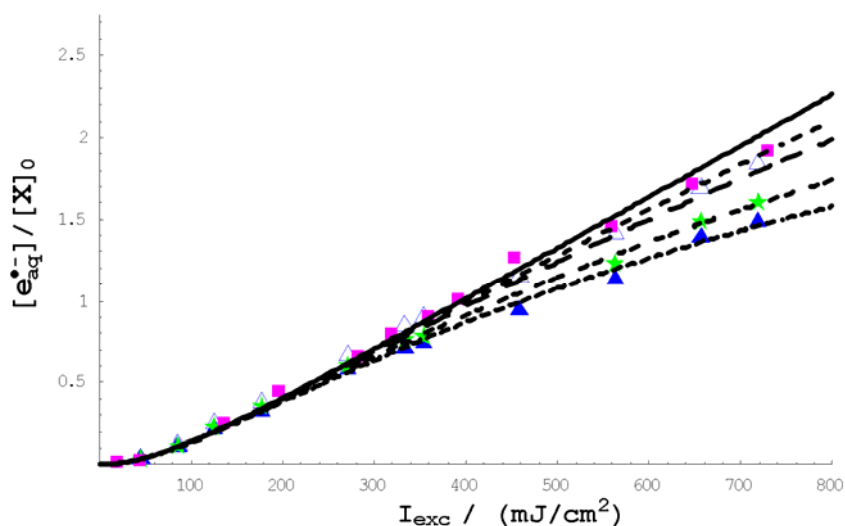


Figure 8.12. Concentration of the hydrated electron $e_{aq}^{\bullet-}$ relative to the starting xanthone concentration $[X]_0$ resulting from the photoreaction of 4×10^{-5} M xanthone in 0.05 M SDS, in the presence of different concentrations of DABCO as functions of the laser intensity (308 nm). The DABCO concentrations: closed triangles, 0.03 M; closed stars, 0.05 M; open triangles, 0.15 M; closed squares, 0.3 M. The kinetic parameters were taken from earlier measurement shown in Figures 5.5, 5.7 and 8.9. The limiting curve was obtained at 1.5 M DABCO (solid line).

It can be assumed that the quenching process is faster than triplet formation even at low quencher concentrations. The kinetic parameters increase with increasing quencher concentration and approach their limiting values. The dependence of the photoionization kinetic constant κ_4 and the photoionization quantum yield (φ_{ion}) on quencher concentrations is given in Table 8.1.

Table 8.1. Effect of quencher concentrations (DABCO) on the photoionization of xanthone following 308 nm light in (a) 0.05 M aqueous SDS solution and (b) methanol-water mixture (1:2 v/v).

(a)

DABCO (M)	κ_4 (cm ² /mJ)	ϕ_{ion}
0.01	3.53×10^{-3}	0.119
0.02	3.86×10^{-3}	0.13
0.05	4.64×10^{-3}	0.156
0.075	4.91×10^{-3}	0.166
0.1	4.97×10^{-3}	0.168

(b)

DABCO (M)	κ_4 (cm ² /mJ)	ϕ_{ion}
0.006	8.806×10^{-4}	0.03
0.035	1.173×10^{-3}	0.04
0.125	1.676×10^{-3}	0.058
0.15	1.92×10^{-3}	0.066
0.3	2.048×10^{-3}	0.071

8.8. Two-color two-laser flash photolysis of xanthone /amine system

Excitation of the xanthone/amine system was conducted by two-laser two-color method (308/532 nm). The transient absorption spectrum obtained after the end of the second laser pulse (532 nm) is assigned to the electron, which can be identified by its characteristic absorption. Both ${}^3X^*$ and $X^{\bullet-}$ exhibit a non-zero absorbance at 532 nm, whereas the xanthone ground state does not absorb light at this wavelength. This means that the electron may be produced from xanthone triplet state and /or xanthone anion radical. To distinguish between the photoionization of the triplet state and that of the radical anion, two-pulse experiments (308/532 nm) were employed to study the possibility of photoionization of ${}^3X^*$. The latter was generated upon excitation of X with laser light at 308 nm. The laser intensity was adjusted to minimize the electron concentration and to produce a triplet concentration as high as possible. No bleaching of the absorption signal at 590 nm was observed when ${}^3X^*$ was irradiated with the second laser at 532 nm. Furthermore, there were no electron absorption signals under these conditions. These observations support the interpretation that ${}^3X^*$ is not ionized to produce hydrated electron.

Two-pulse experiments of xanthone/amine system in methanol/water (1:2 v/v) solution were employed to give more information about the photoionization pathway. In this experiment, a 308 nm laser pulse was used to produce the xanthone radical anion while a second laser at 532 nm laser pulses was used to excite $X^{\bullet-}$. The delay time between the two pulses was 3.9 μ s. The bleaching at 560 nm corresponds to the destruction of $X^{\bullet-}$ by the 532 nm laser pulse and is accompanied by the appearance of absorption in the region 500-829 nm, which is characteristic for the electron (Figure 8.13).

The transient absorption spectra following single and two-laser pulse possess the same shape as the transient absorption spectrum obtained from bleaching but with different intensities. These observations indicate the presence of only one absorbing species during the photoreaction via one or two-laser pulse, which was characterized as X^{\bullet} . No additional absorption could be detected.

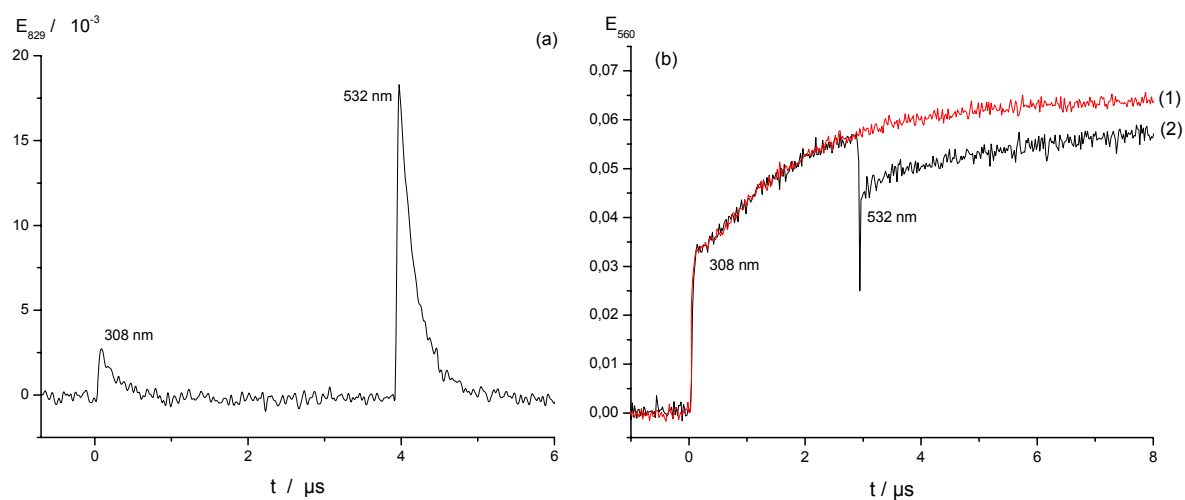
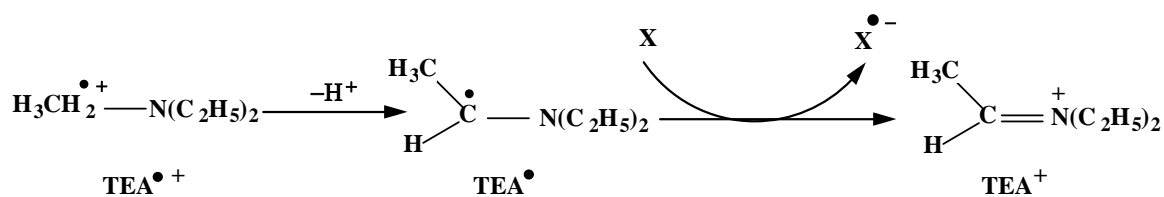


Figure 8.13. Two-laser two-color experiment (308 +532 nm) showing excitation of solution containing 2.1×10^{-4} M of xanthone and 0.3 M of triethylamine in methanol-water (1:2 v/v), at pH 11. **(a)** Electron formation, first pulse, 308 nm, 30 mJ/cm^2 ; second pulse, 532 nm, 1135 mJ/cm^2 . The delay time between the first and the second lasers was $3.9 \mu\text{s}$. E_{829} was the absorption of electron at 829 nm and was measured as difference absorption in argon- and N_2O -saturated solution. **(b)** Decay traces depicting the 532 nm photobleaching of X^{\bullet} monitored at 560 nm (in N_2O -saturated solution) were produced by 308 nm excitation (1) and 308 + 532 nm excitation (2), with the pulses separated by $3 \mu\text{s}$.

As a result of using a constant laser pulse intensity to excite xanthone/amine system in methanol-water solution, the obtained concentrations of the xanthone anion radicals were nearly constant. Figure 8.14 shows the difference in behaviour of the xanthone/ DABCO and X/TEA systems following two-pulse two-color excitation. In case of the photoreaction of X/TEA, a fast absorption signal at 560 nm was observed due to formation of X^{\bullet} . This is followed by a slow rise in the absorption due to the bimolecular reaction between α -aminoalkyl radical (TEA^{\bullet}), which results from the deprotonation of $\text{TEA}^{\bullet+}$ [188], and xanthone ground state resulting in X^{\bullet} and immonium cation (TEA^+) (Scheme 8.3). The advantage of this process is that none of the TEA derived species possesses an absorption above 300 nm [189-191]. Thus, the amount of X^{\bullet} increases with time, and the amount of bleaching increases accordingly.



Scheme 8.3

The transient ascending absorption at the maximum absorption of the xanthone radical anion was not observed in the presence of DABCO. This indicates that the deprotonation of $\text{DABCO}^{\bullet+}$ does not occur in this system. Inbar et al. [192] explained this observation owing to the high stability of $\text{DABCO}^{\bullet+}$ and the decreased overlap between the n-orbital of N and α -C-H orbitals in the bicyclic structure of DABCO.

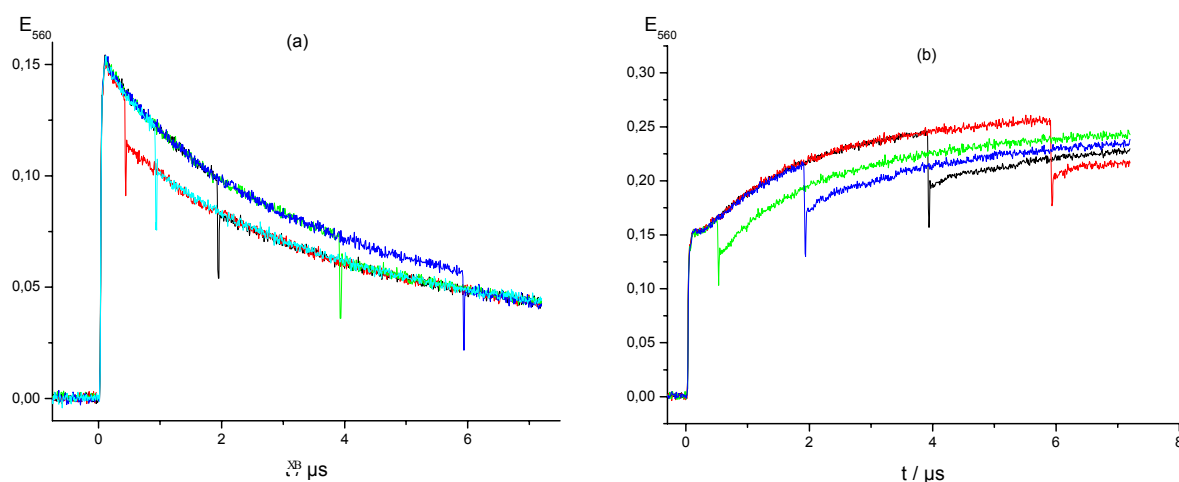


Figure 8.14. Two-pulse experiments in N_2O -saturated solutions in methanol/water (1:2 v/v) at pH 11 of 2.0×10^{-4} M xanthone in the presence of 0.2 M DABCO (a) and 0.3 M triethylamine (b). First pulse, 308 nm, 130 mJ/cm^2 (a) and 180 mJ/cm^2 ; (b) second pulse, 532 nm, and 900 mJ/cm^2 . The delay time between the first and the second laser was a variable. The negative spikes are caused by insufficiently suppressed stray light and/or luminescence of the excited radical anion.

The primary reaction pathway of the DABCO radical cation is a charge recombination process. Consequently, the amount of $\text{X}^{\bullet-}$ decreases with time and its absorption decreases correspondingly as shown in Figure 8.14a. The amount of bleaching increases as the amount of xanthone radical anion increases. There is no contribution from $\text{DABCO}^{\bullet+}$ following the 532 nm laser pulse, because the xanthone and DABCO ground states are completely

transparent at this wavelength. The possibility of the xanthone triplet formation and photoionization of DABCO can be neglected. $\text{DABCO}^{\bullet+}$ resulting from the first laser pulse (308 nm) contributes only slightly to the absorption signal at 560 nm because it has a very low extinction coefficient at this wavelength.

The source of the electron, which was observed following the second laser pulse at 532 nm, is the xanthone radical anion. This can be deduced from the linear relationship between the amount of bleaching and the electron yield (Figure 8.15).

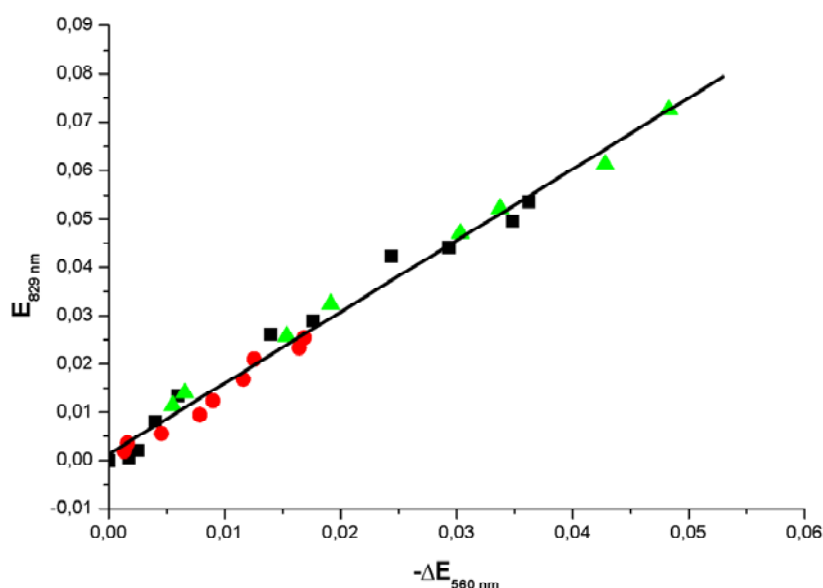


Figure 8.15. Electron absorption ($E_{829 \text{ nm}}$) monitored at 829 nm obtained from two-pulse experiments with $2.1 \times 10^{-4} \text{ M}$ xanthone in methanol-water (1:2 v/v), at pH 11, in the presence of amines, as a function of the bleaching of radical anion absorption ($-\Delta E_{560 \text{ nm}}$) at 560 nm. Electron absorption was obtained following a difference experiment in the absence and in the presence of N_2O . Absorption of radical anion was measured in N_2O -saturated solution. Circles (DABCO); squares and triangles (triethylamine). Experimental conditions as in Fig 8.14, 532 nm, variable intensities. For triangles, the first pulse is changed to 308 nm with intensity 203 mJ/cm^2 .

Figure 8.15 describes the relationship between the absorption of the hydrated electron and the amount of bleaching due to consumption of the xanthone radical anion. The slope of the linear relationship should be equal to the ratio of the extinction coefficient of electron and xanthone radical anion. This ratio was evaluated to be 6.8 and it is almost 4 times greater than the expected value. This means that there is another reaction pathway besides electron formation. This side reaction may be the formation of an undetermined photoproduct. The

ratio of quantum yields of photoproduct (φ_{prod}) and photoionization (φ_{ion}) can be estimated from the slope of the following linear relationship,

$$E_{829}(\text{e}_{\text{aq}}^{\bullet-}) = \frac{\varepsilon_{829}(\text{e}_{\text{aq}}^{\bullet-})}{\varepsilon_{560}(\text{X}^{\bullet-})} \left(\frac{1}{1 + \varphi_{\text{prod}}/\varphi_{\text{ion}}} \right) E_{560}(\text{X}^{\bullet-}). \quad \text{Eq. (8.8)}$$

Thus, it was found that a φ_{prod} is greater than φ_{ion} by a factor of 3.2.

8.9. Linear photonionization of $\text{X}^{\bullet-}$ at green light (532 nm)

Figure 8.16 displays the effect of the intensity of the second laser pulse (at 532 nm) on the electron concentration relative to the concentration of $\text{X}^{\bullet-}$ immediately before that pulse. The excimer laser at 308 nm should be the first pulse in order to generate the xanthone radical anion taking into account the constancy of the laser intensity during these measurements.

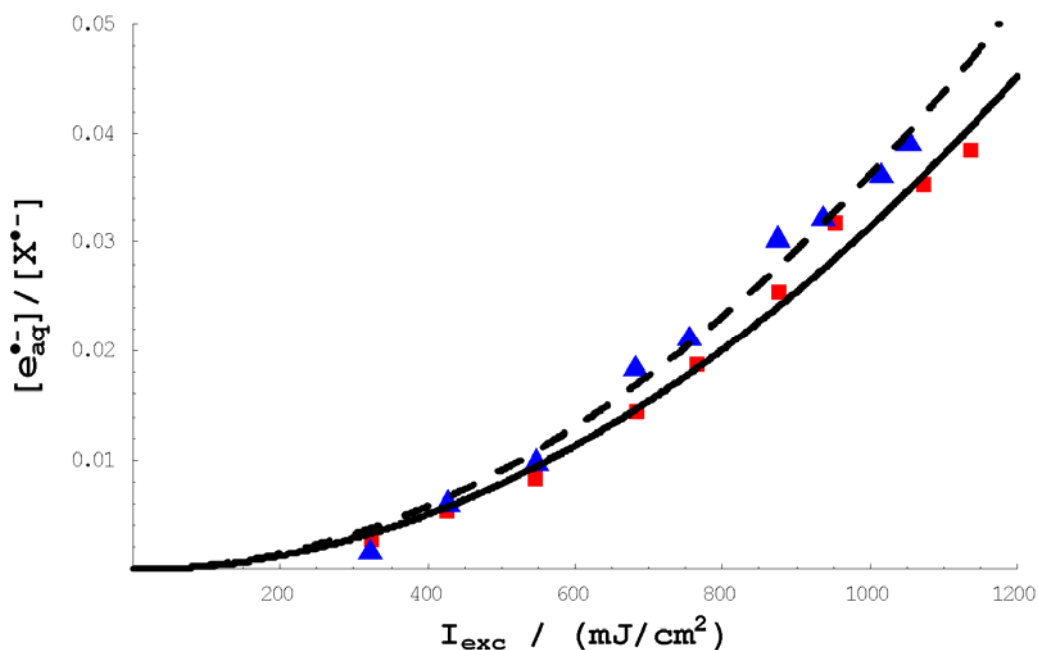


Figure 8.16. Dependence of the concentration of the hydrated electron (monitored at 829 nm) relative to the concentration of xanthone radical anion (produced by 308 nm laser pulse, fixed intensity) on 532 nm laser excitation of a methanol-water 1:2 v/v, pH 11, of 2.1×10^{-4} M xanthone and 0.3 M TEA (triangles, dashed line) or 0.2 M DABCO (squares, solid line). The lines were fitted to the experimental data according to $\propto I_{\text{exc}}^2$. Best-fit values of α : 3.62×10^{-8} (TEA), 3.14×10^{-8} (DABCO).

The variation of the intensity of the second pulse allows investigation of the mechanism of the photoionization process using two different interpretation parameters. Firstly, a strong non-linear relationship between the electron absorption and laser intensity indicates that the

photoionization of xanthone radical anion involves more than one photon. The experimental data are fitted well to Eq. (8.14) as displayed in Figure 8.16.

Secondly, if a substance undergoes a multiphoton reaction, the initial absorption of a transient chemical species can be described as a function of the laser intensity and given by Eq. (8.9)

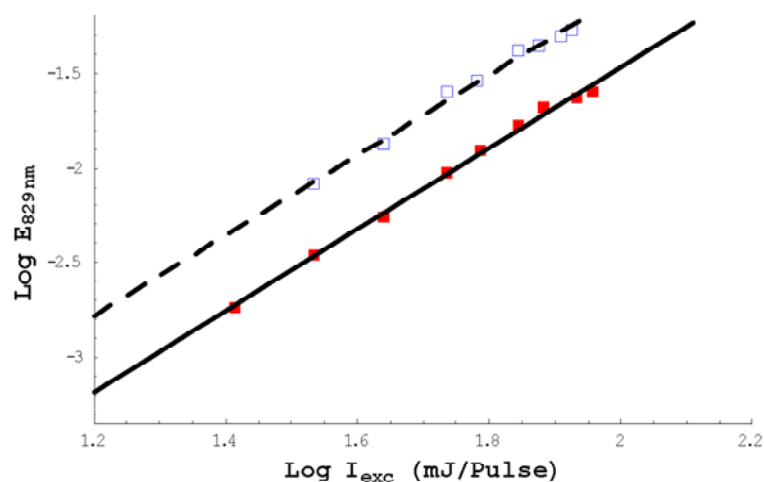
$$E_{\lambda} = kI_{exc}^n \quad \text{Eq. (8.9)}$$

where E_{λ} is the absorbance of $e^{\bullet-}_{aq}$, I_{exc} is the laser intensity, and n is an integer and is equal to the number of photons required for the reaction to occur. k is a kinetic constant depending on the experimental conditions. The value of n can be determined from the slope of the straight line, which results from the logarithmic plot of the absorbance against laser intensity.

$$\log[E_{\lambda}] = \log k + n \log[I_{exc}] \quad \text{Eq. (8.10)}$$

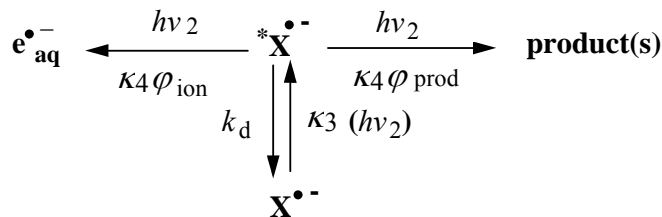
Figure 8.17 represents the plot of $\log [E_{\lambda}]$ due to the absorption of the hydrated electron produced from 532 nm laser pulse vs $\log [I_{exc}]$. The slope was determined to be 2.04, suggesting that the photoionization of $X^{\bullet-}$ by 532 nm light proceeds via a biphotonic ionization process.

Figure 8.17. $\log E (e^{\bullet-}_{aq}, 829 \text{ nm})$ vs $\log (I_{exc})$ for the electron resulting from the excitation of xanthone /amines by 532 nm light in methanol-water 1:2 v/v. Open square and dashed line, 0.3 M TEA and filled squares and solid line, 0.2 M DABCO.



The photoionization of the doublet excited state ($*X^{\bullet-}$) following 532 nm laser excitation can be outlined as shown in Scheme 8.4. The $X^{\bullet-}$ absorbs the first photon and is converted into an excited radical anion $*X^{\bullet-}$. The hydrated electron and a further photoproduct are produced due to the absorption of a second 532 nm photon by $*X^{\bullet-}$. $*X^{\bullet-}$ returns to the doublet ground state $X^{\bullet-}$ with a rate constant k_d . The process of the production of the undetectable product

resulting from the decomposition processes of $X^{\bullet-}$ is represented by $\kappa_4 \varphi_{\text{prod}}$, where κ_4 is the kinetic constant of the excitation process of $X^{\bullet-}$ and φ_{prod} is the respective quantum yield.



Scheme 8.4

The differential rate equations corresponding to Scheme 8.4 can be solved to give a bi-exponential term for the electron concentration as given by Eq. (8.11)

$$\frac{[e_{\text{aq}}^{\bullet-}]}{[X^{\bullet-}]} = \frac{\varphi_{\text{ion}}}{\varphi_{\text{ion}} + \varphi_{\text{prod}}} \left(1 - \frac{k_a \exp(-k_b I_{\text{exc}})}{(k_a - k_b)} + \frac{k_b \exp(-k_a I_{\text{exc}})}{(k_a - k_b)} \right) \quad \text{Eq. (8.11)}$$

where

$$k_{a,b} = \frac{1}{2} (\kappa_3 + (\varphi_{\text{ion}} + \varphi_{\text{prod}}) \kappa_4 + k_d \frac{\tau}{I_{\text{exc}}}) \pm \sqrt{-4(\varphi_{\text{ion}} + \varphi_{\text{prod}}) \kappa_4 \kappa_3 + (\kappa_3 + k_d \frac{\tau}{I_{\text{exc}}})^2 + (\varphi_{\text{ion}} + \varphi_{\text{prod}}) \kappa_4^2} \quad \text{Eq. (8.12)}$$

The above equation can be simplified to give

$$\frac{[e_{\text{aq}}^{\bullet-}]}{[X^{\bullet-}]_0} = \frac{\varphi_{\text{ion}} k_a k_b}{2(\varphi_{\text{ion}} + \varphi_{\text{prod}})} I_{\text{exc}}^2, \quad \text{Eq. (8.13)}$$

which is equivalent to

$$\frac{[e_{\text{aq}}^{\bullet-}]}{[X^{\bullet-}]_0} = \frac{\varphi_{\text{ion}} \kappa_3 \kappa_4}{2} I_{\text{exc}}^2 \quad \text{Eq. (8.14)}$$

When $k_d \gg (\kappa_3 + \kappa_4) I(t)$, Eq. 8.12 can be approximated to

$$k_a = k_d \frac{\tau}{I_{\text{exc}}} \quad \text{Eq. (8.15)}$$

$$k_b = \frac{(\varphi_{\text{ion}} + \varphi_{\text{prod}}) \kappa_4 \kappa_3}{k_d \tau / I_{\text{exc}}} \quad \text{Eq. (8.16)}$$

At low values of $\kappa_3 I(t)$ and $\kappa_4 I(t)$, expanding Eq. 8.11 to second order in the intensity will be give

$$\frac{[e_{\text{aq}}^{\bullet-}]}{[X^{\bullet-}]_0} = \frac{k_d \tau - 1 + \exp(-k_d \tau)}{(k_d \tau)^2} \varphi_{\text{ion}} \kappa_3 \kappa_4 I_{\text{exc}}^2 \quad \text{Eq. (8.17)}$$

The above results reveal that the photoionization mechanism of the xanthone radical anion depends on the photon energy and the physical properties of the xanthone and its radical anion. The photoionization of the $X^{\bullet-}$ requires about 1.4 eV [89]. This implies that the monophotonic ionization of the $X^{\bullet-}$ with near UV-light (308 or 355 nm) is feasible, whereas its biphotonic ionization is a result of the excitation by green light (532 nm) as shown in Figures 8.16 and 8.17. The X molecule resulting from the ionization of $X^{\bullet-}$ has appreciable absorbances at 308 and 355 nm and is transparent at 532 nm. Therefore, the photoionization mechanism of xanthone in the presence of amine with near UV-light (308 or 355 nm) irradiation is cyclic while it occurs via a linear mechanism with green light (532 nm) at the available highest laser intensity.

Interestingly, the photoionization quantum yields and the electron concentrations of the X/amine systems in aqueous SDS micellar solution are greater than that in methanol-water solution. This implies that SDS plays again an important role in the photoionization of X/amine system. SDS may accelerate all photoreaction steps in this system and/or the photoionization may proceed via photoionization of the lowest excited triplet state of xanthone and its radical anion within the pulse duration. Furthermore, $X^{\bullet-}$ was ionized rapidly in micelles giving the xanthone ground state and the electron. Owing to the electrostatic repulsion between the negative charges, the $e_{aq}^{\bullet-}$ exits rapidly from the anionic micelle (SDS) entering the aqueous phase, while xanthone ground state remains inside the micelle. This may enhance the photoionization quantum yield.

9. Summary / Zusammenfassung

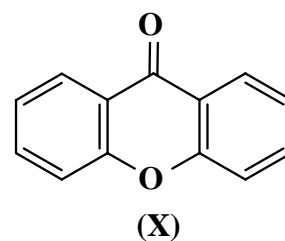
9.1. Summary

The main objective of this thesis was to investigate the photoionization of some hetrocyclic compounds via different linear and cyclic mechanisms, depending on the medium, the physical properties of the intermediates and the laser intensity. The spectroscopy and kinetics of the selected compounds were analysed using nanosecond laser flash photolysis (LFP) with optical detection. Under certain conditions, all these compounds are photoionized by linear two-photon mechanisms. By changing the medium (from methanol-water solution to aqueous SDS solution) or through the addition of an electron donor such as amine in high concentration, we found that new cyclic photoionization pathways can be opened up. The resulting cyclic reaction schemes are investigated in detail in this thesis, and their intensity dependences are compared with those of linear photoionizations. Furthermore, we observed a combination of linear and cyclic photoionizations of an electron acceptor in the presence of low to moderate amine concentrations. The main results are described in the following:

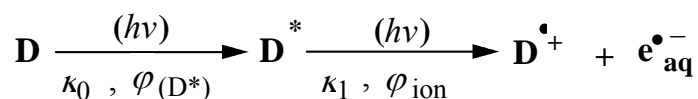
I. Linear photoionizations:

I.A. Electron donor photoionizations:

- The simplest linear photoionization mechanism is a consecutive two-photon ionization as shown in Scheme 9.1. The substrate, D, absorbs a photon with kinetic constant $\kappa_0(h\nu)$ to give an excited state, D*. With a second photon, that state is ionized to give a hydrated electron ($e_{\text{aq}}^{\bullet-}$) and the

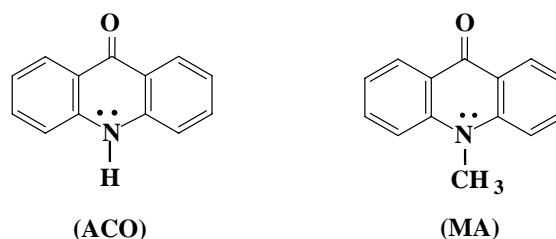


radical cation, D^{•+} with kinetic constant $\kappa_1(h\nu)$. The photoionization of xanthone, X, in methanol-water (1:2 v/v) solution with near-UV light (308 or 355 nm) is an example of this mechanism with a quantum yield of photoionization (ϕ_{ion}) of 8×10^{-3} at both wavelengths. In this case, D* is the triplet state because intersystem crossing is so rapid as to make to intermediacy of ¹D* negligible.

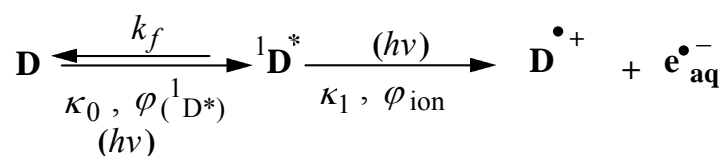


Scheme 9.1

- The excited state to be ionized can also undergo a deactivation process, such as fluorescence emission (rate constant k_f). If the fluorescence lifetime is comparable to the laser pulse duration, the kinetic scheme

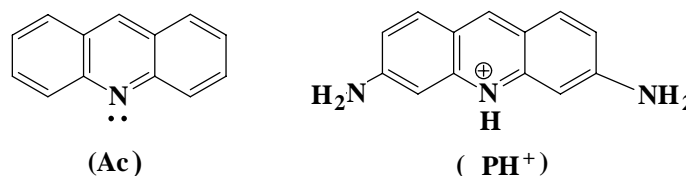


must include this step. The photoionizations of N-methylacridone, MA, or acridone, ACO in alcohol-water (1:2 v/v) at 355 nm or by two superimposed laser pulses (308+355 nm) proceed in that way (Scheme 9.2), with the excited singlet state as intermediate.

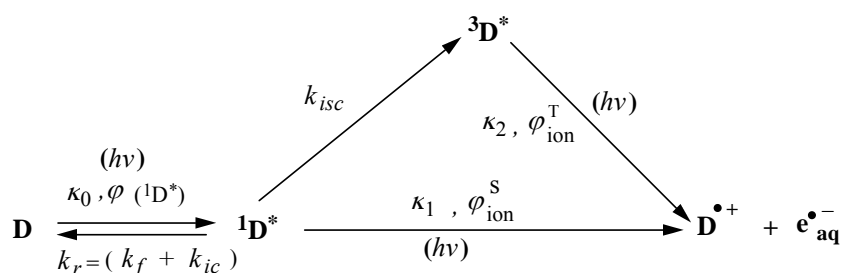


Scheme 9.2

- Scheme 9.3 represents a photoionization through both singlet and triplet state channels. The photoionization of acridine (Ac) in methanol-water (1:2 v/v,



pH 12) at 355 nm is an example of Scheme 9.3, which includes fluorescence, internal conversion (k_{ic}), and intersystem crossing (k_{isc}) of the excited singlet state.

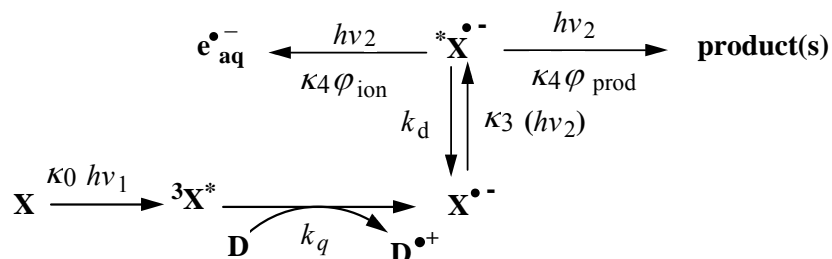


Scheme 9.3

I.B. Electron acceptor photoionization:

- In two-pulse experiment (308/532 nm), an electron acceptor (e.g., xanthone, X) in the presence of a sacrificial donor (e.g., an amine) can be converted into its radical anion ($\text{X}^{\bullet-}$) at 308 nm, which in turn is an electron donor that can be ionized by a linear mechanism.

The radical anion absorbs a photon of 532 nm ($h\nu_2$) light to give its excited state $*X^{\bullet-}$. The latter can undergo a deactivation to $X^{\bullet-}$ with rate constant k_d and also absorb another 532 nm photon to give the hydrated electron and an undetected product, as shown in Scheme 9.4.



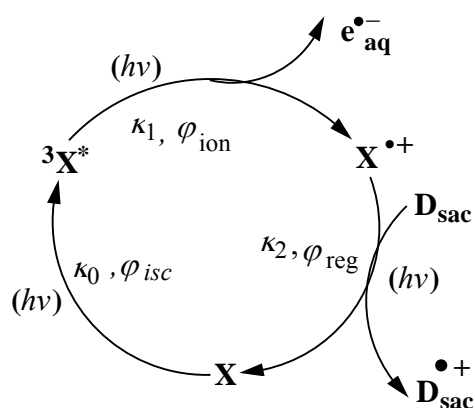
Scheme 9.4

II. Cyclic photoionizations:

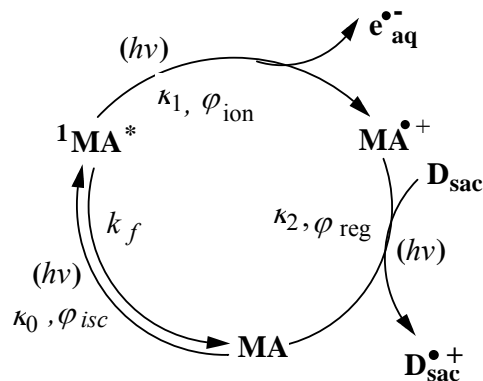
The photoionizations of the investigated electron donors in aqueous SDS micellar solution, or of the investigated electron acceptor in the presence of a sacrificial donor D_{sac} (e.g., an amine) in high concentration occur through different cyclic mechanisms.

II.A. Electron donor photoionizations:

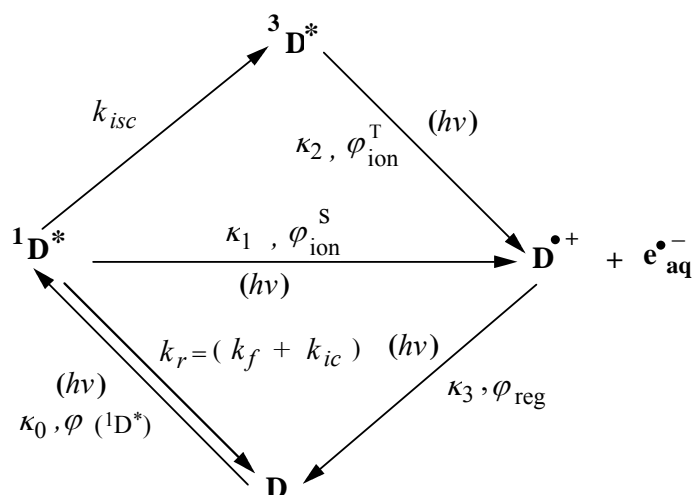
- Cyclic photoionization of xanthone (X) via its excited triplet state (Scheme 9.5)
- Cyclic photoionization of acridone derivatives (e.g., MA or ACO) via their excited singlet state (Scheme 9.6)
- Cyclic photoionization of acridine (Ac) and Proflavine (PH^+) via their excited singlet and triplet states (Scheme 9.7).



Scheme 9.5



Scheme 9.6

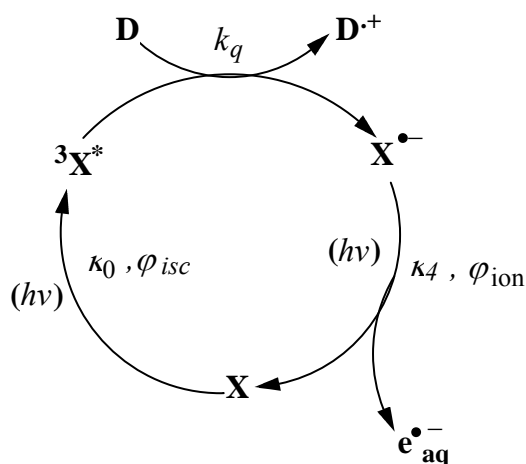


Scheme 9.7

Common to Schemes 9.5-9.7 is that the radical cation absorbs a photon to regenerate the substrate. Evidence that SDS can act as a sacrificial donor is provided by a dependence of the electron yield on the SDS concentration in the case of acridone and xanthone. The quantum yield of the regeneration of the N-methyl acridone-ground state (φ_{reg}) by SDS was found to be 0.051.

II.B. Electron acceptor photoionization:

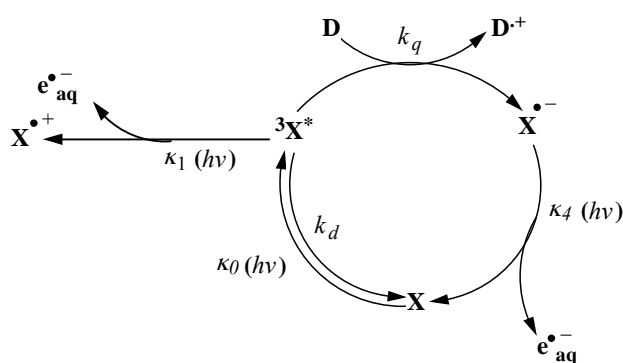
- The photoionization of an electron acceptor (e.g., xanthone) in the presence of an electron donor (e.g., triethylamine, (TEA) or 1,4-Diazabicyclo[2.2.2]octane (DABCO)) occurs via a cyclic mechanism (Scheme 9.8), in which $X^{\bullet-}$ absorbs a second photon to give an electron and regenerate the ground state of X.



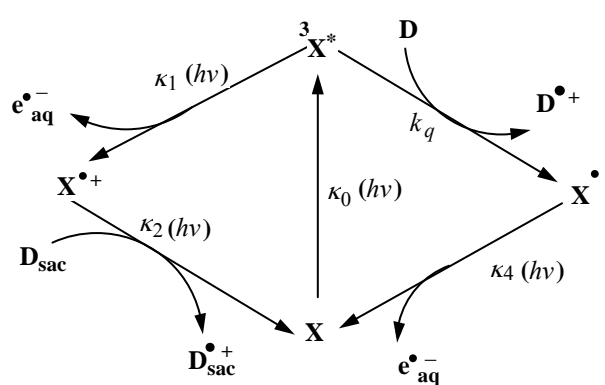
Scheme 9.8

III. Combined linear and cyclic photoionization:

- At low to moderate quencher concentration, the intermediacy of the triplet state cannot be neglected in the photoionization of xanthone. In methanol-water (1:2 v/v) solution a combined linear and cyclic photoionization can occur as shown in. Scheme 9.9. In SDS solution, the mechanism (Scheme 9.10) is the combination of Schemes 9.5 and 9.8. The solution of the rate equations corresponding to these mechanisms was carried out numerically to verify the reaction mechanism and the obtained parameters.



Scheme 9.9



Scheme 9.10

At low light intensities, it is very difficult to distinguish between a linear and cyclic photoionization process, but a differentiation of them is easily possible at high laser intensity. The concentration of the photoionized species proper approaches a steady-state value at high laser intensity in a cyclic reaction while it approaches zero in the case of linear photonization. The electron concentration at high laser intensity is not limited by depletion of substrate with a cyclic mechanism (i.e., the electron yield increases without bounds when the laser intensity is increased), while it reaches saturation with a linear mechanism.

The photoionization of the examined substances in aqueous SDS micellar solutions proceeds via a cyclic mechanism, whereas their photoionization occurs via a linear mechanism in alcohol-water solution. This emphasises the important role of SDS for the photoionization of the examined substances because it can function as an electron donor (i.e., reducing agent). Furthermore, the photoionization quantum yields in SDS are greater than those in methanol-water solution owing to the ability of SDS to decrease the ionization potential of the excited state. Negatively charged micelles (SDS) can inhibit the charge recombination of the electron/radical-cation pair and further enhance the photoionization yield.

This work shows that photoionization should be investigated at high light intensities because under these conditions more reliable evidence as to the actual mechanism is obtained.

9.2. Zusammenfassung

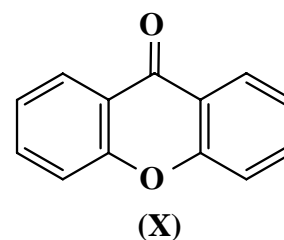
Das Hauptziel dieser Arbeit war es, die Photoionisierung ausgewählter heterozyklischer Verbindungen über verschiedene Mechanismen, lineare und zyklische, in Abhängigkeit von dem Medium und der Laserintensitäten zu studieren. Die Spektroskopie und Kinetik der ausgewählten Verbindungen wurden mit Hilfe der Nanosekunden-Laserblitzlichtphotolyse (LFP) mit optischer Detektion analysiert. Unter gewissen Bedingungen werden alle diese Verbindungen über lineare Zweiphotonenmechanismen photoionisiert. Bei einer Veränderung des Mediums (von Methanol-Wasser-Gemischen zu wässriger SDS-Lösung) oder der Hinzufügung eines Elektronendonors, z.B. eines Amins in hoher Konzentration fanden wir, dass sich neue Reaktionswege für zyklische Photoionisierung eröffnen lassen.

Die resultierenden Reaktionsschemata werden in dieser Arbeit im Detail untersucht und ihre Intensitätsabhängigkeiten werden mit denen linearer Photoionisierung verglichen. Außerdem wurde das Zusammenspiel linearer und zyklischer Photoionisierung eines Elektronenakzeptors in Gegenwart kleiner bis mäßiger Aminkonzentration untersucht. Die wesentlichen Ergebnisse sind:

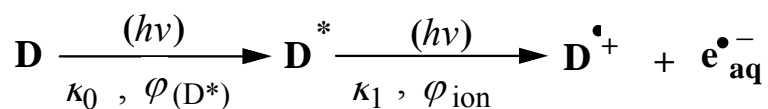
I. Lineare Photoionisierungen:

I.A. Photoionisierungen eines Donors:

- Der einfachste lineare Photoionisierungmechanismus ist eine sequentielle Zweiphotonenionisierung, wie in Schema 9.1 gezeigt. Das Substrat D absorbiert ein Photon mit der kinetischen Konstante κ_0 ($h\nu$), wodurch sich ein angeregter Zustand D^* bildet. Durch ein zweites Photon wird dieser

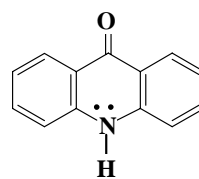


Zustand ionisiert, wobei ein hydratisiertes Elektron $e_{\text{aq}}^{\bullet-}$ und das Radikalkation $D^{\bullet+}$ mit der kinetischen Konstante κ_1 ($h\nu$) entstehen. Die Photoionisierung des Xanthons, X, in Methanol-Wasser (1:2 v/v) mit Licht des nahen UV (308 oder 355 nm) ist ein Beispiel für diesen Mechanismus mit einer Quantenausbeute des Photoionisierungsschrittes (ϕ_{ion}) von 8×10^{-3} bei beiden Wellenlängen. In diesem Fall ist D^* der Triplettzustand, weil die Interkombination so schnell ist, dass $^1D^*$ als Intermediat vernachlässigt werden kann.

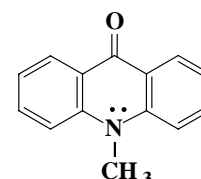


Schema 9.1

- Der zu ionisierende angeregte Zustand kann z. B. durch Fluoreszenz (Geschwindigkeitskonstante k_f) deaktiviert werde. Wenn die Fluoreszenzlebensdauer mit der Dauer des Laserpulses vergleichbar ist, muss das

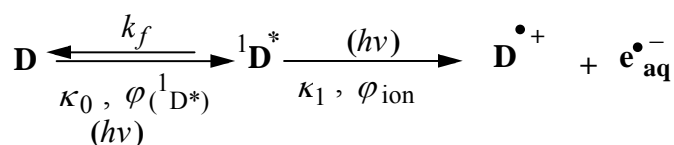


(ACO)



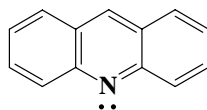
(MA)

kinetische Schema diesen Schritt berichtigen. Die Photoionisierungen von N-Methylacridon, MA oder Acridon ACO in Alkohol-Wasser (1:2 v/v) bei 355 nm oder mit zwei überlagerten Laserpulsen (308+355 nm) verlaufen in dieser Weise (Schema 9.2) mit dem angeregten Singulettzustand als Intermediat.

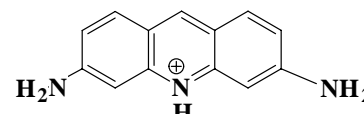


Schema 9.2

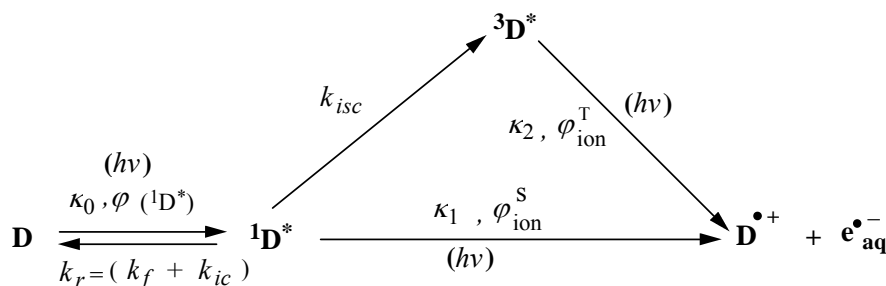
- Schema 9.3 repräsentiert eine Photoionisierung solche über den Singulett- als auch über den Triplettweg. Die Photoionisierung von Acridin (Ac) im Methanol-



(Ac)

(PH⁺)

Wasser (1:2 v/v bei pH 12) bei 355 nm ist ein Beispiel für das Schema 9.3, das auch die Fluoreszenz, die innere Umwandlung k_{ic} , und die Interkombination k_{isc} des angeregten Singulettzustandes umfasst.

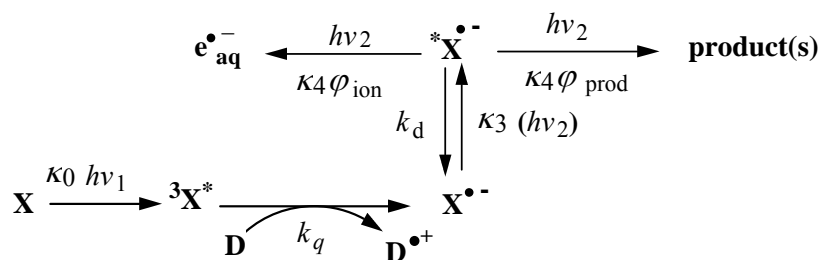


Schema 9.3

I.B. Photoionisierung eines Elektronenakzeptors:

- In einem Zweipulsexperiment (308/532 nm) kann ein Elektronenakzeptor (z.B. Xanthon) durch ein Opferdonor (z.B. ein Amin) in sein Radikalanion, X^{•-} bei 308 nm umgewandelt

werden, welches wiederum ein Elektronendonator ist, der über einen linearen Mechanismus ionisiert werden kann. Das Radikalanion $X^{\bullet-}$ absorbiert ein Photon ($h\nu_2$, 532 nm) und liefert einen angeregten Zustand $^*X^{\bullet-}$. Der Letztere kann mit der Geschwindigkeitskonstante k_d zu $X^{\bullet-}$ deaktiviert werden oder noch ein 532-nm Photon absorbiert, wobei sich ein hydratisiertes Elektron und ein unbeobachtetes Produkt bilden, wie in Schema 9.4 gezeigt.



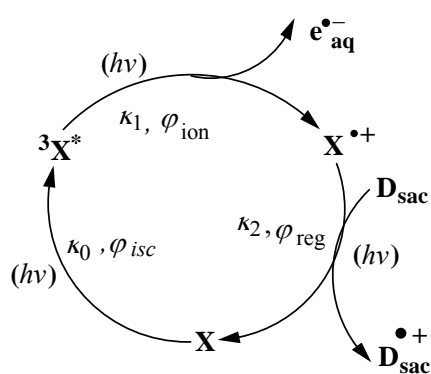
Schema 9.4

II. Zyklische Photoionisierungen:

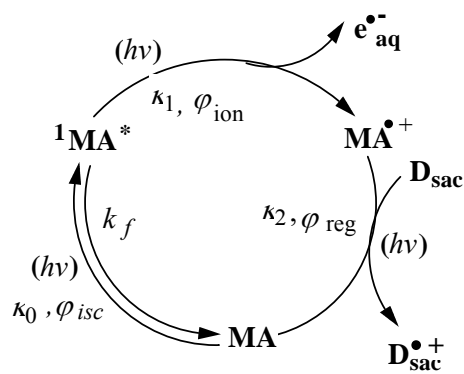
Die Photoionisierungen der untersuchten Elektronendonoren in wässriger Mizellarer Lösung (SDS) oder der untersuchten Elektronenakzeptoren in Gegenwart eines Opferdonors D_{sac} (z.B. eines Amins) in hoher Konzentration verlaufen nach verschiedenen zyklischen Mechanismen.

II.A. Photoionisierungen von Elektronendonoren :

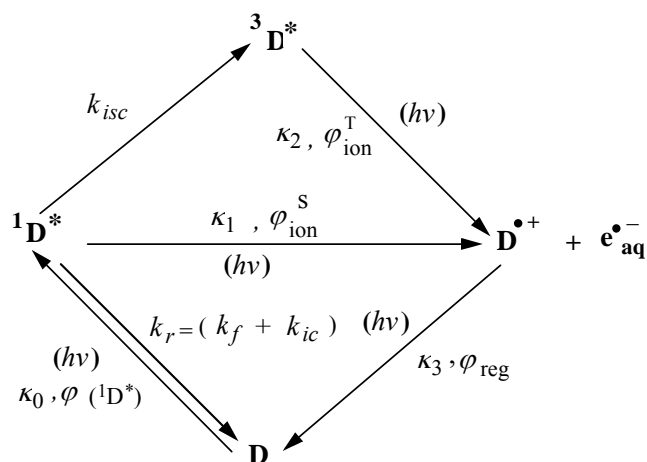
- Zyklische Photoionisierung des Xanthons (X) über seinen angeregten Tripletzustand (Schema 9.5)
- Zyklische Photoionisierung von N-Methylacridon (MA) oder von Acridon (ACO) über ihren angeregten Singulettzustand (Schema 9.6)
- Zyklische Photoionisierung von Acridin (Ac) oder Proflavin (PH^+) über ihre angeregte Singulett- und Tripletzustände (Schema 9.6)



Schema 9.5



Schema 9.6

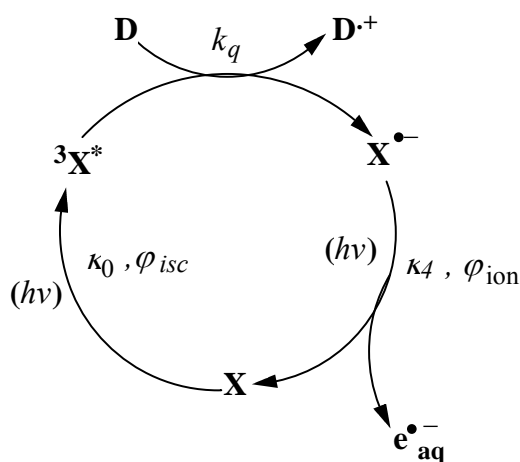


Schema 9.7

Die Schemata 9.5-9.7 haben als Gemeinsamkeit, dass das Radikalkation ein Photon absorbiert und dabei das Substrat zurückbildet. Bei Acridon und Xanthon liefert die Abhängigkeit der Elektronenausbeute von der SDS-Konzentration Evidenz, dass SDS als Opferdonor fügen kann die Quantenausbeute der Rückbildung des Grundzustands des N-Methylacridons (φ_{reg}) durch SDS ergab sich zu 0,051.

II.B. Photoionisierung eines Elektronenakzeptors:

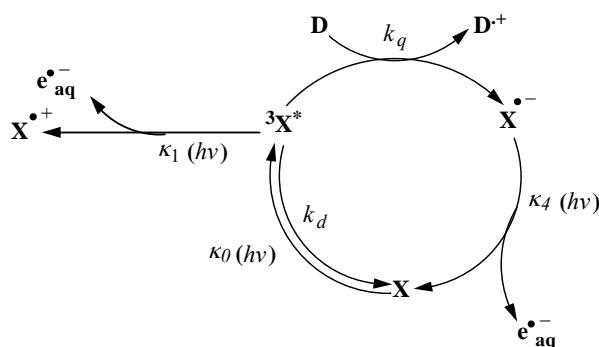
- Die Photoionisierung des Elektronenakzeptors (z.B. Xanthon) in Gegenwart eines Elektronendonors D (z.B. Triethylamin (TEA) oder 1,4-diazabicyclo[2,2,2]octan (DABCO)) erfolgt über einen zyklischen Mechanismus (Schema 9.8), bei dem $X^{\bullet-}$ ein Photon absorbiert, und ein hydratisiertes Elektron sowie den rückgebildeten Grundzustand von X liefert.



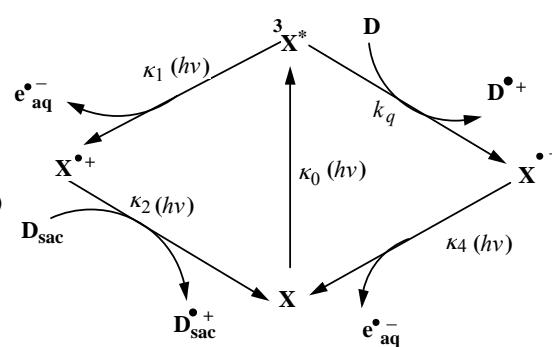
Schema 9.8

III. Kombinierte lineare und zyklische Photoionisierung:

- Bei niedriger bis mäßiger Löschenkonzentration kann den Triplettzustand in der Photoionisierung des Xanthons nicht vernachlässigt werden. In Methanol-Wasser findet eine kombinierte lineare und zyklische Photoionisierung statt, wie in Schema 9.9 gezeigt. In der SDS-Lösung ist der Mechanismus (Schema 9.10) eine Kombination der beiden Mechanismen von Schemata 9.5 und 9.8. Zur Lösung der Differentialgleichungen dieser Mechanismen wurde eine numerische Analyse angewandt, um den Reaktionsmechanismus und die erhaltenen Parameter zu prüfen.



Schema 9.9



Schema 9.10

Bei niedriger Lichtintensität ist es sehr schwierig, zwischen zyklischen und linearen Mechanismen zu unterscheiden, bei hohen dagegen leicht. In einer zyklischen Reaktion erreicht die Konzentration der eigentlichen photoionisierten Spezies einen Stationärzustand, während sie bei einer linearen Photoionisierung gegen null geht. Weiterhin wächst bei einer zyklischen Mechanismus die Elektronenkonzentration mit steigender Laserintensität unbegrenzt an, während sie bei einem linearen Mechanismus in die Sättigung geht.

Die Photoionisierung der untersuchten Substanzen in wäßriger mezzellarer Lösung (SDS) verlaufen über zyklische Mechanismen, während sie in Alkohol-Wasser-Gemischen über eine linearen Mechanismen gehorchen. Dies unterstreicht die wichtige Rolle von SDS für die Photoionisierung der untersuchten Substanzen, weil es als Elektronendonator (d.h. Reduktionsmittel) dienen kann. Außerdem sind die Photoionisierungsquantenausbeuten in SDS größer als in Methanol-Wasser wegen der Fähigkeit von SDS, das Ionisierungspotential des angeregten Zustandes zu senken. Negative geladene Mizellen (SDS) können außerdem die Ladungskombination des Paares Elektron-Radikalkationen hindern und dadurch die Photoionisierungsausbeute weiter erhöhen.

Diese Arbeit zeigt, dass die Photoionisierung bei hohen Lichtintensitäten untersucht werden sollte, weil sich unter diesen Bedingungen verlässliche Informationen über den tatsächlichen Mechanismus erhalten lassen.

10. References

- [1] Görner, H. *J. Photochem. Photobiol. B* **1994**, *26*, 117–139.
- [2] Steenken, S.; Goldbergerova, L. *J. Am. Chem. Soc.* **1998**, *120*, 3928–3934.
- [3] Papadantonakis, G. A.; Tranter, R.; Brezinsky, K.; Yang, Y.; van Breemen, R. B.; LeBreton, P. R. *J. Phys. Chem. B* **2002**, *106*, 7704–7712.
- [4] Crespo-Hernandez, C. E.; Arce, R. *Photochem. Photobiol.* **2002**, *76*, 259–267.
- [5] (a) Sortino, S.; Scaiano, J. C. *Photochem. Photobiol.* **1999**, *70*, 590–95.
(b) Schulte-Frohlinde, D.; Simic, M. G.; Görner, H. *J. Photochem. Photobiol. A* **1990**, *52*, 1137–1151.
- [6] Aloisi, G. G.; Barbafina, A.; Canton, M.; Dall'Acqua, F.; Elisei, F.; Facciolo, G.; Latterini, L.; Viola, G. *Photochem. Photobiol.* **2004**, *79*, 248–258.
- [7] Angelov, A.; Spassky, A.; Berger, M.; Cadet, J. *J. Am. Chem. Soc.* **1997**, *119*, 11373–11380.
- [8] (a) Witt, H. T. *Q. Rev. Biophys.* **1971**, *4*, 365–377.
(b) Czochralska, B.; Lindqvist, L. *Chem. Phys. Lett.* **1983**, *101*, 297–299.
- [9] (a) Lindqvist, L.; Czochralska, B.; Grigorov, I. *Chem. Phys. Lett.* **1985**, *119*, 494–498.
(b) Boldrige, D. W.; Morton, T. H.; Scott, G. W. *Chem. Phys. Lett.* **1984**, *108*, 461–465.
- [10] Masnyk, T. W.; Minton, K. W. *Photochem. Photobiol.* **1991**, *54*, 99–107.
- [11] Croke, D. T.; Blau, W.; OhUigin, C.; Kelly, J. M.; McConnell, D. J. *Photochem. Photobiol.* **1988**, *47*, 527–536.
- [12] (a) Ebbesen, T. W.; Ghiron, C. A. *J. Phys. Chem.* **1989**, *93*, 7139–7143.
(b) Buettner, G. R.; Hall, R. D.; Chignell, C. F.; Motten, A. G. *Photochem. Photobiol.* **1989**, *49*, 249–256.
(c) Johnston, L. J.; Lobaugh, J.; Wintgens, V. *J. Phys. Chem.* **1989**, *93*, 7370–7374.
- [13] Beck, S. M.; Brus, L. E. *J. Am. Chem. Soc.* **1983**, *105*, 1106–1111.
- [14] Hashimoto, S.; Thomas, J. K. *J. Phys. Chem.* **1984**, *88*, 4044–4049.
- [15] (a) Mohanty, J.; Sapre, A. V.; Saini, R. D.; Mukherjee, T.; Pal, H. *Res. Chem. Intermed.* **2005**, *31*, 47–61.
(b) Narayana, P. A.; Li, A. S. W.; Kevan, L. *J. Am. Chem. Soc.* **1982**, *104*, 6502–6505.

- [16] Ohta, N.; Kevan, K. *J. Phys. Chem.* **1985**, *89*, 2415-2419.
- [17] Bemas, A.; Grand, D.; Hauteclouque, S.; Giannotti, C. *J. Phys. Chem.* **1986**, *90*, 6189-6194.
- [18] Grand, D.; Hauteclouque, S. *J. Phys. Chem.* **1990**, *94*, 837-841.
- [19] Stenland, K.; Kevan, L. *J. Phys. Chem.* **1993**, *97*, 5177-5184.
- [20] (a) Trampe, G.; Mattay, J.; Steenken, S. *J. Phys. Chem.* **1989**, *93*, 7157-7160.
(b) Johnston, L. J.; Schepp, N. P. *J. Am. Chem. Soc.* **1993**, *115*, 6564-6571.
- [21] Ghosh, H. N.; Palit, D. K.; Sapre, A. V.; RamaRao, K. V. S.; Mittal, J. P. *Chem. Phys. Lett.* **1993**, *203*, 5-11.
- [22] Gauduel, Y.; Pomerret, S.; Yamada, N.; Migus, A.; Antonetti, A. *J. Am. Chem. Soc.* **1989**, *111*, 4974-4980.
- [23] (a) Ghosh, H. N.; Palit, D. K.; Sapre, A. V.; RamaRao, K. V. S.; Mittal, J. P. *Photochem. Photobiol.* **1994**, *59*, 405-411.
(b) Hashimoto, S.; Thomas, J. K. *J. Photochem. Photobiol. A* **1991**, *55*, 377-386.
- [24] Mittal, L. J.; Mittal, J. P.; Hayon, E. *J. Am. Chem. Soc.* **1973**, *95*, 6203-6210.
- [25] (a) Nakamura, S.; Kanamaru, N.; Nohara, S.; Nakamura, H.; Saito, Y.; Tanaka, J.; Sumitani, M.; Nakashima, N.; Yoshihara, K. *Bull. Chem. Soc. Jpn.* **1984**, *57*, 145-150.
(b) Grand, D. *J. Phys. Chem.* **1990**, *94*, 7585-7588.
(c) Hirata, Y.; Mataga, N. *J. Phys. Chem.* **1990**, *94*, 8503-8505.
- [26] (a) Bhasikuttan, A. C.; Sapre, A. V.; RamaRao, K. V. S.; Mittal, J. P. *Photochem. Photobiol.* **1995**, *62*, 245-250.
(b) Hunter, J. A. A.; Bhutani, L. K.; Magnus, I. A. *Br. J. Dermatol.* **1970**, *82*, 157-168.
(c) Navaratnam, S.; Parsons, B. J.; Phillips, G. O.; Davies, A. K. *J. Chem. Soc., Faraday Trans. 1* **1978**, *74*, 1811-1819.
(d) Hirata, Y.; Ichikawa, M.; Mataga, N. *J. Phys. Chem.* **1990**, *94*, 3872-3874.
- [27] (a) Motten, A. G.; Buettner, G. R.; Chignell, C. F. *Photochem. Photobiol.* **1985**, *42*, 9-15.
(b) Alkaitis, S. A.; Gratzel, M. *J. Am. Chem. Soc.* **1976**, *98*, 3549-3554.
- [28] (a) Smith, G. A.; McGimpsey, W.G. *J. Phys. Chem.* **1994**, *98*, 2923-2329.
(b) Redmond, R. W.; Johnston, L. J. *J. Phys. Chem. A* **1997**, *101*, 4660-4665.

- [29] (a) Garcia, C.; Smith, G. A.; McGimpsey, G. W.; Kochevar, I. E.; Redmond, R. W. *J. Am. Chem. Soc.* **1995**, *117*, 10871-10878.
(b) Mittal, L. J.; Mittal, J. P.; Hayon, E. *Chem. Phys. Lett.* **1973**, *18*, 319-322.
- [30] Hirata, Y.; Mataga, N. *Prog. React. Kinet.* **1993**, *18*, 273-308.
- [31] Ghosh, H. N.; Sapre, A. V.; Palit, D. K.; Mittal, J. P. *J. Phys. Chem. B* **1997**, *101*, 2315-2320.
- [32] Delcourt, M. O.; Rossi, M. J. *J. Phys. Chem.* **1982**, *86*, 3233-3239.
- [33] (a) Vauthey, E.; Haselbach, E.; Suppan, P. *Helv. Chim. Acta* **1987**, *70*, 347-353.
(b) Vauthey, E.; Suppan, P.; Haselbach, E.; Davidson, R. S. *Helv. Chim. Acta* **1986**, *69*, 430-437.
- [34] (a) Grand, D.; Bernas, A.; Amouyal, E. *Chem. Phys.* **1979**, *44*, 73-79.
(b) Bernas, A.; Grand, D.; Amouyal, E. *J. Phys. Chem.* **1980**, *84*, 1259-1262.
(c) Grossweiner, L. S.; Joschek, H. I. *Advances in Chemistry Series*, No. 50 (Solvated electron) p 279.
- [35] (a) Hirata, Y.; Mataga, N. *J. Phys. Chem.* **1991**, *95*, 1640-1644.
(b) Mathivanan, N.; Johnston, L. J.; Wayner, D. D. M. *J. Phys. Chem.* **1995**, *99*, 8190-8195.
(c) Rahn, R.; Schroeder, J.; Troe, J. *J. Phys. Chem.* **1989**, *93*, 7841-7846.
- [36] (a) Shukla, D.; de Rege, F.; Wan, P.; Johnston, L. J. *J. Phys. Chem.* **1991**, *95*, 10240-10246.
(b) Hoffman, G. J.; Albrecht, A. C. *J. Phys. Chem.* **1991**, *94*, 4455-4463.
- [37] Sauberlich, J.; Beckert, D. *J. Phys. Chem.* **1995**, *99*, 12520-12524.
- [38] (a) Shafirovich, V.; Dourandin, A.; Huang, W.; Luneva, P.; Geacintov, N. E. *J. Phys. Chem. B* **1999**, *103*, 10924-10933.
(b) Silva, C.; Walhout, P. K.; Reid, P. J.; Barbara, P. F. *J. Phys. Chem. A* **1998**, *102*, 5701-5707.
- [39] Bensasson, R. V.; Goldschmidt, C. R.; Land, E. J.; Truscott, T. G. *Photochem. Photobiol.* **1978**, *28*, 277-281.
- [40] (a) Boch, M.; Whittlesey, M. K.; Scaiano, J. C. *J. Phys. Chem.* **1994**, *98*, 7854-7857.
(b) Pilloff, H. S.; Abrecht, A. C. *Nature* **1966**, *212*, 499-500.
(c) Pilloff, H. S.; Abrecht, A. C. *J. Chem. Phys.* **1968**, *49*, 4891-4901.
(d) Ray, J. P.; Hamilton, T. D. S. *Nature* **1965**, *206*, 1040-1041.
- [41] (a) Steenken, S.; Warren, C. J.; Gilbert, B. C. *J. Chem. Soc., Perkin Trans. 2* **1990**, 335-342.

- (b) Potashnik, R.; Ottolenghi, M.; Bensasson, R. *J. Phys. Chem.* **1969**, *73*, 1912-1918.
- [42] (a) Jolicard, G.; Billing, G. D. *J. Chem. Phys.* **1989**, *90*, 346-53.
(b) Cai, X.; Sakamoto, M.; Hara, M.; Tojo, S.; Ouchi, A.; Kawai, K.; Endo, M.; Fujitsuka, M.; Majima, T. *J. Am. Chem. Soc.* **2004**, *126*, 7432-7433.
- [43] (a) Narla, R. K.; Dong, Y.; Uckun, F. M. *Leukemia & lymphoma*, **2001**, *41*, 625-34.
(b) Sheng-Tanner, X.; Bump, E. A.; Hedley, D.W. *Rad. Res.* **1998**, *150*, 636-647.
- [44] Lambert, C. R.; Kochevar, I. E.; Redmond, R.W. *J. Phys. Chem. B* **1999**, *103*, 3737-3741.
- [45] (a) Redmond, R. W.; Scaiano, J. C.; Johnston, L. J. *J. Am. Chem. Soc.* **1992**, *114*, 9768-9773.
(b) Scaiano, J. C.; Arnold, B. R.; McGimpsey, W. G. *J. Phys. Chem.* **1994**, *98*, 5431-5434.
- [46] (a) Nagarajan, V.; Fessenden, R. W. *Chem. Phys. Lett.* **1984**, *112*, 207-211.
(b) Cai, X.; Sakamoto, M.; Hara, M.; Tojo, S.; Ouchi, A.; Sugimoto, A.; Kawai, K.; Endo, M.; Fujitsuka, M.; Majima, T. *J. Phys. Chem. A* **2005**, *109*, 3797-3802.
- [47] (a) Weir, D.; Johnston, L. J.; Scaiano, J. C. *J. Phys. Chem.* **1988**, *92*, 1742-1746.
(b) Ouchi, A.; Li, Z.; Sakuragi, M.; Majima, T. *Am. Chem. Soc.* **2003**, *125*, 1104-1108.
(c) Netto-Ferreira, J. C.; Wintgens, V.; Scaiano, J. C. *Tetrahedron Lett.* **1989**, *30*, 6851-6854.
(d) Bendig, J.; Mitzner, R. *Ber. Bunsen-Ges. Phys. Chem.* **1994**, *98*, 1004-008.
(e) Ouchi, A.; Koga, Y. *Tetrahedron Lett.* **1995**, *36*, 8999-9002.
- [48] (a) McGimpsey, W. G.; Scaiano, J. C. *J. Am. Chem. Soc.* **1987**, *109*, 2179-2181.
(b) Ouchi, A.; Koga, Y.; Adam, W. *J. Am. Chem. Soc.* **1997**, *119*, 592-599.
(c) Hara, M.; Tojo, S.; Majima, T. *J. Phys. Chem. A* **2003**, *107*, 4778-4783.
- [49] Redmond, R. W.; Wayner, D. D. M.; Kanabus-Kaminska, J. M.; Scaiano, J. C. *J. Phys. Chem.* **1989**, *93*, 6397-6401.
- [50] Wintgens, V.; Johnston, L. J.; Scaiano, J.C. *J. Am. Chem. Soc.* **1988**, *110*, 511-517.
- [51] (a) Redmond, R. W.; Kochevar, I. E.; Krieg, M.; Smith, G.; McGimpsey, W. G. *J. Phys. Chem. A* **1997**, *101*, 2773-2777.
(b) Pérez-Prieto, J.; Miranda, M. A.; García, H.; Kónya, K.; Scaiano, J. C. *J. Org. Chem.* **1996**, *61*, 3773-3777.
- [52] Goetz, M.; Zubarev, V.; Ekert, G. *J. Am. Chem. Soc.* **1998**, *120*, 5347-5348.

- [53] Goez, M.; Zubarev, V. *Angew. Chem. Int. Ed. Engl.* **1997**, *36*, 2664-2666.
- [54] (a) Schaap, A. P.; Zaklika, K. A.; Kaskar, B.; Fung, L. W. M. *J. Am. Chem. Soc.* **1980**, *102*, 389-391.
(b) Sostero, S.; Traverso, O.; Bernardo, P. D.; Kemp, J. J. *J. Chem. Soc., Dalton Trans.* **1979**, 658-660.
(c) Roth, H. D.; Schilling, M. L. M. *J. Am. Chem. Soc.* **1980**, *102*, 4303-4310.
- [55] (a) Turro, N. J.; Hwang, K. C.; Rao, V. P.; Doubleday, C. J. *J. Phys. Chem.* **1991**, *95*, 1872-1879.
(b) Closs, G. L.; Czeropski, M. S. *Chem. Phys. Lett.* **1978**, *53*, 321-324.
(c) Closs, G. L.; Czeropski, M. S. *J. Am. Chem. Soc.* **1977**, *99*, 6127-6128.
- [56] (a) Matsuyama, A.; Maede, K.; Murai, H. *J. Phys. Chem. A* **1999**, *103*, 4137-40.
(b) Matsuyama, A.; Murai, H. *J. Phys. Chem. A* **2002**, *106*, 2227-2231.
- [57] (a) Miyagawa, K.; Murai, H.; I'Haya, Y. *J. Chem. Phys. Lett.* **1985**, *118*, 140-144.
(b) Clancy, C. M. R.; Forbes, M. D. E. *Photochem. Photobiol.* **1999**, *69*, 16-21.
- [58] (a) Murai, H.; Honma, H.; Kuwata, K. *Res. Chem. Intermed.* **1993**, *19*, 103-118.
(b) Percy, L. T.; Bakker, M. G.; Trifunac, A. D. *J. Phys. Chem.* **1989**, *93*, 4393-96.
(c) Bakker, M. G.; Trifunac, A. D. *J. Phys. Chem.* **1991**, *95*, 550-555.
- [59] (a) Hutton, R. S.; Roth, H. D.; Kraeutler, B.; Cherry, W. R.; Turro, N. J. *J. Am. Chem. Soc.* **1979**, *101*, 2227-2228.
(b) Hwang, K. C.; Turro, N. J.; Doubleday, C. J. *J. Am. Chem. Soc.* **1991**, *113*, 2850-2853.
(c) Jeevarajan, A. S.; Fessenden, R. W. *J. Phys. Chem.* **1992**, *96*, 1520-1523.
- [60] (a) Batchelor, S. N.; Heikkilo, H.; Kay, C. W. M.; McLauchlan, K. A.; Shkrob, A. I. *Chem. Phys.* **1992**, *162*, 29-45.
(b) Batchelor, S. N.; Fischer, H. *J. Phys. Chem.* **1996**, *100*, 9794-9799.
(c) Gridin, V. V.; Korol, A.; Bulatov, V.; Schechter, I. *Anal. Chem.* **1996**, *68*, 3359-3363.
(d) Görner, H.; Curell, L. J. *Rad. Phys. Chem.* **1996**, *48*, 271-279.
(e) Russo-Caia, C.; Steenken, S. *Phys. Chem. Chem. Phys.* **2002**, *4*, 1478-85.
- [61] Turro, N. J.; Grätzel, M.; Braun, A. M. *Angew. Chem.* **1980**, *92*, 712-734; *Angew. Chem. Int. Ed. Engl.* **1980**, *19*, 675-696.
- [62] Mukerjee, P.; Mysels, K. J. in *Critical Micelle Concentration of Aqueous surfactant Systems*, Vol. 36, NSRDS-NBS, Washington DC, 1971.
- [63] Bensasson, R. V.; Land, E. J. *Trans. Faraday Soc.* **1971**, *67*, 1904-1915.

- [64] Lutz, H.; Breheret, E.; Lindqvist, L. *J. Phys. Chem.* **1973**, *77*, 1758-1562.
- [65] Amand, B.; Bensasson, R. *Chem. Phys. Lett.* **1975**, *34*, 44-48.
- [66] Carmichael, I.; Hug, G. L. *J. Phys. Chem. Ref. Data* **1986**, *15*, 1-250.
- [67] Palit, D. K.; Pal, H.; Mukherjee, T.; Mittal, J. P. *J. Photochem.* **1987**, *37*, 95-108.
- [68] Richards, J. T.; Thomas, J. K. *Trans. Faraday Soc.* **1970**, *66*, 621-632.
- [69] (a) Bensasson, R. V.; Land, E. J. "Physical Properties of excited states: A General Method for Measuring Triplet-Triplet Extinction Coefficients, Singlet-Triplet intersystem Crossing Efficiencies, and Related Parameters" in *Photochemical and Photobiological Reviews*, Vol. 3, Smith, K.C. Ed.; Plenum Press: New York, 1978 p.163.
- (b) Land, E. J. *Proc. R. Soc. London, Ser. A* **1968**, *305*, 457-471.
- [70] (a) Backstroem, H. L. J.; Sandros, K. *Acta Chem. Scand.* **1958**, *12*, 823-832.
- (b) Porter, J.; Wilkinson, F. *Trans. Faraday Soc.* **1961**, *57*, 1686-1691.
- (c) Porter, J.; Wilkinson, F. *Proc. Roy. Soc.* **1961**, *264*, 1-18.
- (d) Nielsen, B. R.; Jorgensen, K.; Skibsted, L. H. *J. Photochem. Photobiol. A* **1998**, *112*, 127-133.
- (e) Biczok, L.; Linschitz, H.; Walter, R. I. *Chem. Phys. Lett.* **1992**, *195*, 339-46.
- [71] (a) Carmichael, I.; Hug, G. L. *Appl. Spect.* **1987**, *41*, 1033-8.
- (b) Alfimov, M. V.; Batekha, Y. B.; Shekk, Y. B.; Gerko, V. I. *Spectrochimica Acta A* **1971**, *27*, 329-41.
- (c) Brinen, J. S.; Gerhardt, G. E.; Kazan, J. *Chem. Phys. Lett.* **1970**, *5*, 150-152.
- [72] Maciejewski, A.; Steer, R. P. *Chem. Rev.* **1993**, *93*, 67-98.
- [73] Islam, S. D. M.; Yoshikawa, Y.; Fujitsuka, M.; Ito, O.; Komatsu, S.; Usui, Y. *J. Photochem. Photobiol. A* **2000**, *134*, 155-161.
- [74] Alam, M. M.; Ito, O.; Adam, W.; Grimm, G. N.; Saha-Moeller, C. R. *Phys. Chem. Chem. Phys.* **1999**, *1*, 1851-1857.
- [75] Kunieda, R.; Fujitsuka, M.; Ito, O.; Ito, M.; Murata, Y.; Komatsu, K. *J. Phys. Chem. B* **2002**, *106*, 7193-7199.
- [76] Islam, S. D. M.; Fujitsuka, M.; Ito, O. *Phys. Chem. Chem. Phys.* **1999**, *1*, 3737-3742.
- [77] Kuzmin, V. A.; Dourandin, A.; Shafirovich, V.; Geacintov, N. E. *Phys. Chem. Chem. Phys.* **2002**, *2*, 1531-1535.
- [78] (a) Alam, M. M.; Fujitsuka, M.; Watanabe, A.; Ito, O. *J. Phys. Chem. A* **1998**, *102*, 1338-1344.

- (b) Alam, M. M.; Ito, O.; Grimm, G. N.; Adam, W. *J. Chem. Soc., Perkin Trans. 2* **1998**, 2471-2476.
- [79] (a) Birks, J. B., Ed. "Photophysics of Aromatic Molecules"; Wiley: New York, 1970.
(b) Butler, R. P.; Pilling, M. J. *J. Chem. Soc., Faraday Trans. 2* **1977**, 73, 886-894.
(c) Fang, T. S.; Fukuda, R.; Brown, R. E.; Singer, L. A. *J. Phys. Chem.* **1978**, 82, 246-248.
(d) Rothenberger, G.; Infelta, P. P.; Grätzel, M. *J. Phys. Chem.* **1981**, 85, 1850-1856.
- [80] Zwicker, E. F.; Grossweiner, L. I. *J. Phys. Chem.* **1963**, 67, 549-455.
- [81] (a) Bachilo, S. M.; Weisman, R. B. *J. Phys. Chem. A* **2000**, 104, 7711-7713.
(b) Kremer, M. J.; Connery, K. A.; Dipippo, M. M.; Feng, J.; Chateauneuf, J. E.; Brennecke, J. F. *J. Phys. Chem. A* **1999**, 103, 6591-6598.
(c) Saltiel, J.; Marchand, G.; Smothers, W. K.; Stout, S. A.; Charlton, J. *J. Am. Chem. Soc.* **1981**, 103, 7159-7164.
- [82] Okamoto, M.; Teratsuji, T.; Tazuke, Y.; Hirayama, S. *J. Phys. Chem. A* **2001**, 105, 4574-4578.
- [83] Spinks, J. W. T.; Woods, R. J. *An Introduction to Radiation Chemistry*, 2nd ed.; Wiley: New York, 1976.
- [84] (a) Hush, N. S.; Cheung, A. S. *Chem. Phys. Lett.* **1975**, 34, 11-13.
(b) Fielden, E. M.; Hart, E. *J. Radiat. Res.* **1967**, 32, 564-580.
- [85] Trenin, A.; Hayon, E. *J. Am. Chem. Soc.* **1976**, 98, 3884-3891.
- [86] Goetz, M.; Hussein, B.H.M. *Phys. Chem. Chem. Phys.* **2004**, 6, 5490-5497.
- [87] Goetz, M.; Schiewek, M.; Musa, M. H. O. *Angew. Chem. Int. Ed. Engl.* **2002**, 41, 1535-1538.
- [88] Goetz, M.; Von Ramin-Marro, D.; Musa, M. H. O.; Schiewek, M. *J. Phys. Chem. A* **2004**, 108, 1090-1100.
- [89] Goetz, M.; Hussein, B. H. M. *Angew. Chem. Int. Ed. Engl.* **2003**, 42, 1659-1661.
- [90] Goetz, M.; Zubarev, V. *Chem. Phys.* **2000**, 256, 107-116.
- [91] Becker, H.G.O.; Böttcher, H.; Dietz, F.; Rehorek, D.; Roewer, G.; Schiller, K.; Timpe, H. J. *Einführung in die Photochemie*, ed.; Becker, H.G.O., Deutscher Verlag der Wissenschaften: Berlin 1991.p114.
- [92] Lachish, U.; Shafferman, A.; Stein, G. *J. Chem. Phys.* **1976**, 64, 4205-2411.
- [93] Saito, T.; Haida, K.; Sano, M.; Hirata, Y.; Mataga, N. *J. Phys. Chem.* **1986**, 90, 4017-420.

- [94] Miranda, M. A.; Font-Sanchis, E.; Pérez-Prieto, J.; Scaiano, J. C. *Chem. Commun.* **1998**, 1541-1542.
- [95] Goetz, M.; Zubarev, V. *Angew. Chem. Int. Ed. Engl.* **2001**, *40*, 2867-2869.
- [96] (a) Shoute, L. C. T.; Mittal, J. P. *J. Phys. Chem.* **1993**, *97*, 8630-8637.
(b) Bhattacharyya, K.; Das, P. K. *J. Phys. Chem.* **1986**, *90*, 3987-3993.
(c) Scaiano, J. C. *J. Photochem.* **1973**, *74*, 81-118.
- [97] Davidson, R. S.; Santhanam, M. *J. Chem. Soc., Perkin Trans. 2* **1972**, 2355-2359.
- [98] Bartholomew, R. F.; Davidson, R. S.; Lambeth, P. H.; McKellar, J. F.; Turner, P.H. *J. Chem. Soc., Perkin Trans. 2* **1972**, 2351-2355.
- [99] Arimitsu, S.; Masuhara, H.; Mataga, N.; Tsubomura, H. *J. Phys. Chem.* **1975**, *79*, 1255-1259.
- [100] Arimitsu, S.; Masuhara, H. *Chem. Phys. Lett.* **1973**, *22*, 543-546.
- [101] Siegmund, M.; Bending, J. *Ber. Bunsen. Phys. Chem.* **1978**, *82*, 1061-1068.
- [102] (a) Kokubun, H.; Kobayashi, M. *Z. Phys. Chem.* **1964**, *41*, 245-247.
(b) Fushimi, K.; Kikuchi, K.; Kokubun, H. *J. Photochem.* **1976**, *5*, 457-468.
(c) Kokubun, H. *Z. Phys. Chem.* **1976**, *101*, 137-142.
(d) Val'kova, G. A.; Shcherbo, S. N.; Shigorin, D. N. *Docl. Acad. Nauk USSR* **1978**, *240*, 884-887.
- [103] Abdullah, K. A.; Kemp, T. J. *J. Photochem.* **1986**, *32*, 49-57.
- [104] Shcherbo, S. N.; Val'kova, G. A.; Shigorin, D. N. *Russ. J. Phys. Chem.* **1981**, *55*, 452-453.
- [105] Joschek, H. I.; Grossweiner, L. I. *J. Am. Chem. Soc.* **1966**, *88*, 3261-2368.
- [106] Stein, G. in: *Actions Chimiques et biologiques des radiations*. Vol. 13, ed.; Haissinski, M., Masson: Paris, 1969, p. 119.
- [107] Leslaux, R.; Jousot-Dubien, J. in *Organic molecular photophysics*, Vol. 1, ed.; Birks, J.B., Wiley-Interscience: New York, 1973, p. 457.
- [108] Matsuzaki, A.; Kobayashi, T.; Nagakura, S. *J. Phys. Chem.* **1978**, *82*, 1201-1202.
- [109] Kawata, H.; Shimada, K.; Kumagai, T.; S. Niizuma, *J. Chem. Soc., Perkin Trans. 2* **1993**, 1395-1398.
- [110] Hinze, W. L.; Reihl, T. E.; Singh, H. N.; Baba, Y. *Anal. Chem.* **1984**, *56*, 2180-2191.
- [111] Bending, J.; Siegmund, M. *J. Prakt. Chem.* **1979**, *321*, 587-600.
- [112] Siegmund, M.; Bending, J. *Z. Naturforsch.* **1980**, *35a*, 1076-1086.
- [113] Mory, S.; Weigmann, H.-J.; Rosenfeld, A.; Siegmund, M.; Mitzner, R.; Bendig, J. *Chem. Phys. Lett.* **1985**, *115*, 201-204.

- [114] Kawata, H.; Niizuma, S. *J. prakt. Chem.* **1993**, 336, 425–428.
- [115] (a) Hart, E. J.; Boag, J. W. *J. Am. Chem. Soc.* **1962**, 84, 4090-4095.
(b) Hart, E. J.; Anbar, M. *The Hydrated Electron*, WILEY-Interscience: New York, 1970.
- [116] Nemoto, M.; Kokubun, H.; Koizumi, M. *Bull. Chem. Soc. Jpn.* **1969**, 42, 2464-7240.
- [117] Harriman, A.; Mills, A. *J. Chem. Soc., Faraday Trans. 2.* **1981**, 77, 2111-2124.
- [118] Watanabe, T.; Honda, K. *J. Phys. Chem.* **1982**, 86, 2617-2618.
- [119] Kim, Y. S.; McNiven, S.; Ikebukuro, K.; Karube, I. *Photochem. Photobiol.* **1997**, 66, 180-184.
- [120] Kalyanasundaram, K. *J. Chem. Soc., Chem. Commun.* **1978**, 628-630.
- [121] Méndez, E. E.; Crespo-Hernández, C.; Figueroa, R.; Arce, R.; Quiñones, E. *J. Photochem. Photobiol. A* **2001**, 142, 19-24.
- [122] Ebbesen, T. W.; Levey, G.; Patterson, L. K. *Nature* **1982**, 298, 545-548.
- [123] (a) Ware, W.R.; Doemeny, L. J.; Nemzek, T. L. *J. Phys. Chem.* **1973**, 77, 2038-2048.
(b) McKinnon, A. E.; Szabo, A.G.; Miller, D. R. *J. Phys. Chem.* **1977**, 81, 1564-1570.
- [124] Ishiwata, N.; Murai, H.; Kuwata, K. *J. Phys. Chem.* **1993**, 97, 7129–7131.
- [125] (a) Gibbs, R. C.; Johnson, J. R.; Hughes, E. C. *J. Am. Chem. Soc.* **1930**, 52, 4895-4904.
(b) Lamb, F.; Suschitzky, H. *Tetrahedron* **1959**, 5, 1-9.
- [126] (a) Garner, A.; Wilkinson, F. *J. Chem. Soc., Faraday Trans. 2.* **1976**, 72, 1010-1020.
(b) Ley, C.; Morlet-Savary, F.; Fouassier, J. P.; Jacques, P. *J. Photochem. Photobiol. A* **2000**, 137, 87-92.
- [127] (a) Okano, L. T.; Barros, T. C.; Chou, D. T. H.; Bennet, A. J.; Bohne, C. *J. Phys. Chem. B* **2001**, 105, 2122-2128.
(b) Scaiano, J. C.; Selwyn, J. C. *Can. J. Chem.* **1981**, 59, 2368-2372.
- [128] (a) Wagner, P.J.; Nakahira, T. *J. Am. Chem. Soc.* **1973**, 95, 8474-8475.
(b) Fessenden, R. W.; Carton, P. M.; Shimamori, H.; Scaiano, J. C. *J. Phys. Chem.* **1982**, 86, 3803-3811.
- [129] (a) Encia, M. V.; Lissi, E. A.; Lemp, E.; Zanocco, A.; Scaiano, J. C. *J. Am. Chem. Soc.* **1983**, 105, 1856-1860.
(b) Mohtat, N.; Cozens, F.; Scaiano, J. C. *J. Phys. Chem. B* **1998**, 102, 7557-7562.
(c) Scaiano, J. C. *J. Am. Chem. Soc.* **1980**, 102, 7747-7753.

- [130] Scaiano, J. C.; Weldom, D.; Pliva, C. N.; Martínez, J. *J. Phys. Chem. A* **1998**, *102*, 6898-6903.
- [131] (a) Evans, C. H.; Prud'homme, N.; King M.; Scaiano, J. C. *J. Photochem. Photobiol. A* **1999**, *121*, 105-110.
(b) Barra, M.; Bohne, C.; Scaiano, J. C. *J. Am. Chem. Soc.* **1990**, *112*, 8075-8079.
- [132] (a) Ferguson, M. W.; Beaumont, P. C.; Jones, S.E.; Navaratnam, S.; Parson, B. *Phys. Chem. Chem. Phys.* **1999**, *1*, 261-268.
(b) Yamaji, M.; Inomata, S.; Nakajima, S.; Akiyama, K.; Tobita, S.; Marciniak, B. *J. Phys. Chem. A* **2005**, *109*, 3843-3848.
(c) Murov, S. L.; Carmichael, I.; Hug, G. *Handbook of Photochemistry*, 2nd ed.; Mercel Dekker: New York, 1993.
- [133] Hurely, J. K.; Linschitz, H.; Treinin, A. *J. Phys. Chem.* **1988**, *92*, 5151-5159.
- [134] Damschen, D. E.; Merritt, C. D.; Perry, D. L.; Scott, G. W.; Talley, L. D. *J. Phys. Chem.* **1978**, *82*, 2268-2272.
- [135] Cavaleri, J. J.; Prater, K.; Bowman, R. M. *Chem. Phys. Lett.* **1996**, *259*, 495-502.
- [136] (a) Grand, D. Hautecioque, S.; Bernas, A.; Petit, A. *J. Phys. Chem.* **1983**, *87*, 5236-5240.
(b) Thomas, J. K.; Piciulo, P. *J. Am. Chem. Soc.* **1978**, *100*, 3239-3240.
- [137] Atherton, S. J. *J. Phys. Chem.* **1984**, *88*, 2840-2844.
- [138] Alkaitis, S. A.; Beck, G.; Gräzel, M. *J. Am. Chem. Soc.* **1975**, *97*, 5723-5729.
- [139] (a) Naik, D. B.; Schnabel, W. *Chem. Phys. Lett.* **1999**, *315*, 416-420.
(b) Naik, D. B.; Schnabel, W. *Chem. Phys. Lett.* **1994**, *228*, 616-620.
- [140] Kellmann, A.; Tfibel, F. *Chem. Phys. Lett.* **1980**, *69*, 61-65.
- [141] Ryan, E.T.; Xiang, T.; Johnston, K. P.; Fox, M. A. *J. Phys. Chem. A* **1997**, *101*, 1827-1835.
- [142] Kasama, K.; Kikuchi, K.; Yamamoto, S. A.; Uji-Ie, K.; Nishida, Y.; Kokubun, H. *J. Phys. Chem.* **1981**, *85*, 1291-1296.
- [143] Ito, S.; Ito, E.; Yoshikawa, Y.; Watanabe, A.; Kokubun, H. *J. Chem. Soc., Faraday Trans.* **1996**, *92*, 227-230.
- [144] Kellmann, A.; Lindqvist, L. "The Triplet State", Zahlan, A. B. Ed. Cambridge University Press: New York, 1967, p 439.
- [145] Medeiros, G. M: M.; Leitão, M. F.; Costa, S. M. B. *J. Photochem. Photobiol. A* **1993**, *72*, 225-233.

- [146] (a) Bowen, E. J.; Holder, N. J.; Woodger, G. B. *J. Phys. Chem.* **1962**, *66*, 2491-2492.
(b) Weller, A. Z. *Elektrochem.* **1957**, *61*, 956-961.
- [147] Wolff, T. *Ber. Bunsen. Phys. Chem.* **1981**, *85*, 145-148.
- [148] Periasamy, N. *Chem. Phys. Lett.* **1983**, *99*, 322-325.
- [149] Meisel, D.; Matheson, M. S.; Mulac, W. A.; Rabani, J. *J. Phys. Chem.* **1977**, *81*, 1449-1455.
- [150] Kikuchi, K. In *Triplet-Triplet Absorption Spectra*, Bunshin Publishing Co., Tokyo, 1989.
- [151] Kellmann, A. *J. Phys. Chem.* **1977**, *81*, 1195-1198.
- [152] Nishida, Y.; Kikuchi, K.; Kokubun, H. *J. Photochem.* **1980**, *13*, 75-81.
- [153] Kasama, K.; Kikuchi, K.; Nishida, Y.; Kokubun, H. *J. Phys. Chem.* **1981**, *85*, 4148-4153.
- [154] Kellmann, A.; Tfibel, F. *J. Photochem.* **1982**, *18*, 81-88.
- [155] Wehry, E.L. In *Practical Fluorescence*; Guilbaut, G. G., Ed.; Marcel Dekker, Inc.: New York, 1990.
- [156] Kikuchi, K.; Kasama, K.; Kanemoto, A.; Uji-ie, K.; Kokubun, H. *J. Phys. Chem.* **1985**, *89*, 868-871.
- [157] Bent, D.V.; Hayon, E. *J. Am. Soc.* **1975**, *97*, 2599, 2606, 2612.
- [158] Krasna, A. I. *Photochem. Photobiol.* **1980**, *31*, 75-82.
- [159] (a) Oncescu, T.; Stefan, M. *New. J. Chem.* **1993**, *17*, 495-498.
(b) Oncescu, T.; Stefan, M.; Ionescu, G.; Contineanu, M. *Rev. Roum. Chim* **1987**, *32*, 953-960.
- [160] Koryakin, B. V.; Dzhabiev, T. S.; Shilov, A. E. *Dokl. Akad. Nauk. SSSR*, **1977**, *233*, 620-622.
- [161] (a) Grimaldi, J. J.; Bioleau, S.; Lehn, J. M. *Nature* **1977**, *265*, 229-230.
(b) Krasna, A. I. *Photochem. Photobiol.* **1979**, *29*, 267-276.
(c) Oncescu, T.; Stefan, M.; Ionescu, G. *Rev. Roum. Chim.* **1993**, *38*, 791-798.
- [162] (a) Kalyanasundaram, K.; Grätzel, M. *J. Chem. Soc. Chem. Comm.* **1979**, *24*, 1137-1138.
(b) Nenadovic, M. T.; Micic, O. I.; Kosanic, M. M. *Rad. Phys. Chem.* **1981**, *17*, 159-61.
(c) Neumann-Spallart, M.; Kalyanasundaram, K. *J. Phys. Chem.* **1982**, *86*, 2681-90.
(d) Micic, O. I.; Nenadovic, M. T. *Energy Storage, Trans. Int. Assem* **1980**, 445-449.
- [163] Kalyanasundaram, K.; Dung, D. *J. Phys. Chem.* **1980**, *84*, 2551-2556.

- [164] Pileni, M. P.; Gräzel, M. *J. Phys. Chem.* **1980**, *84*, 2402–2406.
- [165] Kiwamv, Y.; Sumihare, N.; Mamoru, Y. *Bull. Chem. Soc. Jpn.* **1981**, *54*, 31-34.
- [166] Schwarz, G.; Klose, S.; Balthasar, W. *Eur. J. Biochem.* **1970**, *12*, 454-460.
- [167] (a) Haugen, G. R.; Melhuish, W. H. *Trans. Faraday. Soc.* **1964**, *60*, 386-394.
(b) Melhuish, W. H. *J. Opt. Soc. Am.* **1964**, *54*, 183-186.
- [168] Armstrong, R. W.; Panzer, N. M. *J. Am. Chem. Soc.* **1972**, *94*, 7650-58.
- [169] (a) Du, H.; Fuh, R. C. A.; Li, J.; Corkan, L. A.; Lindsey, J. S. *Photochem. Photobiol.* **1998**, *68*, 141-142.
(b) Kubota, Y.; Steiner, R. F. *Chem. Lett.* **1973**, *3*, 299-304.
(c) Roberts, J. E. *Photochem. Photobiol.* **1981**, *33*, 61-64.
- [170] Kikuchi, K.; Koizumi, M. *Bull. Chem. Soc. Jpn.* **1967**, *40*, 736-743.
- [171] Kikuchi, K.; Kokubun, H.; Koizumi, M. *Bull. Chem. Soc. Jpn.* **1971**, *44*, 1545-51.
- [172] Lim, E. C.; Swenson, G. W. *J. Chem. Phys.* **1963**, *39*, 2768-2769.
- [173] Lim, E. C.; Lazzara, C. P.; Yang, M. Y.; Swenson, G. W. *J. Chem. Phys.* **1965**, *43*, 970-974.
- [174] (a) Magata, N.; Kaifu, Y.; Koizumi, M. *Bull. Chem. Soc. Jpn.* **1956**, *29*, 373-379.
(b) Kaye, R. C.; Stonehill, M. I. *J. Chem. Soc.* **1951**, 2638-2646.
(c) Solar, S.; Solar, W.; Getoff, N. *Z. Naturforsch.* **1982**, *37a*, 1077-1082.
- [175] Goez, M.; Sartorius, I. *J. Phys. Chem. A* **2003**, *107*, 8539-8546.
- [176] Kavarnos, G. J.; Turro, N. J. *Chem. Rev.* **1986**, *86*, 401–449.
- [177] (a) Cohen, S. G.; Chao, H. M.; Stein, N. J. *J. Am. Chem. Soc.* **1969**, *90*, 521-522.
(b) Cohen, S. G.; Stein, N. J. *J. Chem. Soc.* **1969**, *91*, 3690-3691.
- [178] (a) Shaefer, C. G.; Peters, K. S. *J. Am. Chem. Soc.* **1980**, *102*, 7566-7567.
(b) Peters, K. S.; Freilich, S. C.; Shaefer, C. G. *J. Am. Chem. Soc.* **1980**, *102*, 5701-5702.
(c) Simon, J. D.; Peters, K. S. *J. Am. Chem. Soc.* **1981**, *103*, 6403-6406.
- [179] (a) Cohen, S. G.; Parola, A. H.; Jr, G. H. *Chem. Rev.* **1973**, *73*, 141-161.
(b) Parola, A. H.; Rose, W.; Cohen, S.G. *J. Am. Chem. Soc.* **1975**, *97*, 6202-6209.
(c) Parola, A. H.; Cohen, S. G. *J. Photochem.* **1980**, *12*, 41-50.
- [180] Gardini G. P.; Bargon, J. *J. Chem. Soc., Chem. Commun.* **1980**, 757-758.
- [181] (a) Devadoss, C.; Fessenden, R. W. *J. Phys. Chem.* **1990**, *94*, 4540-4549.
(b) Devadoss, C.; Fessenden, R. W. *J. Phys. Chem.* **1991**, *95*, 7253-7260.
(c) Peters, K. S.; Lee, J. *J. Phys. Chem.* **1993**, *97*, 3761-3764.
- [182] Kajii, Y.; Itabashi, H.; Shibuya, K.; Obi, K. *J. Phys. Chem.* **1992**, *96*, 7244-7247.

- [183] Yanimoto, Y.; Fujiwara, Y.; Jinda, C.; Itoh, M. *J. Photochem. Photobiol. A* **1994**, *79*, 89-94.
- [184] Abe, T.; Kawai, A.; Kajii, Y.; Shibuya, K.; Obi, K. *J. Phys. Chem. A* **1999**, *103*, 1457-1462.
- [185] Igarashi, M.; Sakaguchi, Y.; Hayashi, H. *Chem. Phys. Lett.* **1995**, *243*, 545-551.
- [186] (a) Aloisi, G.G.; Elisei, F.; Latterini, L.; Galiazzo, G.; Goerner, H. *J. Chem. Soc., Faraday Trans.* **1995**, *91*, 3117-3121.
(b) Aloisi, G. G.; Elisei, F.; Latterini, L. *J. Chem. Soc., Faraday Trans.* **1992**, *88*, 2139-2145.
- [187] Goerner, H.; Elisei, F.; Aloisi, G.G. *J. Chem. Soc., Faraday Trans.* **1992**, *88*, 29-34.
- [188] Hiller, K. O.; Asmus, K. D. *J. Phys. Chem.* **1983**, *87*, 3682-3688.
- [189] Goez, M.; Rozwadowizki, J.; Marciniak, B. *J. Am. Chem. Soc.* **1996**, *118*, 2882-91.
- [190] Bonnett, R. *J. Chem. Soc.* **1965**, 2313-2318.
- [191] Pittacco, G.; Valentin, E. In the Chemistry of Amino, Nitroso and Nitro compounds and their derivatives, Part 1; Patai, S., Ed.; Wiley: New York, 1982; p 623-714.
- [192] Inbar, S.; Linschitz, H.; Cohen, S. G. *J. Am. Chem. Soc.* **1981**, *103*, 1048-1054.
- [193] Redmond, R. W.; Scaiano, J. C.; Johnston, L. J. *J. Am. Chem. Soc.* **1990**, *112*, 398-402.
- [194] (a) Workentin, M. S.; Johnston, L. J.; Wayner, D. D. M.; Parker, V. D. *J. Am. Chem. Soc.* **1994**, *116*, 8279-8287.
(b) Dunn, D. A.; Schuster, D. I.; Bonneau, R. *J. Am. Chem. Soc.* **1985**, *107*, 2802-2804.
(c) Halpern, A. M.; Forsyth, D. A.; Nosowitz, M. *J. Phys. Chem.* **1986**, *90*, 2677-2679.
- [195] Davis, G. T.; Demek, M. M.; Rosenblatt, D. H. *J. Am. Chem. Soc.* **1972**, *94*, 3321-3325.

Abbreviations and symbols

$e_{aq}^{\bullet-}$	Hydrated electron	k_{1st}	Unimolecular decay rate constant
$I(t)$	Envelope of laser pulse	k_{obs}	Observed decay rate constant (First- order decay constant)
τ	Laser pulse duration	k_q	Rate constant of self-quenching
φ	Quantum yield	k_{T-T}	Rate constant of triplet-triplet annihilation
ε	Extinction coefficient	r_i	Rate of photoinduced reaction step
E	Absorbance	I_{abs}	Absorbed light intensity
ΔE	Absorbance difference	I_{exc}	Laser excitation intensity
τ_0^D	Triplet lifetime	I	Total intensity of the exciting light
τ_f	Fluorescence lifetime	c	Concentration
η	Efficiency	c_0	Initial concentration of substrate
D	Donor	M	Substance under study
A	Acceptor	St	Standard substance
A	Irradiated area	MA	N-Methylacridone
V	Excited volume	ACO	Acridone
λ	Wavelength	X	Xanthone
d	Optical path length of cell	Ac	Acridine
N_a	Avogadro number	Me	Methanol
c_l	Speed of light	H ₂ O	Water
h	Planck's constant	v/v	Volume/volume
$h\nu$	Photon energy	SDS	Sodium hydroxide
ν	Frequency	D _{sac}	Sacrificial electron donor
κ_1	Kinetic constant (Constant of proportionality)	ET	Electron transfer
k_i	Associated rate "constant"	EnT	Energy Transfer
k_f	Fluorescence rate constant		
k_{ic}	Internal conversion rate constant		
k_{isc}	Intersystem crossing rate constant		
k_d	Radiationless decay		

T	Triplet		
BC	Benzophenone-4-carboxylate	TEA	Triethylamine
PH ⁺	Proflavine hemisulfate dihydrate	SDS	Sodium dodecylsulfate
MV ²⁺	Methylviologen (1,1'-dimethyl-4,4'-bipyridinium chloride)	cmc	Critical micellar concentration
ESR	Electron spin resonance	NADH	Dihyronicotinamide adenine dinucleotide
ESR	Electron spin resonance	DNA	Deoxyribonucleic acid
CINP	Chemically induced nuclear polarization		
LFP	Laser flash photolysis		
FWHM	Full width at half-maximum		
UV-vis	Ultraviolet-visible		
PMT	Photomultiplier tube		
NDS	1,5-Naphthalene-disulfonate		
DABCO	1,4-Diazabicyclo[2.2.2]octane		

Superscripts

(*)	Excited state
(* , 1)	Excited singlet state
(* , 3)	Excited triplet state
(•+)	Radical cation
(•-)	Radical anion
(* , •-)	Excited radical anion
(•)	Radical

Curriculum Vitae

Personal data:

Name : Belal Hussein Mohamed Hussein
Date of birth : January 2, 1970
Place of birth : Sharkia (Egypt)
Marital status : Married

Education :

1988-1991 : B. Sc in Chemistry. Suez Canal University, Faculty of Science
Department of Chemistry
1992-1993 : Post Graduate (Organic Chemistry)
1993-1997 : M. Sc. in Chemistry. Suez Canal University, Faculty of Science
Department of Chemistry
2000-2005 : Ph. D. studentship at Martin-Luther-Universität Halle-Wittenberg,
Institute of Organic Chemistry, under Supervision of Prof. Dr. M. Göz.

Job experience:

1994-1997 : Demonstrator in the Chemistry Department, Faculty of Science, Suez
Canal University.
1997-1999 : Assistant Lecture. Department of Chemistry, Faculty of Science, Suez
Canal University.

Publications

Results of the work are presented in the following publications:

Goez, Martin; **Hussein, Belal Hussein Mohammed. Generation of hydrated electrons by an acridone-sensitized three-photon cycle.** *Angew. Chem. Int. Ed. Engl.* 2003, 42, 1659-1661.

Goez, Martin; **Hussein, Belal Hussein Mohammed. Photoionization of xanthone via its triplet state or via its radical anion.** *Phys. Chem. Chem. Phys.* **2004**, 6, 5490-5497.

Acknowledgment

I would like to express my deepest gratitude to Prof. Dr. M. Goez, my advisor for this thesis, for the opportunity to do such an interesting research under his supervision. Also, I am particularly thankful for his guidance, advice, patience, fruitful discussions, and encouragements during the whole period of my PhD work.

I would like to thank the members of our research group in photochemistry of Prof. Goez: Especially, Dr. V. Zubarev for advising me in my first steps in the laboratory, as well as Dipl.-Chem. Daniel von Ramin-Marro and Dipl.-Chem. Martin Schiewek for fruitful discussions. My thanks are extended to all the staff of the Institute of Organic Chemistry in university of Halle (Saale) for their cooperation during the preparation of my thesis.

My special thanks are due to my parents and to my wife for their mental, practical support, and encouragement, as well as to our children for their love and patience during all the years of my research work.

Author's declaration

This thesis is an account of work carried out at the Martin-Luther-Universität Halle-Wittenberg under the supervision of Prof. Dr. Martin Goez.

I declare that this work was carried out in accordance with the Regulations of the Martin-Luther-Universität Halle-Wittenberg. The work is original except where indicated by special references in the text and no part of the dissertation has not been presented to any other University for examination.

Eidesstattliche Erklärung

Ich erkläre hiermit, die vorliegende Dissertationsschrift selbständig und nur unter Verwendung der angegebenen Quellen und Hilfsmittel angefertigt zu haben.

Die Arbeit wurde bisher an keiner weiteren Hochschule oder Universität zur Promotion eingereicht.

Halle (Saale), October, 19, 2004